



MINISTÉRIO DA CIÊNCIA, TECNOLOGIA, INOVAÇÕES E COMUNICAÇÕES
INSTITUTO NACIONAL DE PESQUISAS ESPACIAIS

sid.inpe.br/mtc-m21c/2018/08.21.18.18-TDI

EXPERIMENTAL INVESTIGATION OF THE THERMAL PERFORMANCE OF SCREEN MESH WICK HEAT PIPES OPERATING IN MID-LEVEL TEMPERATURES

Débora de Oliveira Silva

Doctorate Thesis of the Graduate Course in Engineering and Space Technology/Space Mechanics and Control, guided by Dr. Roger Ribeiro Riehl, approved in august 31, 2018.

URL of the original document:

<<http://urlib.net/8JMKD3MGP3W34R/3RM6TQ2>>

INPE
São José dos Campos
2018

PUBLISHED BY:

Instituto Nacional de Pesquisas Espaciais - INPE

Gabinete do Diretor (GBDIR)

Serviço de Informação e Documentação (SESID)

CEP 12.227-010

São José dos Campos - SP - Brasil

Tel.:(012) 3208-6923/7348

E-mail: pubtc@inpe.br

**COMMISSION OF BOARD OF PUBLISHING AND PRESERVATION
OF INPE INTELLECTUAL PRODUCTION (DE/DIR-544):****Chairperson:**

Dr. Marley Cavalcante de Lima Moscati - Centro de Previsão de Tempo e Estudos Climáticos (CGCPT)

Members:

Dra. Carina Barros Mello - Coordenação de Laboratórios Associados (COCTE)

Dr. Alisson Dal Lago - Coordenação-Geral de Ciências Espaciais e Atmosféricas (CGCEA)

Dr. Evandro Albiach Branco - Centro de Ciência do Sistema Terrestre (COCST)

Dr. Evandro Marconi Rocco - Coordenação-Geral de Engenharia e Tecnologia Espacial (CGETE)

Dr. Hermann Johann Heinrich Kux - Coordenação-Geral de Observação da Terra (CGOBT)

Dra. Ieda Del Arco Sanches - Conselho de Pós-Graduação - (CPG)

Silvia Castro Marcelino - Serviço de Informação e Documentação (SESID)

DIGITAL LIBRARY:

Dr. Gerald Jean Francis Banon

Clayton Martins Pereira - Serviço de Informação e Documentação (SESID)

DOCUMENT REVIEW:

Simone Angélica Del Ducca Barbedo - Serviço de Informação e Documentação (SESID)

André Luis Dias Fernandes - Serviço de Informação e Documentação (SESID)

ELECTRONIC EDITING:

Marcelo de Castro Pazos - Serviço de Informação e Documentação (SESID)

Murilo Luiz Silva Gino - Serviço de Informação e Documentação (SESID)



MINISTÉRIO DA CIÊNCIA, TECNOLOGIA, INOVAÇÕES E COMUNICAÇÕES
INSTITUTO NACIONAL DE PESQUISAS ESPACIAIS

sid.inpe.br/mtc-m21c/2018/08.21.18.18-TDI

EXPERIMENTAL INVESTIGATION OF THE THERMAL PERFORMANCE OF SCREEN MESH WICK HEAT PIPES OPERATING IN MID-LEVEL TEMPERATURES

Débora de Oliveira Silva

Doctorate Thesis of the Graduate Course in Engineering and Space Technology/Space Mechanics and Control, guided by Dr. Roger Ribeiro Riehl, approved in august 31, 2018.

URL of the original document:

<<http://urlib.net/8JMKD3MGP3W34R/3RM6TQ2>>

INPE
São José dos Campos
2018

Cataloging in Publication Data

Silva, Débora de Oliveira.

Si38e Experimental investigation of the thermal performance of screen mesh wick heat pipes operating in mid-level temperatures / Débora de Oliveira Silva. – São José dos Campos : INPE, 2018.

xxviii + 151 p. ; (sid.inpe.br/mtc-m21c/2018/08.21.18.18-TDI)

Thesis (Doctorate in Engineering and Space Technology/Space Mechanics and Control) – Instituto Nacional de Pesquisas Espaciais, São José dos Campos, 2018.

Guiding : Dr. Roger Ribeiro Riehl.

1. Heat pipes. 2. Thermal control. 3. Thermal conductance.
4. Experimental heat pipes. 5. Two-phase flow. I.Title.

CDU 536.2:620.1



Esta obra foi licenciada sob uma Licença [Creative Commons Atribuição-NãoComercial 3.0 Não Adaptada](https://creativecommons.org/licenses/by-nc/3.0/).

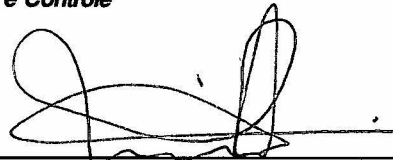
This work is licensed under a [Creative Commons Attribution-NonCommercial 3.0 Unported License](https://creativecommons.org/licenses/by-nc/3.0/).

Aluno (a): *Débora de Oliveira Silva*

Título: "EXPERIMENTAL INVESTIGATION OF THE THERMAL PERFORMANCE OF SCREEN MESH WICK HEAT PIPES OPERATING IN MID-LEVEL TEMPERATURES"

Aprovado (a) pela Banca Examinadora em cumprimento ao requisito exigido para obtenção do Título de *Doutor(a)* em *Engenharia e Tecnologia Espaciais/Mecânica Espacial e Controle*

Dr. Paulo Giácomo Milani



Presidente / INPE / SJC Campos - SP

() *Participação por Vídeo - Conferência*

Aprovado () *Reprovado*

Dr. Roger Ribeiro Riehl

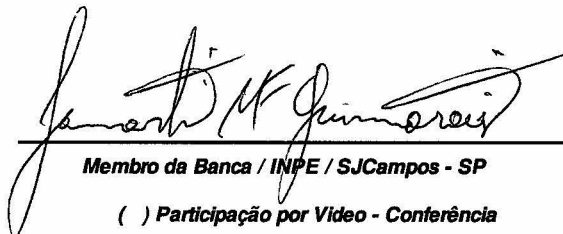


Orientador(a) / INPE / SJC Campos - SP

() *Participação por Vídeo - Conferência*

Aprovado () *Reprovado*

Dr. Lamartine Nogueira Frutuoso Guimaraes



Membro da Banca / INPE / SJC Campos - SP

() *Participação por Vídeo - Conferência*

Aprovado () *Reprovado*

Dr. Heraldo da Silva Couto



Membro da Banca / INPE / São José dos Campos - SP

() *Participação por Vídeo - Conferência*

() *Aprovado* () *Reprovado*

Este trabalho foi aprovado por:

() *maioria simples*

unanimidade

São José dos Campos, 31 de agosto de 2018

Aprovado (a) pela Banca Examinadora
em cumprimento ao requisito exigido para
obtenção do Título de **Doutor(a)** em
**Engenharia e Tecnologia Espaciais/Mecânica
Espacial e Controle**

Dr. Demétrio Bastos Netto

Membro da Banca / INPE / São José dos Campos - SP

() Participação por Vídeo - Conferência

() Aprovado () Reprovado

Dr. Sebastião Cardoso

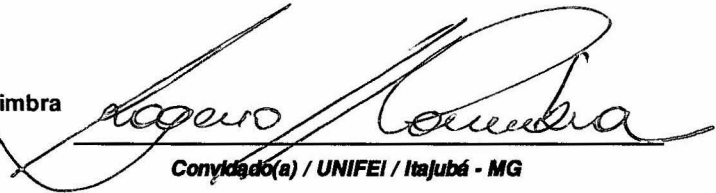


Convidado(a) / ITA/DCTA / São José dos Campos - SP

() Participação por Vídeo - Conferência

() Aprovado () Reprovado

Dr. Rogério Frauendorf de Faria Coimbra



Convidado(a) / UNIFEI / Itajubá - MG

() Participação por Vídeo - Conferência

Aprovado () Reprovado

Este trabalho foi aprovado por:

() maioria simples

() unanimidade

São José dos Campos, 31 de agosto de 2018

“A verdadeira viagem de descobrimento não consiste em procurar novas paisagens, mas em ter novos olhos”.

MARCEL PROUST

*To my parents Benedito Nelson and Célia Maria, to my
sisters Bruna and Bárbara, and to my daughter Isabela*

ACKNOWLEDGEMENTS

Firstly to my parents Nelson e Célia, for always being at my side, supporting in every decision.

To my daughter Isabela, who was able to understand all times that I have not been at her side.

To my teachers at the National Institute for Space Research (INPE) than with their knowledge, they formed the basis for the development of this research, with special attention to my advisor, Dr. Roger Ribeiro Riehl.

To my really friends, especially to Paulo Henrique Mineiro Leite, Roberta Lee Alcaide, Eli Maciviero Alcaide, Luciana Souza, Maria José Souza, Danilo Homem de Melo, Marcia Homem de Melo, Elaine Santos, Marcelo Asato, Gabriela Romeiro, Herly Brazolin, Letícia Marcato, Pedro Moniz, Thiago Godoy and to my nephew Pedro.

To Coordenação de Aperfeiçoamento de Pessoal de Nível Superior - CAPES for the financial support.

To everybody that in their way, helped me to complete this work.

ABSTRACT

Heat pipes are two-phase heat transfer devices with the capacity of transfer large amounts of heat with a small temperature difference between the evaporation section and the condensation section, making the heat transfer process be highly efficient. The robust and simple tubular structure with no moving parts makes the heat pipe a perfect choice for different applications such as industrial or aerospace sector. Heat pipe technology has been widely applied in various areas, such as heat exchangers, spacecraft thermal control and cooling systems for electronic components. This technology has found increasing application in improving the thermal performance of heat exchangers in many industrial environments. The use of heat pipes in heat exchangers allows the development of more compact and efficient equipment, when compared to traditional heat exchangers. For some applications, such as heat recovery in industrial process, the use of heat pipes on heat exchangers presents to be rather interesting due to their direct influence on increasing the efficiency, allowing a more compact design. However, in many thermal control applications, heat pipes using mid-level temperature working fluids, such as water or ammonia, with operating temperatures between 200 K (-73°C) and 550 K (277°C), can hardly operate at steady state conditions. The heat pipe performance depends on its geometry, working fluid, wick structure, and operating conditions. The working fluid is one of the most important parameters as the heat pipe utilizes the phase change to transport the heat. Therefore, the selection of the working fluid is of great importance to enhance the thermal performance of the heat pipe. Heat pipes operating at mid-level temperatures have found several applications in industrial sector. In this work, heat pipes were designed and manufactured with the objective of investigating the potential application of heat pipes operating at mid-level temperature. The thermal conductance obtained from the experimental tests were used to correlate the thermal conductances obtained analytically, with results showing high accuracy based on the adjustment factor applied. The numerical model results were compared with experimental measurements at the same condition. Good agreement was observed between numerical predicted temperature profiles and experimental temperature data. Test results showed reliable operation during the power step and power cycles, with fast start ups, achieving thermal conductances of up $26.59\text{W}/^{\circ}\text{C}$.

INVESTIGAÇÃO EXPERIMENTAL DO DESEMPENHO TÉRMICO DE TUBOS CALOR COM MALHA DE TELA METÁLICA OPERANDO EM TEMPERATURA MODERADA

RESUMO

Os tubos de calor são dispositivos que utilizam a mudança de fase de um fluido para transferir grandes quantidades de calor com uma pequena diferença de temperatura entre a seção de evaporação e a seção de condensação, tornando o processo de transferência de calor altamente eficiente. A estrutura tubular robusta e simples, sem peças móveis, faz do tubo de calor uma escolha perfeita para diferentes aplicações, tanto no setor industrial como no aeroespacial. A tecnologia de tubos de calor tem sido amplamente aplicada em várias áreas de transferência de calor, inclusive em sistemas de controle térmico e sistemas de refrigeração para componentes eletrônicos. Esta tecnologia encontrou uma aplicação crescente na melhoria do desempenho térmico dos permutadores de calor em muitos ambientes industriais. O uso de tubos de calor em trocadores de calor permite o desenvolvimento de equipamentos mais compactos e eficientes, quando comparados aos trocadores de calor tradicionais. Para algumas aplicações, como a recuperação de calor em processos industriais, o uso destes dispositivos apresenta-se bastante interessante devido à sua influência direta no aumento da eficiência, permitindo um design mais compacto. No entanto, em muitas aplicações de controle térmico, tubos de calor que utilizam fluidos de trabalho de temperatura intermediária, como água ou amônia, com temperaturas de operação entre 200 K (-73°C) e 550 K (277°C), dificilmente podem operar em condições de estado estacionário. O desempenho do tubo de calor depende da sua geometria, fluido de trabalho, estrutura porosa e condições de operação. O fluido de trabalho é um dos parâmetros mais importantes, pois o tubo de calor utiliza a mudança de fase deste para transportar o calor. Portanto, a seleção do fluido de trabalho é de grande importância para melhorar o desempenho térmico do tubo de calor. Os tubos de calor que operam a temperatura intermediária encontraram várias aplicações no setor industrial e aeroespacial. Neste trabalho, os tubos de calor foram projetados e fabricados com o objetivo de investigar o potencial aplicação em temperatura intermediária. Os resultados do modelo numérico foram comparados com resultados experimentais nas mesmas condições. Boa concordância foi observada entre os perfis de temperatura numéricos e os resultados experimentais de temperatura. A condutância térmica obtida a partir dos testes experimentais foi utilizada para correlacionar as condutâncias térmicas obtidas de forma analítica, com resultados com alta precisão com base no fator de ajuste aplicado. Os resultados do teste mostraram operação confiável durante o incremento e ciclagem das potências, com rápida inicialização, atingindo conduções térmicas de até $26,59\text{W}/^{\circ}\text{C}$.

LIST OF FIGURES

	<u>Pág.</u>
1.1 (a) Thermosyphon, (b) Heat Pipe.	2
1.2 Heat Pipes used in Thermal Control of Satellites - CBERS	7
1.3 Miniature heat pipe.	9
1.4 Micro-heat pipe operation.	10
1.5 (a) Condenser partially active and (b) Condenser fully active.	12
1.6 Multiple evaporator LHP.	15
1.7 Operating principle of loop heat pipe.	16
1.8 Pulsating heat pipe configurations:(a) closed loop, (b) closed loop with check valve, (c) open loop.	17
1.9 PHP application for PCB temperature control.	18
1.10 Schematics of the PHP used for the thermal control.	19
3.1 (a) Components and principle of operation of a conventional heat pipe and (b) Development of capillary pressure at liquid-vapour interface. . .	24
3.2 Heat Pipe design flow chart.	27
3.3 Operating temperature ranges of various working fluid.	30
3.4 Figure of Merit for various working fluids.	32
3.5 Different types of wick structure.	34
3.6 (a) Wire mesh heat pipe, (b) Stainless steel wire mesh.	36
3.7 (a) Sintered wick heat pipe, (b) Sintered metal powder.	37
3.8 Grooved wick in a copper tube.	38
4.1 Interfacial tensions acting on a contact line.	42
4.2 Wetting and nonwetting contact.	44
4.3 Geometry of meniscus at liquid-vapour interface.	45
4.4 Limitations to heat transport in a heat pipe.	53
4.5 Liquid and Vapour pressure distributions in a heat pipe.	55
4.6 Temperature as a function of axial position.	59
4.7 Overall thermal resistance of a heat pipe.	64
5.1 Tilt angle on the heat pipes (a) HP1, HP2 and HP3, (b) HP4, HP5 and HP6	73
5.2 (a) HP1, (b) HP2 and (c) HP3.	74
5.3 (a) HP4, (b) HP5 and (c) HP6.	76
5.4 Maximum capillary pressure for screen wicks	78

5.5	Container and screen mesh wick (a) Stainless steel container, (b) Stainless steel screen mesh wick	79
5.6	Heat Pipes Experimental Bench (a) Experimental test rig 0°, (b) Experimental test rig 30°	81
5.7	(a) Data acquisition system and power controller, (b) Position of thermocouples on the heat pipes and data acquisition system.	83
5.8	NCG generation rate for the heat pipe	85
6.1	Temperature profiles of HP1, HP2 and HP3: (a) Power Step, (b) Power Cycles by Table 5.3.	91
6.2	Thermal conductance experimental x calculated for HP1, HP2 and HP3: Cycle 2 by Table 5.3.	93
6.3	Temperature profiles of HP1, HP2 and HP3 for power step.	95
6.4	Temperature profiles of HP1, HP2 and HP3: (a) Cycle 1 and (b) Cycle 2 by Table 5.3.	96
6.5	Thermal conductance experimental x calculated for HP1, HP2 and HP3: Cycle 1 by Table 5.3.	97
6.6	Temperature profiles of HP1, HP2 and HP3 for power step	99
6.7	Thermal conductance experimental x calculated for HP1, HP2 and HP3: Power step.	100
6.8	Temperature profiles of HP1, HP2 and HP3 for cycle 1	102
6.9	Thermal conductance experimental x calculated for HP1, HP2 and HP3: Cycle 1.	103
6.10	Temperature profiles of HP4, HP5 and HP6 for cycle 2	105
6.11	Thermal conductance experimental x calculated for HP4, HP5 and HP6: Cycle 2.	106
6.12	Temperature profiles of HP4, HP5 and HP6 for cycle 1	108
6.13	Thermal conductance experimental x calculated for HP4, HP5 and HP6: Cycle 1.	109
6.14	Temperature profiles of HP4, HP5 and HP6 for cycle 1	111
6.15	Thermal conductance experimental x calculated for HP4, HP5 and HP6: Cycle 1.	112
6.16	Temperature profiles of HP4, HP5 and HP6 for cycle 1.	114
6.17	Thermal conductance experimental x calculated for HP4, HP5 and HP6: Cycle 1.	115
6.18	The effects of inclination on the heat pipes performance(a) Stainless steel heat pipes and (b) Copper heat pipes.	116
6.19	Heat pipes in a storage tank.	118

6.20	(a) Temperature distribution in the PAC tank, (b) Speed vector in the PAC tank (3D model).	119
6.21	(a) Temperature distribution in the PAC tank (3D model, (b) Speed vector in the PAC tank (3D model).	119
6.22	Position of electronic equipment on honeycomb panel.	121
6.23	Temperature distribution on honeycomb panel.	122
6.24	(a) Aluminum extruded profile with flanges for panel heat pipes and for panel connecting pipes with radiator, (b) Aluminum extruded profile without flanges for adiabatic section of panel heat pipes with radiator.	123
6.25	Position of the heat pipes in the panel.	124
6.26	Pressure drops	125
6.27	Operating Limits	125
6.28	Arrangement of the panel in relation to the radiator.	127
6.29	Heat pipe arrangement for connecting the panel to the radiator.	127
7.1	Boundary conditions of heat pipe.	131
7.2	Temperature comparison between experimental and numerical for different heat inputs.(a) HP1, (b) HP2, (c) HP3, (d) HP4 and (e) HP5.	134
7.3	Thermal conductance comparison between experimental and numerical for different heat inputs.(a) HP1, (b) HP2, (c) HP3, (d) HP4 and (e) HP5.	138

LIST OF TABLES

	<u>Pág.</u>
3.1 Heat Pipe components and their influence on design requirements	28
3.2 Results of experimental compatibility tests	29
5.1 Characteristics of heat pipes HP1, HP2 and HP3	71
5.2 Characteristics of heat pipes HP4, HP5 and HP6	71
5.3 Applied power	87
5.4 Schedule of tests realized with the heat pipes: power step	87
5.5 Schedule of tests realized with the heat pipes: power cycles	87
6.1 Thermal performance for the HP1 operating with power cycles - Cycle 2	93
6.2 Thermal performance for the HP2 operating with power cycles - Cycle 2	94
6.3 Thermal performance for the HP3 operating with power cycles - Cycle 2	94
6.4 Thermal performance for the HP1 (power step) with the thermal con- ductance uncertainty of 11%	98
6.5 Thermal performance for the HP1 (power step) with the thermal con- ductance uncertainty of 14%	101
6.6 Thermal performance for the HP3 (cycle 1) with the thermal conductance uncertainty of 11%	102
6.7 Thermal performance for the HP4 (cycle 2) with the thermal conductance uncertainty of 15%	107
6.8 Thermal performance for the HP4 (cycle 1) with the thermal conductance uncertainty of 19%	110
6.9 Thermal performance for the HP4 (cycle 1) with the thermal conductance uncertainty of 14%	112
6.10 Thermal performance for the HP6 (cycle 1) with the thermal conductance uncertainty of 19%	114
6.11 Boundary conditions	118
6.12 Geometric characteristics of the heat pipe (panel)	122
6.13 Geometric characteristics of the heat pipe (panel/radiator)	126
7.1 Boundary Conditions	132
7.2 Comparison between experimental and numerical results for different heat inputs - HP2	137
7.3 Comparison between experimental and numerical results for different heat inputs - HP4	137

Nomenclature

A	Pre-exponential factor, s^{-1}
$AHPE$	Ames Heat Pipe Experiment
CPL	Capillary Pump Loop Pipe
HP	Heat Pipe
LHP	Loop Heat Pipe
N_l	Liquid Figure of Merit
NCG	Non-Condensable Gas
PAC	Petroleum Asphalt Cement
PCB	Printed Circuit Board
PHP	Pulsating Heat Pipe
OBP	Onboard Processor
OHP	Oscillating Heat Pipe
$VCHP$	Variable Conductance Heat Pipe
A	Area, m^2
C	Constant
C_p	Specific heat at constant pressure, J/kgK
C_v	Specific heat at constant volume, J/kgK
d	Diameter, m
E	Energy, J
E_{act}	Activation energy, J/mol
f	Friction factor
g	Gravitational acceleration, m/s^2
G	Thermal conductance, $W/^\circ C/$
h	Heat transfer coefficient, W/m^2K
k	Thermal conductivity, W/mK
I	Amperage, A
K	Wick permeability, m^2 or Rate of decomposition, s^{-1}
L	Length, m
\dot{m}	Mass flow rate, kg/s
M	Mach number
N	Screen mesh number, m^{-1}
N_1	Liquid figure of merit, W/m^2
N_u	Nusselt number
P	Pressure, N/m^2
P_r	Prandtl number

Q	Heat transfer, W
r	Radius, m
r_c	Effective capillary radius, m
$r_{h,v}$	Hydraulic radius for vapour flow, m
R	Radius of curvature, m or Thermal resistance, $^{\circ}C/W$ or Universal gas constant
Ra	Rayleigh number
Re	Reynolds number
S	Surface area or Crimping factor, m^2
T	Temperature, $^{\circ}C$
u	Axial component of velocity, m/s
v	Radial component of velocity, m/s
V	Voltage, V
x	Axial position, coordinate, m
y	Position coordinate, m
W	Screen mesh pore width, m
We	Weber number

Greek Symbols

λ	Latent heat vaporization, J/Kg
μ	Viscosity coefficient, Ns/m^2
ν	Kinematic viscosity, m^2/s
ρ	Density, kg/m^3
γ	Ratio of specific heats
ϵ	Wick porosity
σ	Surface Tension Coefficient N/m
θ	Contact angle
ω	Wire spacing, m
ψ	Heat pipe inclination measured from horizontal position
α	Coefficient for global thermal conductance or Thermal diffusivity, m^2/s
β	Volumetric thermal expansion coefficient, $^{\circ}C^{-1}$

Subscripts and superscripts

a	Refers to adiabatic section
b	Refers to boiling
c	Refers to capillary, capillary limitation, condenser

<i>C</i>	Refers to calculated
<i>e</i>	Refers to entrainment, evaporator
<i>E</i>	Refers to experimental
<i>eff</i>	Refers to effective
<i>h</i>	Refers to hydraulic
<i>i</i>	Refers to inner
<i>l</i>	Refers to liquid
<i>max</i>	Refers to maximum
<i>n</i>	Refers to nucleation
<i>p</i>	Refers to pipe
<i>s</i>	Refers to solid
<i>sat</i>	Refers to saturation temperature
<i>T</i>	Refers to total
<i>v</i>	Refers to vapour
ω	Refers to wick
	Refers to axial hydrostatic pressure
+	Refers to normal hydrostatic pressure

CONTENTS

	<u>Pág.</u>
1 INTRODUCTION	1
1.1 Historical Development	1
1.2 Applications of the Heat Pipe	3
1.3 Types of Heat Pipes	7
1.3.1 Micro/Miniature Heat Pipes	8
1.3.2 Variable Conductance Heat Pipes	11
1.3.3 Loop Heat Pipe	13
1.3.4 Pulsating Heat Pipe	16
2 OBJECTIVES	21
3 HEAT PIPE	23
3.1 Principles of Operation	23
3.2 Components, Design and Materials: Manufacturing Considerations	25
3.2.1 The Working Fluid	28
3.2.2 Wick Structures	32
3.2.3 Wick material and form	35
3.2.3.1 Wire mesh	35
3.2.3.2 Sintering	36
3.2.3.3 Grooves	37
3.2.4 The Container	38
3.2.5 Cleaning of container and wick	40
4 HEAT TRANSFER AND FLUID FLOW THEORY	41
4.1 Introduction	41
4.2 Surface tension and capillarity	41
4.3 Liquid pressure drop	47
4.4 Effective thermal conductivity of wick structures	49
4.5 Vapour pressure drop	49
4.6 Normal hydrostatic pressure	51
4.7 Axial hydrostatic pressure	52
4.8 Operating limits	52
4.8.1 Capillary limitation on heat transport capability	54

4.8.2	Viscous limitation	56
4.8.3	Sonic limitation	57
4.8.4	Entrainment limitation	61
4.8.5	Boiling limitation	62
4.9	Heat pipe thermal resistance	63
4.10	Uncertainties Analysis	67
5	EXPERIMENTAL PROGRAM	69
5.1	Introduction	69
5.2	Heat pipe design	69
5.3	Limits for the heat pipes	72
5.4	Experimental Procedure	77
5.4.1	Materials Selection	78
5.4.2	Cleaning and Fabrication Procedures	79
5.4.3	Test Apparatus and Instrumentation	80
5.4.4	Aging Process	82
5.4.5	Test Sequence for the Heat Pipes	86
6	EXPERIMENTAL RESULTS AND DISCUSSION	89
6.1	Stainless Steel Heat Pipes - 0° of inclination	89
6.1.1	The effects of input heat	89
6.2	Stainless Steel Heat Pipes - 30° of inclination	94
6.2.1	The effects of input heat	94
6.3	Stainless Steel Heat Pipes - 60° of inclination	98
6.3.1	The effects of input heat	98
6.4	Stainless Steel Heat Pipes - 90° of inclination	101
6.4.1	The effects of input heat	101
6.5	Copper Heat Pipes - 0° of inclination	104
6.5.1	The effects of input heat	104
6.6	Copper Heat Pipes - 30° of inclination	107
6.6.1	The effects of input heat	107
6.7	Copper Heat Pipes - 60° of inclination	110
6.7.1	The effects of input heat	110
6.8	Copper Heat Pipes - 90° of inclination	113
6.8.1	The effects of input heat	113
6.9	The effects of inclination angle on the heat pipe performance	115
6.10	Application of screen mesh wick heat pipes operating in mid-level temperature	117

6.11 Application of heat pipes for thermal control of electronic equipment in a honeycomb panel	120
6.11.1 Heat pipe for honeycomb panel	121
6.11.2 Capillary Pressure/Pressure Drops and Operating Limits	123
6.11.3 Heat pipes for connecting the honeycomb panel to the radiator	124
7 NUMERICAL MODEL	129
7.1 Governing Equations	129
7.1.1 Vapour Flow Region	129
7.1.2 Liquid Flow Region	130
7.2 Boundary Conditions	130
7.3 Method of Solution	132
7.4 Numerical Results	133
8 CONCLUSIONS	141
REFERENCES	145

1 INTRODUCTION

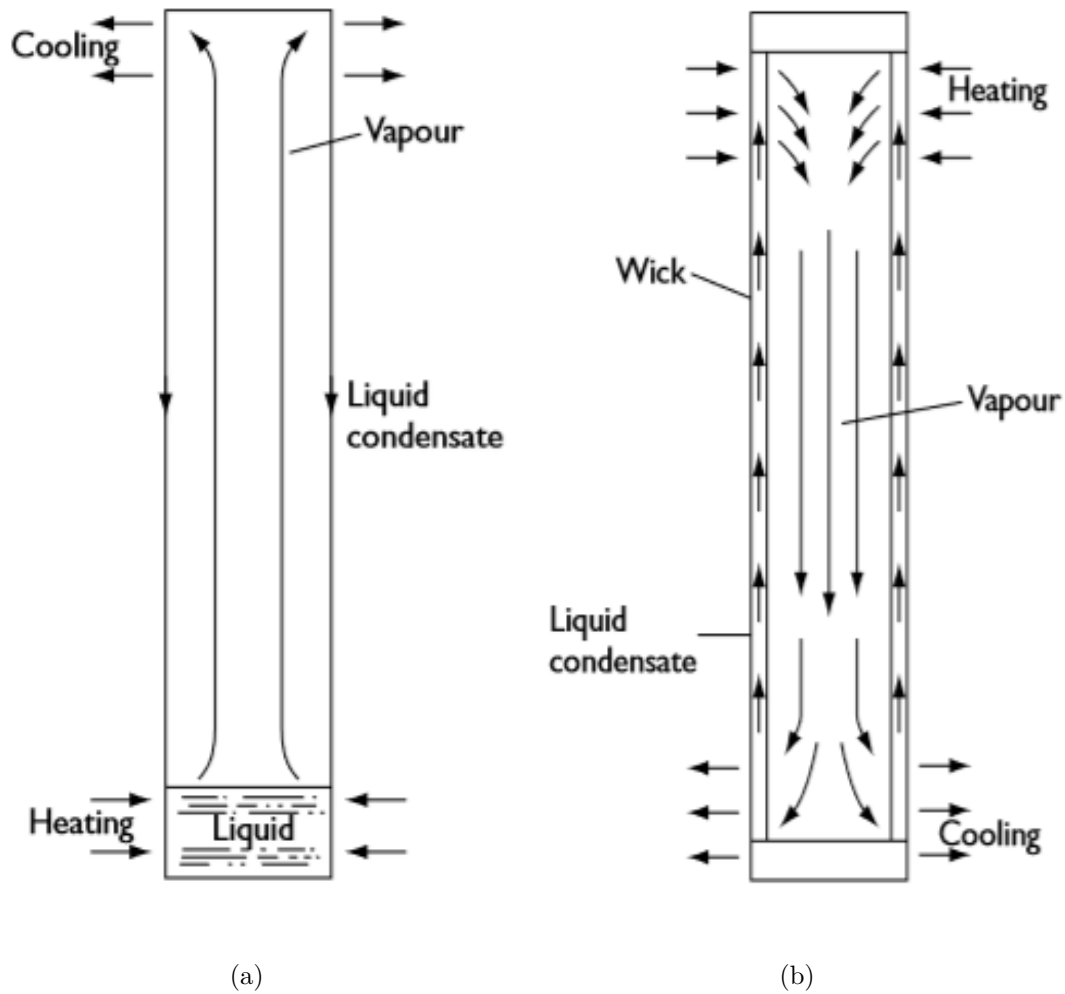
1.1 Historical Development

The concept of passive two-phase heat transfer device capable of transferring large quantities of heat with a minimal temperature drop was first introduced by Gaugler in 1942 (PETERSON, 1994). Gaugler, who was working on refrigeration problems at that time, envisioned a device that would evaporate a liquid from a place and would condensate it at a higher elevation place, without requiring any additional work to move the liquid. The device consists of a closed tube in which the liquid absorbs heat at one location causing the liquid to evaporate. The vapor then travels down the length of the tube, where it releases its latent heat and condenses. It then travels back up the tube due to capillarity pressure to start the process again (FAGHRI, 1995). The independent invention by Grover in the early 1960s showed the remarkable properties of the heat pipes and became appreciated when development work took place (KEW; REAY, 2006). The heat pipe concept received relatively little attention, until Grover et al (GROVER et al., 1964) published the results of an independent investigation and first applied the term heat pipe. It was used to describe a "synergistic engineering structure, which is equivalent to a material having a thermal conductivity greatly exceeding that of any known metal" (PETERSON, 1994).

The "Grover Heat Pipe" is a device that exhibits a thermal conductance greatly in excess of what could be obtained by the use of an homogeneous piece of any known metal. This property is achieved within the containing envelope by the evaporation of a liquid, transport of the vapor to another part of the container, condensation of the vapor and returning of the condensate liquid to the evaporator through a wick of suitable capillary structure. The first heat pipe used water as working fluid and was soon followed by a sodium heat pipe which operated at 1100 K (FAGHRI, 1995).

Heat pipes are similar in some respect with the thermosyphon and it is helpful to describe its operation. In the thermosyphon Fig. 1.1(a) a small quantity of water is placed in a tube from which the air is then evacuated and the container sealed. The lower end of the container is heated causing the liquid to evaporate and the vapor to move to the cold end of the container, where it is condensed. The condensed liquid is returned to the hot end by gravity. Since the latent heat of evaporation is large, considerable quantities of heat can be transported with a very small temperature difference from one end to another. Thus, the thermosyphon will also have a high effective thermal conductance. One limitation of the basic thermosyphon is that, in order to the condensed liquid to be returned to the evaporator region by gravitational

Figure 1.1 - (a) Thermosyphon, (b) Heat Pipe.



Source: Kew e Reay (2006)

force, the latter must be situated at the lowest end of the device. The basic heat pipe differs from the thermosyphon by the fact that a porous structure (wick) is fixed to the inside surface of the container. This wick is responsible for the generation of capillary forces used to return the condensed liquid to the evaporator Fig. 1.1(b). In the heat pipe, the evaporator position is not restricted and it may be used at any orientation, considering that the total pressure drop shall be lower than the maximum capillary pressure generated by the porous structure (KEW; REAY, 2006).

From the many different types of systems which transport heat, the heat pipe is one of the most efficient systems known today. The advantage of using a heat pipe over other conventional methods is that large quantities of heat can be transported through a small end-to-end temperature drop, and the ability to control and trans-

port high heat rates at various temperature levels are unique features of heat pipe (FAGHRI, 1995).

The material selection and compatibility between the porous structure, container and working fluid are major factors to be considered upon designing heat pipes. Besides the proper material compatibility, there are other factors that may be of great importance and may indeed influence the heat pipe design, such as weight, operation temperature, fabrication and material costs (CHI, 1976). A lot of research material has been generated on heat pipes during the last 30 years and several different designs, such as axially grooved, arterial and even pulsating heat pipes have been applied to many projects. However, there are always new and challenging applications for heat pipes where adjustments on their designs need to be made, in order to meet the thermal management requirements.

Heat pipes are typically made using copper due to their inherent high thermal conductivity. To manufacture lighter heat pipes without compromising thermal conductivity, alloys of aluminium, titanium and magnesium have been used but they are susceptible to corrosion (YANG et al., 2012). These alloys must be corrosion protected, otherwise non-condensable gas generated as a result of the corrosion will jeopardise the performance of the heat pipes. Using lighter wick materials could also be an option, but most progress has been made by improving the mass transfer performance of the wick rather than making it lighter. Alternatively, miniaturisation of the heat pipe can also be an option (CHAN et al., 2015).

The early development of terrestrial applications of heat pipes proceeded at a slow pace. Since heat pipes can operate in microgravitational fields due to capillary action without any external force field or pump, most early efforts were directed toward space applications. However, due to the high cost of energy, especially in Japan and Europe, the industrial community began to appreciate the significance of heat pipes and thermosyphons in energy saving design improvements in various applications. Today, all developed countries have been involved in research, development, and commercialization of heat pipes (FAGHRI, 1995)

1.2 Applications of the Heat Pipe

One of the most important subjects ultimately under global discussions have been the energy efficiency and energy optimization or even the proper energy management, therefore thermal energy efficiency augmentation also has been of great interest lately. Indeed the discussions for the augmentation of efficiency in thermal

systems has meaningfully increased not only within the aerospace industry but also within the industry in a general manner (SILVA et al., 2015)

Heat pipe have been applied in many ways since their introduction em 1964. The late 90's has seen mass production of heat pipes on a scale not provided before, millions of units per month being fabricated for thermal management (generally cooling) of processors in desktop and notebook computers. The position of heat pipes in spacecraft has been challenged by developments in lightweight mechanical pumps (for fluid pumping) and by some thermal storage technologies (KEW; REAY, 2006).

Liquid metal heat pipes have been widely used in energetics for cooling nuclear and isotope reactors, for building thermionic and thermoelectric generators, and for heat recovery in gasification plants. Moderate-temperature heat pipes have been used in electronics to cool such items as generator tubes, travelling wave tubes, and instrument packages while in energetics they have been used to cool shafts, turbine blades, generators motors, and transformers. In heat recovery they have been applied to collect heat from exhaust gases, solar energy, and geothermal energy. And, finally, in spacecraft they have served to control the temperature of vehicles, instruments, and space suits. The cryogenic heat pipes have been used in communication for cooling infrared sensors, parametric amplifiers and laser systems (FAGHRI, 1995). Due to their extremely high thermal conductivity, heat pipe can efficiently transport heat from a concentrated source to a remotely mounted sink. This property can enable dense packing of electronics, for example, without undue regard for heat sink space requirements. Another benefit of the high thermal conductivity is the ability to provide an accurate method of temperature equalization. For example, a heat pipe assembled between two opposing faces of an orbiting platform will enable both faces to maintain constant and equal temperatures, thus minimizing thermal stresses (FAGHRI, 1995).

The first application of heat pipes in the space program was the thermal equilibration of satellite transponders. As satellites orbit the Earth, one side is exposed to the direct radiation of the sun while the opposite side is completely dark and exposed to the deep cold of outer space. This cause severe temperature gradients affecting thus the reliability and accuracy of the transponders. The heat pipe cooling system designed for the purpose managed the high heat fluxes and demonstrated flawless operation with or without the gravitational influence. The cooling system developed was the first used of variable conductance heat pipes (VCHP) to actively regulate

heat flow or evaporator temperature (SHUKLA, 2015).

The variable conductance heat pipes offers temperature control within narrow limits, in addition to the simple heat transport function performed by basic heat pipes. Kirkpatrick e Marcus (1971) studied the VCHP concept for electronics temperatures control. They designed and manufactured a variable conductance heat pipe, referred to as the Ames Heat Pipe Experiment (AHPE), in which the heat pipe provided temperature stability for an onboard processor (OBP), by maintaining the OBP plataform/AHPE interface at $17 \pm 3^\circ\text{C}$. Power dissipation from the electronics processor varied between 10 and 30 W (KEW; REAY, 2006).

Heat pipes, certainly at vapour temperatures up to 200°C , have probably gained more from the developments associated with spacecraft applications (KEW; REAY, 2006) than from any other area due to their low weight penalty, zero maintenance and reliability. Maintaining isothermal structures is an important task with respect to orbiting astronomy experiments under the adverse solar heating. During orbit, an observatory is fixed on a single point such as a star. Therefore, one side of the spacecraft will be subjected to intense solar radiation, while the other is exposed to deep space. Heat pipes have been used to transport the heat from the side irradiated by the sun to the cold side in order to equalize the temperature of the structure. Heat pipes are also being used to dissipate heat generated by electronic components in satellites. Early experiments of heat pipes for aerospace applications were conducted in sounding rockets which provided six to eight minutes of zero-g conditions. In 1974, ten separate heat pipe experiments were flown in the International Heat Pipe Experiment. Also heat pipe experiments were conducted aboard the Applications Technology Satellite-6, in which an ammonia heat pipe with a spiral artery wick was used as a thermal diode. With the use of the space shuttle, flight testing of prototype heat pipe designs continued at a much larger scale. A 6-ft. mono groove heat pipe radiator with Freon 21 as the working fluid was flight tested on the eighth space shuttle flight. The Space Station Heat Pipe Advanced Radiator Element, consisting of a 50-ft. long high capacity mono groove heat pipe encased in a radiator panel, was flown on the space shuttle during 1989 and also, two heat pipe radiator panels were separately flight tested in a shuttle flight of 1991. Heat pipe thermal buses were proposed to facilitate a connection between heat-generating components and external radiator. The components may be designed with a clamping device which can be directly attached to the heat pipe thermal bus at various points in the spacecraft. In 1992, two different axially grooved oxygen heat pipes were tested in a Hitchhiker Canister experiment that was flown aboard the Shuttle Discovery

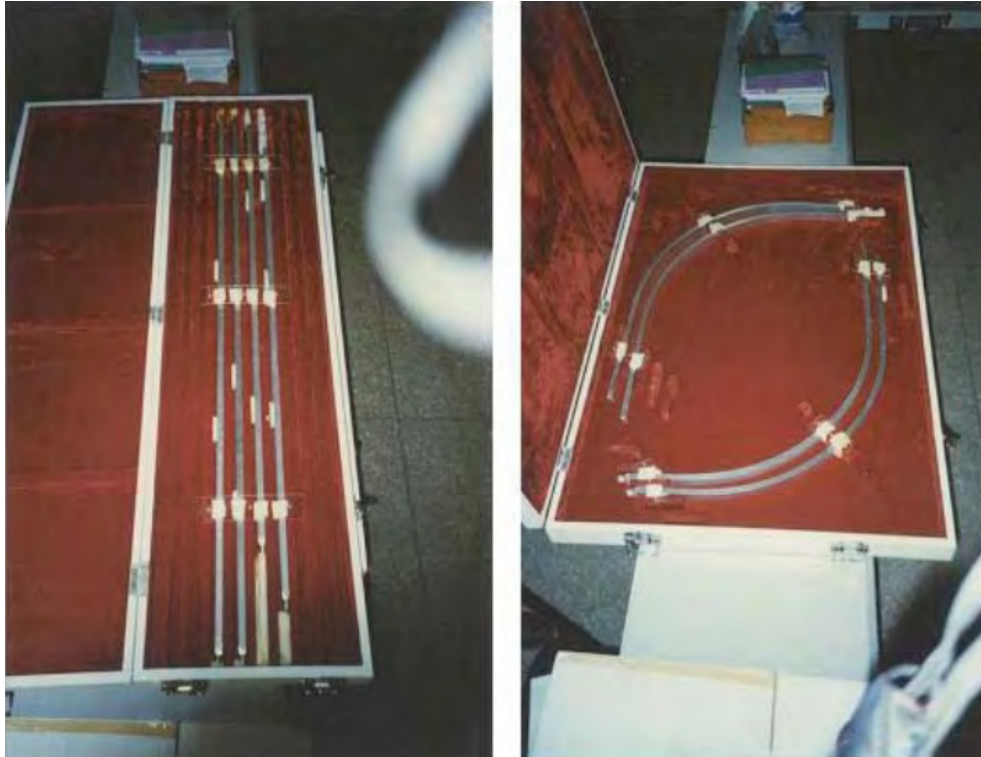
(STS-53) by NASA and the Air Force to determine startup behaviour and transport capabilities in micro gravity (FAGHRI, 1995).

Thermal control devices of passive action as heat pipe have been extensively applied in several space missions whether for low or geo-stationary orbit or instruments sent to other planets for scientific purposes (BIRUR et al., 2002). Good example of those missions have been observed in missions to Mars, such as Cassini-Huygens and Mars Rovers, as well as several satellites applications such as the CBERS (China-Brazil Earth Resources Satellite). Heat pipes, as for example in Fig. 1.2, were used in the thermal control of the CBERS and embedded in several honeycomb panels to control the temperature of several electronic instruments and cameras installed on it (VLASSOV et al., 2007). The use of heat pipes as thermal control device in space applications is well known and has proved their ability to manage the temperature of equipments within a tight range, as well as equalize the temperature of honeycomb panels in order to avoid thermal stress of structures (RIEHL; SANTOS, 2008; RIEHL; SANTOS, ; RIEHL, b).

They can easily be implemented as heat exchangers inside sorption and vapor-compression heat pumps, refrigerators and other types of heat transfer devices, to secure the energy saving and environmental protection (VASILIEV, 2005). Heat exchangers made of heat pipes are one of the most effective devices for heat recovery. The operation of a heat pipe involves phase changes (i.e., condensation and evaporation) and so large amounts of heat can be transferred between the ends of the tube. In practice, the thermal conductance of a heat pipe may be over 500 times than that the best available thermal conductors (LIU et al., 2006).

Heat pipes (HPs), pulsating heat pipes (PHPs), and loop heat pipes (LHPs) have been applied to many thermal management designs due to the fact that the new equipment is requiring more efficient ways to dissipate heat. Since those technologies have been successfully applied for space missions where the operational conditions are extremely severe, ground applications have found them very important devices to be considered for the heat dissipation issues faced by new projects (RIEHL; CACHUTÉ, 2013; RIEHL, 2015; RIEHL, 2016b; SILVA; RIEHL, 2014). Applications vary from satellites and spacecrafts to computer's cooling (KEW; REAY, 2006), but heat pipes have gained attention for other applications as well, especially those related to military and surveillance systems (SILVA; RIEHL, 2014). The continuous development of the heat pipe technology has given to this passive thermal control device a great interest for the new applications that were not considered before. It is well known that

Figure 1.2 - Heat Pipes used in Thermal Control of Satellites - CBERS



Source: Santos (2009).

heat pipes are reliable two-phase passive thermal control devices, and their applications have spread out over many fields, from aerospace to computer cooling as well as industrial sector. Special attention should be given to heat pipes that operate at mid-level temperatures (up to 200 °C), which have found several applications in both aerospace and industrial areas (SILVA; RIEHL, 2014). New applications are constantly being suggested for heat pipes which has called attention from many sensitive fields such as military and surveillance. This is especially important to consider because of the new developments of electronic systems devoted to military applications, regarding data and communication hardware. Previous investigations have addressed this issue, where the potential of applying heat pipes and also pulsating heat pipes have been demonstrated (RIEHL; CACHUTÉ, 2013; SILVA; RIEHL, 2014; RIEHL, 2016b)

1.3 Types of Heat Pipes

Heat pipes can be classified in several different ways: by operating temperature range (cryogenic, ambient, or liquid metal), by wicking structure (arterial or composite), or by function (rotating/revolving heat pipes, micro-heat pipes, variable conductance heat pipes, or thermal diodes) (COTTER, 1965). Heat pipes have been designed and

built with various cross-sectional areas as small as 0.6 mm x 0.6 mm and 25 mm in length. All heat pipes have an evaporator and condenser section where the working fluid evaporates and condenses respectively. Many heat pipes also have a transport or adiabatic section which separates the evaporator and condenser sections by an appropriate distance intended to satisfy the heat pipe limitations and the design constraints of the applications. A given heat pipe may have multiple evaporators, condensers and adiabatic sections. The working fluid is usually circulated by capillary forces in a wick. However, gravitational, centrifugal, electrostatic, and osmotic forces can also be used to return the liquid from the condenser to the evaporator (FAGHRI, 1995).

1.3.1 Micro/Miniature Heat Pipes

Thermal management is one of most critical technologies in electronic product development, and directly influences the cost, reliability, and performance of the considered product. As the number of circuits on a computer chips increases, it becomes more difficult to dissipate the heat which is generated. The limitations on the maximum chip temperature, there may be further requirements on the level of temperature uniformity. Because of the high heat flux and temperature uniformity consideration, it is necessary to develop new methods for distributing and removing heat from modern electronic devices (FAGHRI, 1995).

In 1984, Cotter first introduced the concept of very small "micro" heat pipes incorporated into semiconductor devices to promote more uniform temperature distributions and improve thermal control (COTTER, 1984). At that time a micro-heat pipe as one "so small that the mean curvature of the liquid-vapor interface is necessary comparable in magnitude to the reciprocal of the hydraulic radius of the total flow channel", significant additional work has been performed (PETERSON, 1992).

The initial applications proposed by Cotter (1984) involved the thermal control of semiconductor devices, a wide variety of other uses have been investigated or proposed. Since 1984, numerous analytical and experimental investigations of micro-heat pipes have been conducted (PETERSON, 1994). In order that the micro heat pipe finds more commercial applications in microelectronic cooling, it must compete with other cooling methods, such as forced convection, impingement and two phase direct cooling in areas such as manufacturing cost and reliability. Because of the extremely small dimensions of micro heat pipes, difficulties in manufacturing and the subsequent degassing and charging are expected. Furthermore, the "true" micro heat pipe built directly into the silicon must compete with the miniature heat pipe

attached on the chip surface in this area, which is much less viable (FAGHRI, 2014). It was found that the methanol is a better suited working fluid for the micro heat pipe with triangular cross section. The capillary limit calculated in Shukla (2009) was almost double the value obtained elsewhere (GERNER et al., 1992). There is an enormous interest in the satellite building programs by the universities. Several micro and nano satellites are built and launched for experimental purposes. The thermal management of these satellites have looked upon the micro heat pipes or micro loop heat pipes (SHUKLA, 2015).

Recently, designs for communication and surveillance devices have shown the application of heat pipes as a device to assist in the dissipation issues found in those equipments. In a specific application, which is an in-house development, miniature copper heat pipes have been designed to perform heat transport of up to 12 W using methanol as working fluid. A 200 screen mesh wick heat pipe was developed by Riehl (2016b). The main objective of these miniature heat pipes was to spread the heat generated over the heat dissipation area in order to enhance the process. Figure 1.3 presents the heat pipes designed for this application (RIEHL, 2016b; RIEHL, 2016a).

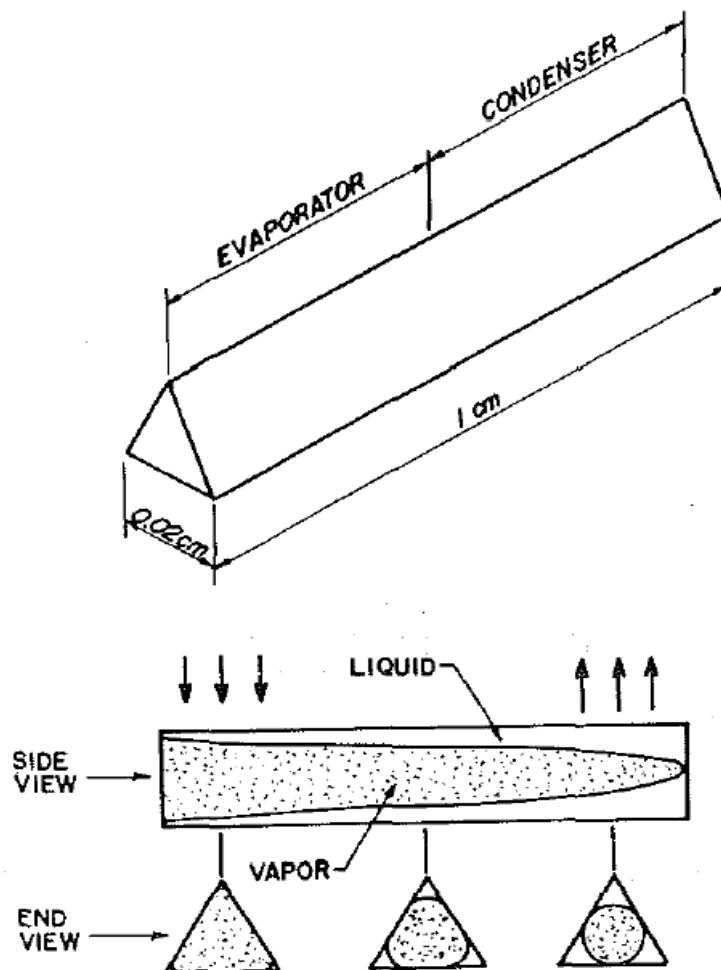
Figure 1.3 - Miniature heat pipe.



Source: Riehl (2016b).

The fundamental operating principles of micro heat pipes are essentially the same of those occurring in larger, more conventional heat pipes. Heat applied to one end of the heat pipe vaporizes the liquid in that region and forces it to move to the cooler end where it condenses and gives up the latent heat of vaporization. This vaporization and condensation process causes the liquid-vapor interface in the liquid arteries to change continually along the pipe, as illustrated in Fig. 1.4 and results in a capillary pressure difference between the evaporator and condenser sections. This capillary pressure difference promotes the flow of the working fluid from the condenser back to the evaporator through the triangular shaped corner regions. These corner regions serve as liquid arteries, thus no wicking structure is required (PETERSON, 1994). Since the initial conceptualization, numerous analytical and experimental investigation of micro-heat pipes have been conducted.

Figure 1.4 - Micro-heat pipe operation.



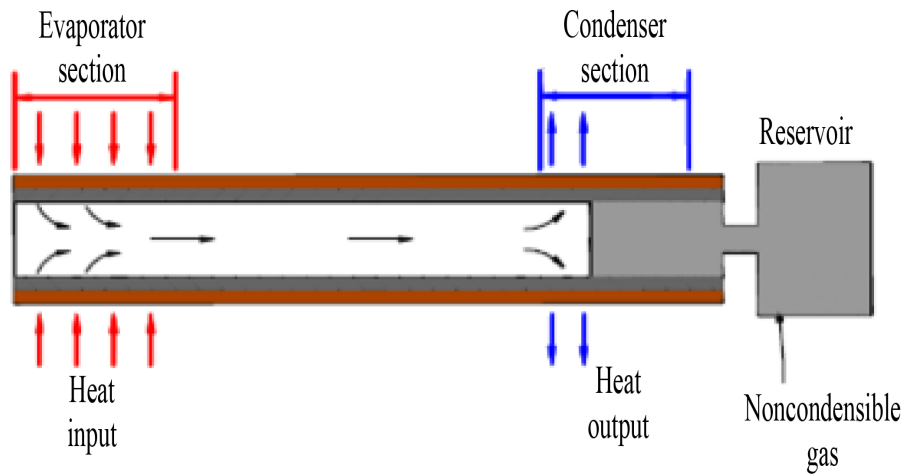
Source: Peterson (1992).

1.3.2 Variable Conductance Heat Pipes

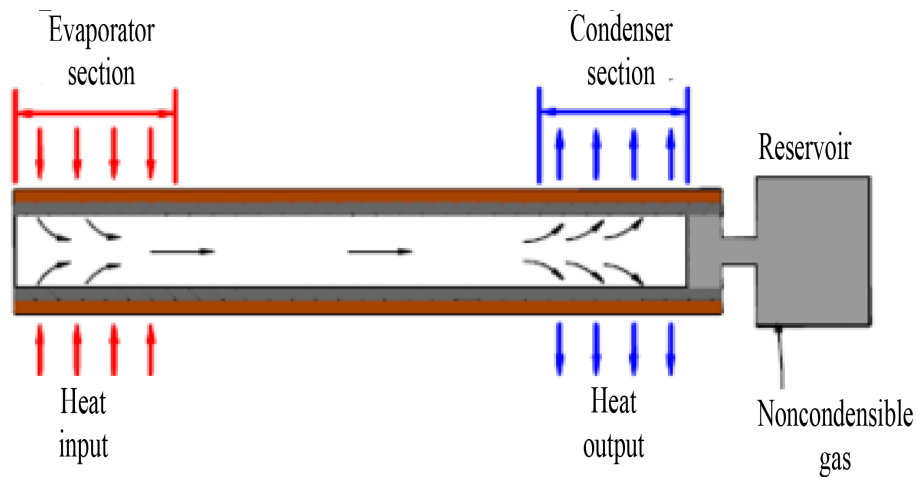
Variable Conductance Heat Pipes were discovered in the early 1960's, soon after the initial work by Los Alamos on the first heat pipes. At the time, there was no good method for sealing a refractory metal heat pipe, so a lower temperature valve was left on condenser end of the heat pipe. Non-Condensable Gas (NCG) was added to the heat pipe to protect it by providing a blanket of gas between the working fluid and the valve. VCHP, sometimes called in a specific variant the gas-controlled or gas-loaded heat pipe, has a unique feature that sets it apart from other types of heat pipe. A typical Variable Conductance Heat Pipe (VCHP) has an evaporator, a single condenser, and an electrically heated reservoir in the end of the condenser. This system is commonly used in spacecraft thermal control to provide $\pm 1\text{-}2^\circ\text{C}$ temperature control over widely varying powers and sink temperatures (ANDERSON et al., 2012). This is to maintain a device mounted at the evaporator at a near constant temperature, independent of the amount of power being generated by the device. A variable conductance heat pipe is able to maintain its own temperature nearly constant while heat input or ambient conditions are changed and are now routinely used in many applications. These applications range from thermal control of components and systems on satellites precise temperature calibration duties and conventional electronics temperature control (KEW; REAY, 2006).

The heat pipe conductance in a VCHP is reduced or blocked by the introduction of a certain amount of Non-Condensable Gas (NCG) in the condensing section of the heat pipe. VCHP controls the evaporator temperature change by altering the amount of condenser area available (Fig. 1.5(a)). Decreasing ambient temperatures reduces the vapor pressure of the working fluid and increases the volume of NCG, thus reducing the available condenser area. Because NCG is swept to the end of the condenser by the condensing working fluid vapor, it blocks a portion of the condenser, effectively lowering its conductance. If the ambient temperature increases, decreasing the available temperature difference between the condenser and the environment, the operating temperature of the heat pipe will increase. This causes the operating pressure to increase, compressing the NCG into a smaller volume. The result is that more of the condenser area is available for condensing working fluid (Fig. 1.5(b)). The level of control depends on the working fluid saturation curve, the desired operating temperature set point, the ranges of the ambient temperatures and the heat loads, and the volume of gas relative to the volume of the vapor space in the condenser (LERICHE et al., 2012).

Figure 1.5 - (a) Condenser partially active and (b) Condenser fully active.



(a)



(b)

Source: Shukla (2015).

Lerliche et al. (2012) investigated the use of VCHP with water as the working fluid and nitrogen as non-condensable gas in vehicle thermal management. They found that the performance of VCHP is a function of inclination angle and that the non-condensable gas reservoir connected to the VCHP, can control the delay in the VCHP start-up. In an air preheated for industrial boilers device, Shi et al. (2011) confirmed that the VCHP has excellent anti-corrosion and anti-ash-deposition performance due to the fact that VCHP can prevent corrosion and ash deposition on to heat exchangers caused by low temperatures. In process(or reaction)engineering, VCHP can also be effective in reactor temperature control but is yet to be fully exploited (CHAN et al., 2015).

1.3.3 Loop Heat Pipe

The history of development of loop heat pipes (LHPs) originates from 1972, when the first such device with a length of 1.2 m and a capacity of about 1 kW, with water as a working fluid, was created and tested successfully by the Russian scientists Gerasimov and Maydanik from the Ural Polytechnical Institute (GERASIMOV et al., 1974; GERASIMOV et al., 1975).

Loop heat pipes (LHPs) also referred to as capillary pump loop pipe (CPL) are basically composed of the following parts: a capillary evaporator, a compensation chamber (or a two-phase reservoir), vapor and liquid lines, and a condenser (RIEHL, 2016b). They are considered reliable two-phase thermal control devices and have been extensively investigated for application in Space conditions during the last years by many researchers, with the aim to use them in satellites and spacecrafts that have been already launched and their missions were accomplished (RIEHL; SANTOS, 2008; BIRUR et al., 2002; MAYDANIK, 2005). At present the main area of application of loop heat pipes is space technology. The first flight experiment in conditions of microgravitation was conducted in 1989 aboard the Russian spacecraft 'Gorizont' (MAYDANIK et al., 1992). Several other applications for LHPs are also interesting and have been already presented (MAYDANIK, 2005) and this technology has shown to be important for the future of satellites that require high heat transport capabilities and considerable advances on de-freezing methods of working fluid in Space radiators (RIEHL; SANTOS, 2008).

During the last years, the development of LHP technology has been performed and the entire technological cycle required to have a domain of the constraints related to these thermal control devices have been obtained. LHPs have been designed and fabricated according to their needs as thermal control devices operating in tight temperature ranges with reliable performances (RIEHL, a; RIEHL; SIQUEIRA, 2006; RIEHL; SANTOS, 2008; RIEHL; SANTOS,). A constant question always rise when preparing this device for a specific mission, which is related to the parameters for their previous acceptance and integration in satellites structures or instrumentation. In this case, proper testing and evaluation of LHPs operating during the acceptance procedure requires the identification of variables that need to be checked, which might lead to accept or reject the device for the purpose for which it was designed (RIEHL, b). LHPs are embedded in the honeycomb panels (TULIN et al., 2011) or directly attached to an electronic module dissipating heat that needs to be rejected by means of a space radiator or condenser (GONCHAROV, 2011). Due to the reliability

and the fine temperature control capability provided by LHPs, their applications have also gained a growing interest for terrestrial applications, especially for defense and military use (RIEHL, 2016b).

The LHPs are able to transport large amounts of heat over long distances. This is possible due to the fact that its capillary evaporator is able to generate substantial capillary pumping pressure to drive the working fluid from the heat source to the heat sink because of the small pore size present in its primary wick, which can overcome the loop's overall pressure drop, while controlling the heat source's temperature. Since its capillary evaporator is the most important component, the LHP can be designed to operate either with gravity assistance or under adverse condition as long as enough pumping pressure is generated. Usually, the capillary evaporator is built with the following components: housing, primary wick with fine pore sizes, secondary wick (usually made from screen mesh) that connects the evaporator liquid core to its compensation chamber, vapor and liquid seals, a bayonet to deliver the working fluid (most of the times with some degree of sub cooling) to the evaporator liquid core and, in some cases, a pressure control regulator that is used to set the LHP operation temperature (RIEHL, 2013; RIEHL, 2016b).

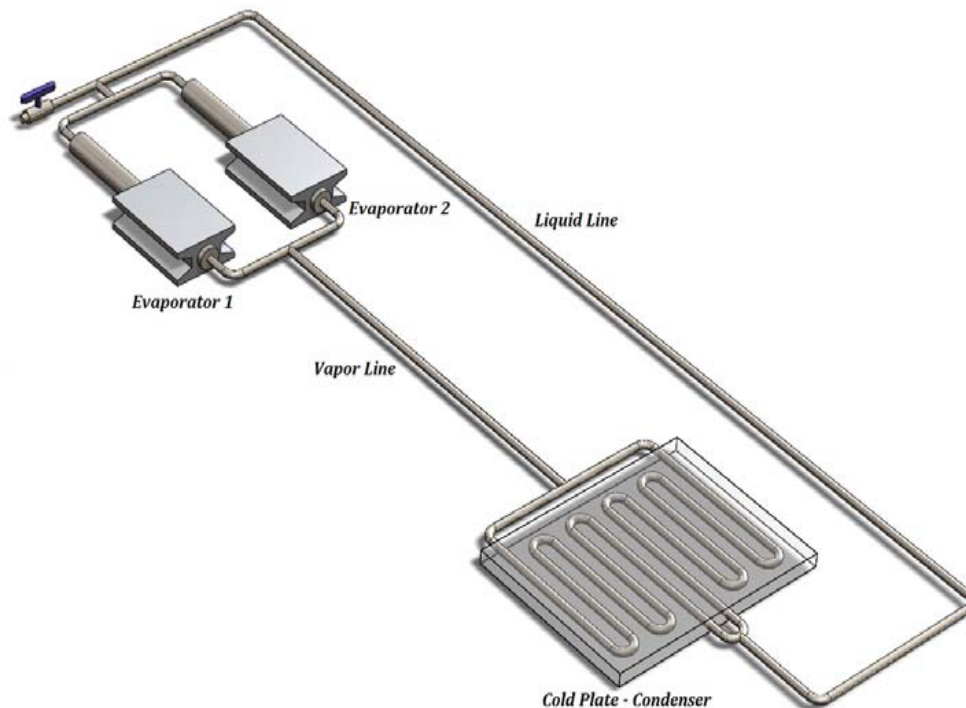
There are many types of evaporator design. Singh et al. (2008) found that the volume of the compensation chamber determines the thickness of the evaporator in an LHP with disk-shaped evaporator. An increase in the length of the transportation section (vapour line and the condenser) will increase the thickness (volume) of the compensation chamber. For rectangular and flat oval evaporators, the compensation chamber is usually situated along the evaporator. Both width or/and length of the compensation chamber can be altered to allow increased chamber volume when required (CHAN et al., 2015). Figure 1.6 is a representation when more than one heat source needs to be controlled by an LHP-based system. This is due to the difficulties associated with the availability of the multiple evaporator designs sharing the condenser and transport lines, which are called multiple evaporator LHP (RIEHL, 2016b).

A simple LHP is shown in Fig. 1.7. The operation of LHPs is based on the same physical processes as those used in conventional heat pipes. However, they are organized in a quite different way. First of all, it concerns the functions of the wick, which plays here a more complicated role (MAYDANIK, 2005). In a start-up, the liquid load is sufficient to fill the condenser, the liquid and vapour lines and there is sufficient liquid in the evaporator and compensation chamber to saturate the wick.

When a heat load is applied to the evaporator fluid it evaporates from the surface of the wick, and to a lesser extent in the compensation chamber, but as the wick has an appreciable thermal resistance the temperature and pressure within the compensation chamber is less than that in the evaporator. The capillary forces in the wick prevent the flow of the vapour from evaporator to compensate chamber increases, the liquid is displaced from the vapour line and the condenser, and returned to the compensation chamber (KEW; REAY, 2006).

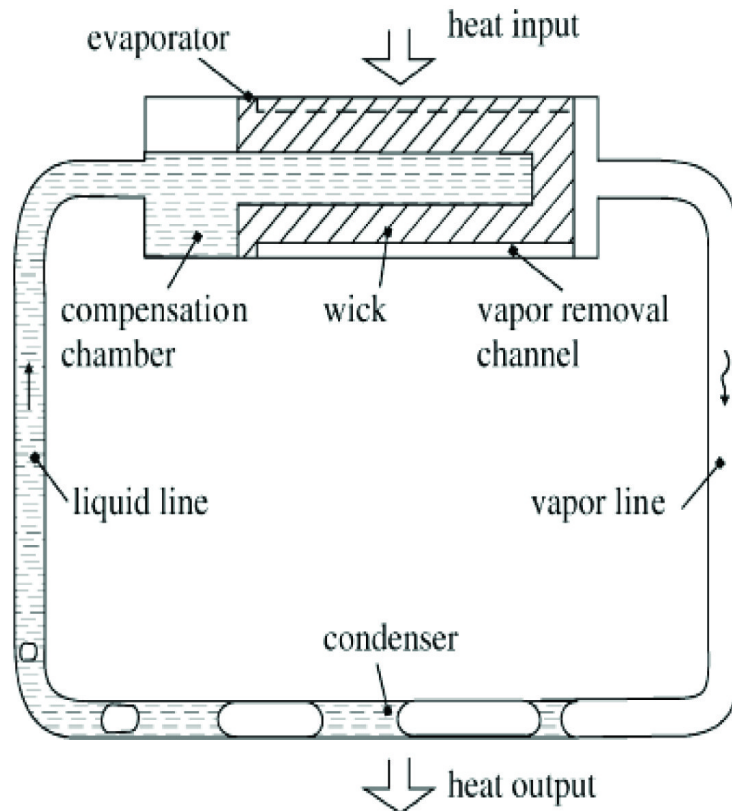
Many authors have reported the development of such LHPs with different configurations on the transport lines as well as in regard to their porous (wick) structure (RIEHL; SANTOS, 2008; RIEHL, 2013). Depending on the requirement, a pressure regulation valve can be installed on the LHP at its vapor line, which automatically controls the heat source temperature independent of the heat power applied to the evaporator (TORRES et al., 2010; RIEHL, 2013).

Figure 1.6 - Multiple evaporator LHP.



Source: Riehl (2013).

Figure 1.7 - Operating principle of loop heat pipe.

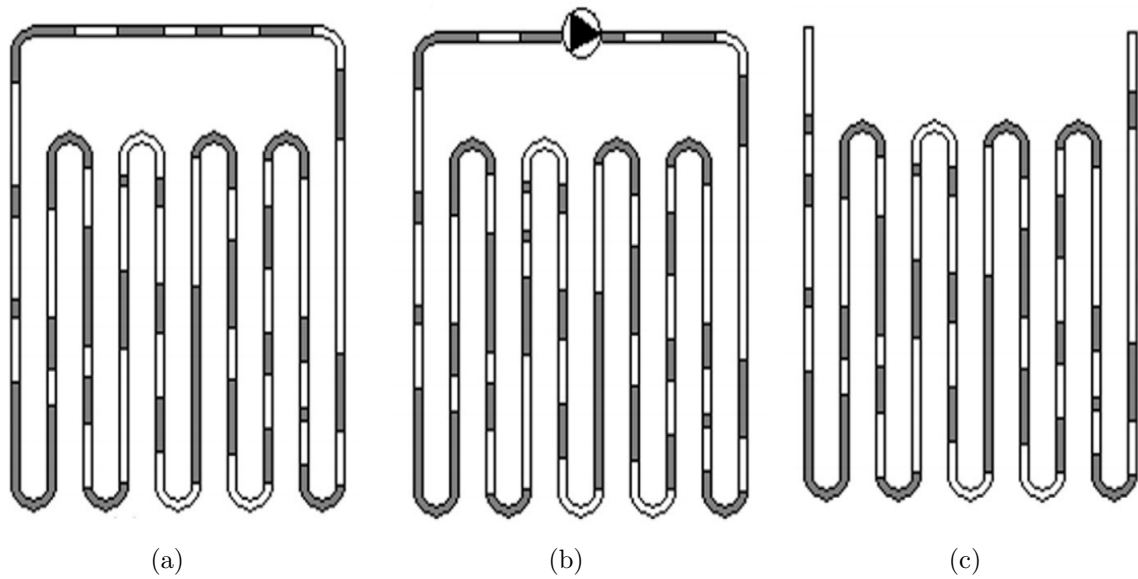


Source: Maydanik (2005).

1.3.4 Pulsating Heat Pipe

Pulsating (PHPs) or oscillating (OHPs) heat pipes comprise a tube of capillary diameter, evacuated and partially filled with the working fluid (KEW; REAY, 2006), which distributes itself naturally in the form of liquid-vapor plugs and slugs inside the capillary tube. It consists in a simple meandering tube bent with several curves forming several parallel channels, without the presence of a wick structure. The channels are formed from capillary tube and a working fluid is responsible for acquiring the heat from a source and dissipating it in a sink. This kind of device can be considered as a special type of heat pipe and was introduced by Akachi et al. (1996). When one end of the capillary tube is heated (the evaporator), the working fluid evaporates and increases the vapour pressure, causing the bubbles in the evaporator section to grow. This pushes the liquid towards the low-temperature end (the condenser). Cooling of the condenser results in a reduction of vapour pressure and condensation of bubbles in that section of the heat pipe. The growth and collapse

Figure 1.8 - Pulsating heat pipe configurations:(a) closed loop, (b) closed loop with check valve, (c) open loop.



Source: Chan et al. (2015).

of bubbles in the evaporator and condenser sections, respectively, results in an oscillating motion within the tube. Heat is transferred through latent heat in the vapour and through sensible heat transported by the liquid slugs (KEW; REAY, 2006).

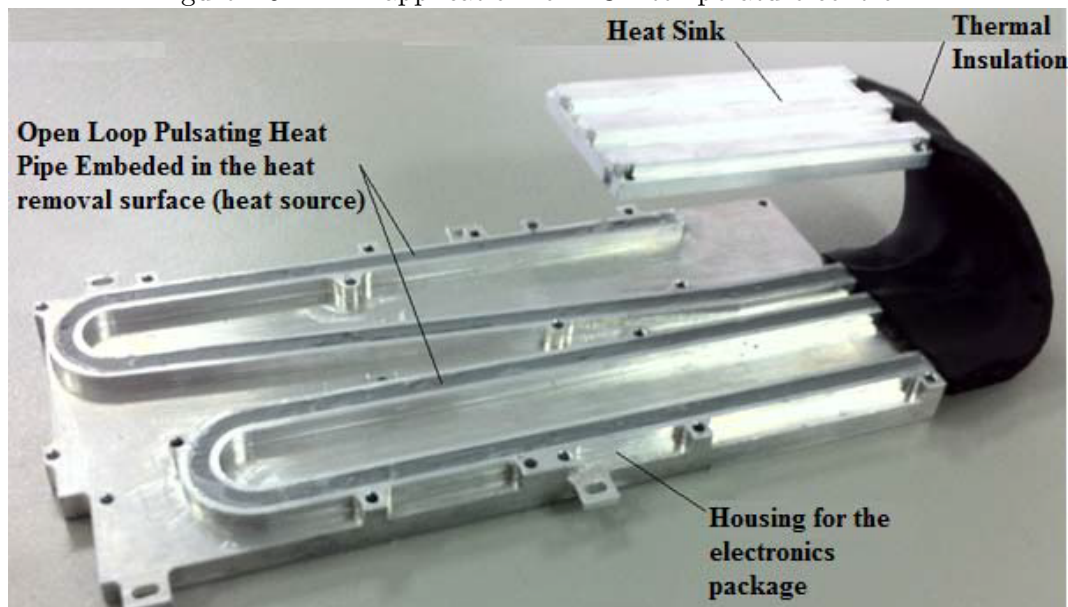
Pulsating heat pipes can present three configurations: closed loop, where the endings are connected (Fig. 1.8(a)); closed loop with a check valve, which is used to regulate the fluid flow and its direction (Fig. 1.8(b)); open loop, where the endings are not connected (Fig. 1.8(c)). For the first 2 configurations, there is circulation of the working fluid, and this can be regulated especially with the use of a check valve. Therefore, a closed loop device without a check valve is the most practicable implementation of the pulsating heat pipe (KEW; REAY, 2006; RIEHL, 2016b). In the last configuration, the dynamics involving the plug/slug movement is rather chaotic and difficult to simulate, but it presents reliable operation, and it is able to promote the thermal control once its design and manufacturing procedures are well controlled (RIEHL, 2016b).

PHPs can be applied in several thermal control problems, such as microelectronics cooling, but recently have gained interest in applications such as those for Space, Aeronautics and Surveillance systems used on the ground. As PHPs operate by means of slug/plug dynamics, several investigations have been performed in order

to improve their efficiency, also focusing on working fluids with the presence of solid nanoparticles, which can improve this dynamics as well as the thermal conductivity of the fluid. PHPs have been under investigation in the last years with great development regarding the phenomenon involved in their operation, but further investigations are still required (RIEHL; CACHUTÉ, 2013). Yang et al. (2008) present an experimental investigation of an open loop PHP, where the maximum heat transport capability was investigated, showing the great perspective of using PHP as a thermal control device. The first investigations regarding the operation of PHPs were important to guide future studies and applications, focusing on the use of this technology where a temperature difference greater than those observed on regular heat pipes, between the heat source and sink, was not an issue as this is a characteristic of this device (RIEHL, 2016b; RIEHL; CACHUTÉ, 2013)

Surveillance system has shown potential applications for PHPs due to their particular configuration on their PCBs and construction, as most of them are far away from possible heat sinks and the use of other passive thermal control system would result in the increase of costs. The Figure. 1.9 presents a configuration for a PHP applied for the thermal control of high density heat management PCB, which is able to control the electronic components.

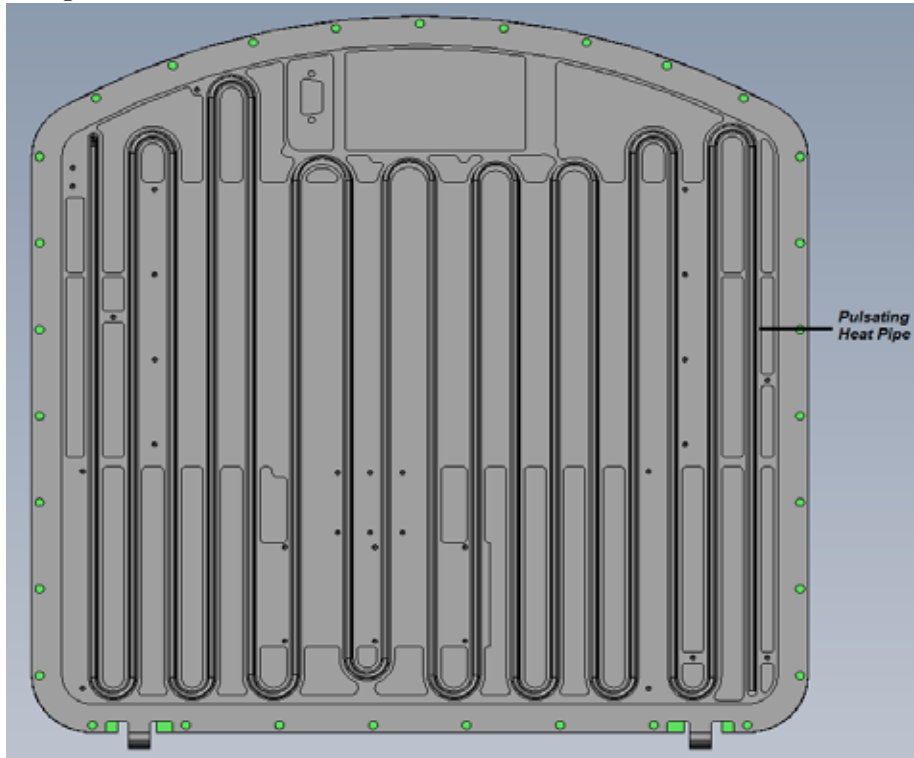
Figure 1.9 - PHP application for PCB temperature control.



Source: Riehl (2016b).

Another application for a surveillance system using the thermal control promoted by PHPs is presented in Fig. 1.10. In this case, a PHP was embedded in heat dissipation structure in order to collect the heat from several components located in the electronic setup and spread throughout the available area, in order to enhance the heat dissipation process (RIEHL, 2016b).

Figure 1.10 - Schematics of the PHP used for the thermal control.



Source: Riehl (2016b).

2 OBJECTIVES

This work aims to present a novel application of heat pipes for future aerospace and industrial applications, operating in temperature levels up to 200°C . This temperature level has many needs related to its control by using heat pipes, ranging from sensors to structures in satellites and spacecrafts, as well as heat recovery systems in industrial operation.

The main contribution of this work to this area is related to obtaining extensive experimental data related to heat pipes tests under different inclinations and heat loads applied to their evaporator, which greatly contributes to validate the proposed numerical simulation model as presented. With this model being validated, a powerful tool is obtained for new heat pipe designs and their application at both aerospace and industrial needs. From this base point, future developments can be expected for a wider temperature range by using other working fluids than those proposed in this work. The literature review about heat pipes presented before has helped in the construction of this work. Based on recent developments, the application for the heat pipes has shown maturity for implementation in several industrial and aerospace projects where mid-levels temperature are necessary.

Therefore, the main goal of this investigation was to analyze the thermal behaviour in the steady-state and transient regime for each power level when operated with the power step and power cycles in mid-level temperature. The calculated thermal conductances based on the thermal resistance analysis were used to be compared with the obtained experimental thermal conductances. An adjustment factor was calculated with the objective of being used in the results of the calculated thermal conductances, to bring them closer to the actual results that were obtained experimentally with the stainless steel heat pipes and copper heat pipes. Such an adjustment was necessary as this takes into account factors that are not considered during the design, which are inherent to the manufacturing of heat pipes. This background was necessary to develop this work, where the objectives are presented below:

- Design of stainless steel and copper heat pipes with metal mesh as a porous structure, considering compatibility between materials, permeability, porosity, operating limits and pressure losses, in order to guarantee heat pipes with a life time of approximately 15 years to be applied in several industrial and aerospace projects;

- Construct a test bench with three stainless steel container and wick tubes with mesh is of 100, 200 and 400 wires per inch and three copper heat pipes with mesh is of 100 and 200 (container and wick of copper) and 200 (copper container and stainless steel wick) wires per inch using water as working fluid and Conduct experimental tests with the power step and power cycles with applied powers of 25W, 50W, 75W, 100W and 125W and verify the temperature along the heat pipes in order to obtain temperature profiles in different inclinations;
- Analyze the thermal stability during the start-up, transient and steady-state regime and obtain the temperature difference between the evaporator and the condenser to verify drying tendency in the evaporator and the generation of non-condensable gases in the condenser;
- Obtain a calculated thermal conductance based on the thermal resistance analysis to be compared with the experimental thermal conductance. An adjustment factor will be calculated to be used in the results of the calculated thermal conductances to bring them closer to the actual results that were obtained experimentally with the heat pipes;
- Present applications of heat pipes operating at mid-level temperature for the industrial and space sector;
- Develop a numerical model and optimization of heat pipes, which can predict the temperature along the length of the heat pipe, this model should be used as a design tool for future land and aerospace applications.

3 HEAT PIPE

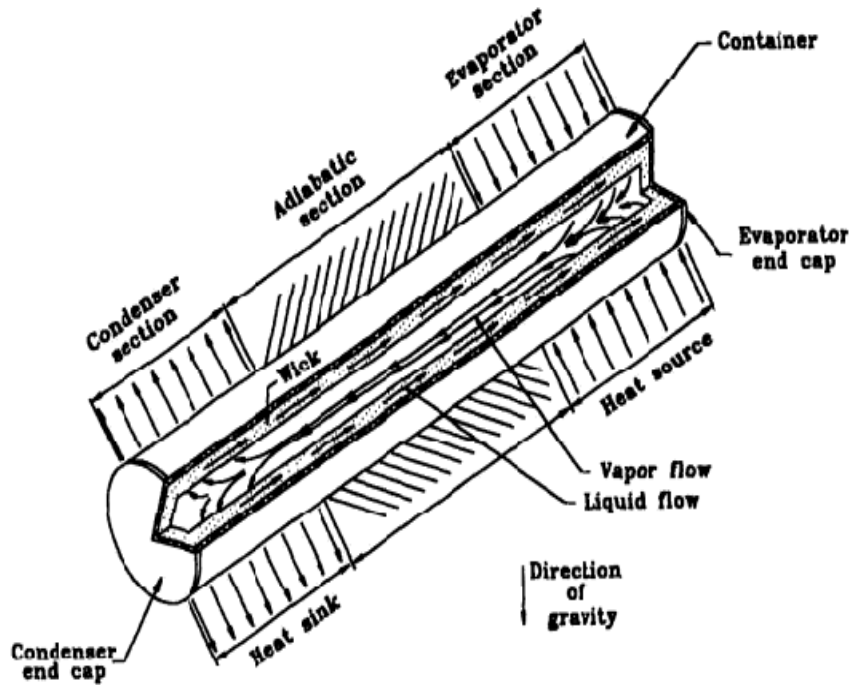
3.1 Principles of Operation

Capillary-driven two-phase systems offer significant advantages over traditional single-phase systems. With the typical increased thermal capacity associated with the phase change of a working fluid, considerably smaller mass flow rates are required to transport equivalent amounts of heat than in single-phase liquid or gas systems for a given temperature range. Moreover, heat transfer coefficients two-phase systems are much greater than of single-phase flows and result in enhanced heat transfer. Lower mass flow rates and enhanced thermal characteristics provide the benefits of smaller system size (and weight) while providing increased performance. The thermal capacity of a single-phase system depends on the temperature change of the working fluid; thus, a large temperature gradient or a high mass flow rate is required to transfer a large amount of heat. However, a two-phase system can provide essentially isothermal operation regardless of variations in the heat load (BEJAN; KRAUS, 2003).

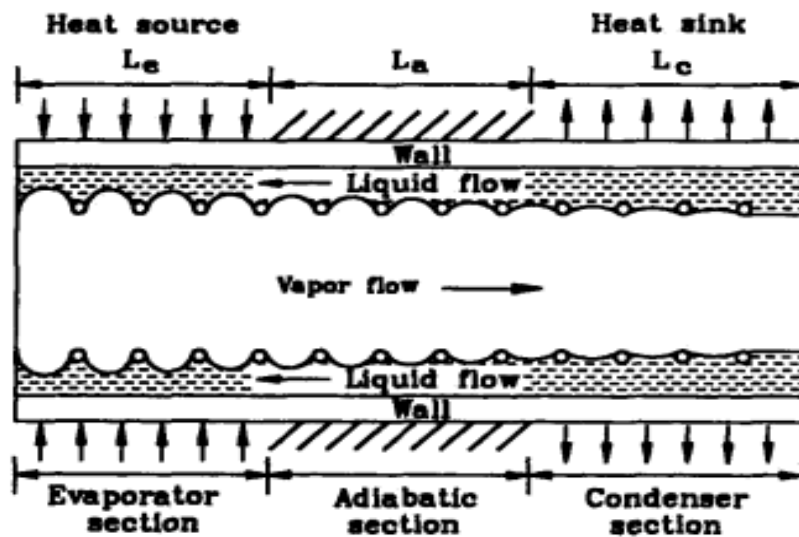
The operation of a heat pipe is easily understood by using a cylindrical geometry, as shown in Fig. 3.1(a) In its conventional form, the heat pipe is a closed tube with a wick structure, where a small amount of working fluid is inserted into the tube at its saturated condition. The length of the heat pipe is divided in three parts: evaporator, adiabatic, and condenser sections. The heat pipe may have multiple heat sources or sinks with or without adiabatic sections, depending on a specific application and design. Heat is applied to the evaporator section by an external source and then conducted through the tube wall and wick structure, where it evaporates the working fluid. The vapor then flows through the adiabatic section to the condenser where it is condensed, releasing its latent heat of vaporization to the provided heat sink (FAGHRI, 1995). Depletion of liquid by evaporation causes the liquid-vapor interface in the evaporator to enter into the wick surface and capillary pressure is developed there (Fig. 3.1(b)). The capillary pressure pumps the condensed liquid back to the evaporator, closing the cycle. The heat pipe can consequently transport the latent heat of vaporization from the evaporator section to the condenser without drying out the wick. This process will continue as long as the flow passage for the working fluid is not blocked and a sufficient capillary pressure is maintained (CHI, 1976).

Heat Pipes have been developed with working fluids ranging from cryogenic liquids to liquid metals. Accordingly, heat pipes can be categorized in cryogenic, moderate-temperature, and liquid-metal types. The most important differences among these

Figure 3.1 - (a) Components and principle of operation of a conventional heat pipe and
 (b) Development of capillary pressure at liquid-vapour interface.



(a)



(b)

Source: Faghri (1995).

three classes of heat pipes are their maximum heat transport capabilities. Temperature drops should be compatible with their designs and applications, giving the fact that the material and working fluid selection shall consider their useful operation temperature ranges (CHI, 1976).

As heat pipes work through capillary forces, then the wick structure becomes a very important component to be properly designed. Capillary pressures tend to be higher while pore sizes of wick structure get smaller. On the other hand, larger pores are preferred for the liquid movement within the wick structure to minimize the pressure drop. However, the wick characteristics regarding minimum pore size, porosity, permeability and effective thermal conductivity are not simple to be designed. Those factors indeed demand specific investigations depending on the application and will directly affect the heat pipe's capillary limit, boiling limit, entrainment limit, etc. For this reason, many different types of wick structures have been developed in order to optimize the performance into two categories: homogeneous and composite wicks. Homogeneous wicks have the benefit of being relatively simple to be designed, manufactured and installed. Composite wicks, however, can significantly increase the capillary pressure, but they have the drawback of high manufacturing costs.

Homogeneous wicks are constructed with one type of material or machining technique. The screen mesh wick is probably the most simple and common type of wick structure. It consists of a metal or cloth fabric that is wrapped around a mandrel and inserted into the heat pipe. After placing it in the heat pipe the mandrel is removed, leaving the wick held by the tension of the wrapped screen mesh in the case of a metal fabric. For a cloth fabric, a spring may be inserted into the heat pipe to hold the wick against inner wall of the tube (FAGHRI, 1995).

3.2 Components, Design and Materials: Manufacturing Considerations

Choice of components and materials used for heat pipes is an extremely complex process involving many different physical variable such as size, shape, weight, and volume; thermophysical properties such as working fluid, wicking structure, and material properties; and other design aspects, such as thermal load, transport length, evaporator/condenser length, acceptable temperature drop, operating temperature range, gravitational environment, source-sink interfaces, fluid inventory, life/reliability, and safety (PETERSON, 1994).

The design and manufacturing of heat pipes is governed by three operational considerations: the effective operating temperature range, which is determined by the

selection of the working fluid, the maximum power the heat pipe is capable of transporting, which is determined by the ultimate pumping capacity of the wick structure, and the maximum evaporator heat flux, which is determined by the point at which nucleate boiling occurs. As shown in the Fig. 3.2, all three of these operational considerations must be included, the design specifications for the problem under consideration be clearly identified (PETERSON, 1994).

The manufacture involves a number of comparatively simple operations, particularly when the units is designed for operation at temperatures of the order of 50-200 °C, which embraces skills such as welding, machining, chemical cleaning and nondestructive testing, and can be carried out following a relatively small outlay on capital equipment. The prime importance to ensure that no incompatibilities exist is the cleanliness, assuming that the materials selected for the wick, wall and working fluid are themselves compatible, and make certain that the wick and wall will be wet by the working fluid. As well as affecting the life of the heat pipe, negligence in assembly procedures can lead to inferior performance, due to poor wetting among other reasons. Atmospheric contaminants, in addition to those likely to be present in the raw working fluid, must be avoided (KEW; REAY, 2006).

The most difficult part of the design process is determining how the various components utilized in heat pipe construction affect the different design requirements. Indications of how each of the three primary components, the working fluid, wick material, and heat pipe case material, affect the various design requirements are presented in the Table 3.1. As shown, no single component appears to be more important than any other, and very few design requirements are affected by only one of these three components (PETERSON, 1994).

Compatibility and the results of life tests on heat pipe remain as one critical aspect of heat pipe design and manufacture. In particular, the generation of non-condensable gases that adversely affects the performance of heat pipes in either short-term or long-term. An aspect of heat pipes that has always been of interest is the compatibility of water with steel, because the superior properties of water and the low cost of some steels, together with their strength, make the combination of water-steel more attractive (KEW; REAY, 2006). Water is an ideal working fluid for heat pipes and it is compatible with a number of container materials, the most popular being copper. However, ever since heat pipes were first conceived, experimenters have experienced difficulty in operating a water/steel heat pipe without obtaining the generation of hydrogen in the container. This gas generation always manifests itself

Source: Adapted from Peterson (1994).

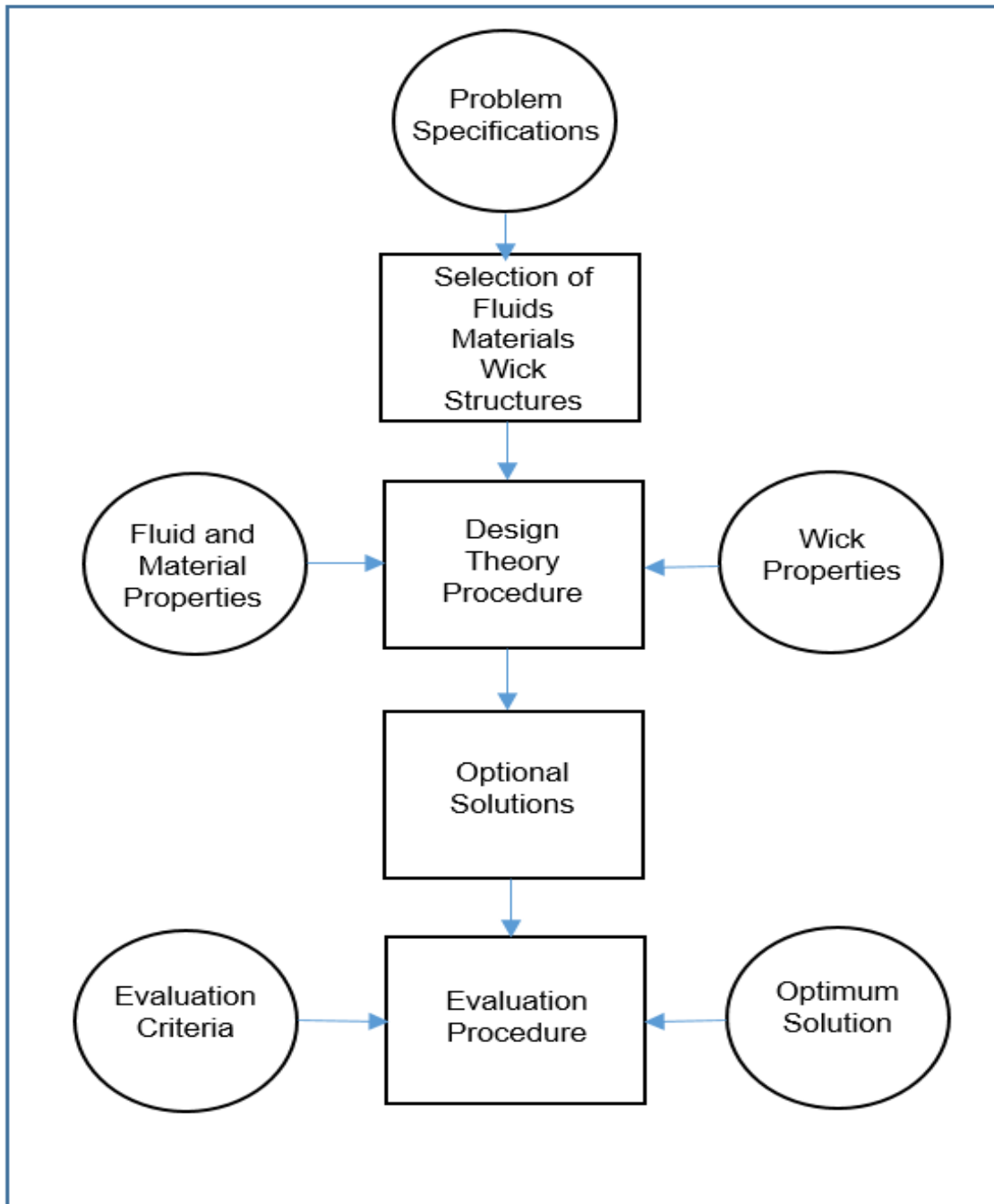


Figure 3.2 - Heat Pipe design flow chart.

as a cold plug of gas at the condenser section of the heat pipe, blocking off surface for heat rejection. There is a sharp defined interface between the water vapour and the non-condensable gas, making the presence readily identifiable (KEW; REAY, 2006).

Table 3.1 - Heat Pipe components and their influence on design requirements

Design Requirements	Working Fluid	Wick Material	Case Material
Thermal Performance			
Transport capacity	S	S	W
Operating temperature range	S	W	W
Temperature drop	M	W	W
Mechanical			
Physical requirements	W	W	M
Wall thickness-internal pressure	W	N	S
Sink-source interface	N	N	S
Dynamic/static loads	W	S	M
Reliability and Safety			
Material compatibility	S	S	S
External corrosion	N	N	
Fabrication	M	M	M
Pressure containment/leakage	W	M	S
Toxicity	S	W	W
Gravitational environment			
>1g	M	M	W
1g	W	M	W
<1g			

S, strong factor; M, moderate factor; W, weak factor; N, negligible

Source: Adapted from [Peterson \(1994\)](#).

3.2.1 The Working Fluid

Each heat pipe application has a particular temperature range in which the heat pipe needs to operate. Therefore, the design of the heat pipe must account for the intended temperature range by specifying the proper working fluid. A first consideration in the identification of suitable fluid is the operating vapour temperature range. Factors that affect the selection of an appropriate working fluid include the operating temperature range, the vapour pressure, the thermal conductivity, the compatibility with the wick and case materials, the stability, the toxicity, wettability of wick and case materials, the high surface tension, the low liquid, vapour viscosities, high latent heat and vapour pressures not too high or too low over the operating temperature range ([FAGHRI, 1995](#); [KEW](#); [REAY, 2006](#); [PETERSON, 1994](#)).

The selection of the working fluid must be based on thermodynamic considerations which are concerned with the various limitations to heat flow occurring within the heat pipe. Many of the problems associated with long-life heat pipe operation are a direct consequence of material incompatibility. Longevity of a heat pipe can be assured by selecting a case material, wick and welding materials that are compati-

ble with each other and with the working fluid of interest. One aspect peculiar to the working fluid, however, is the possibility of thermal degradation. With certain organic fluids, it is necessary to keep the film temperature below an specific value to prevent the fluid breaking down into different compounds. A good thermal stability is therefore a necessary feature of the working fluid over its likely operating temperature range. A compilation of the most up-to-date information concerning compatibility of metals with working fluid for heat pipes is given in Table 3.2 (FAGHRI, 1995; KEW; REAY, 2006).

Table 3.2 - Results of experimental compatibility tests

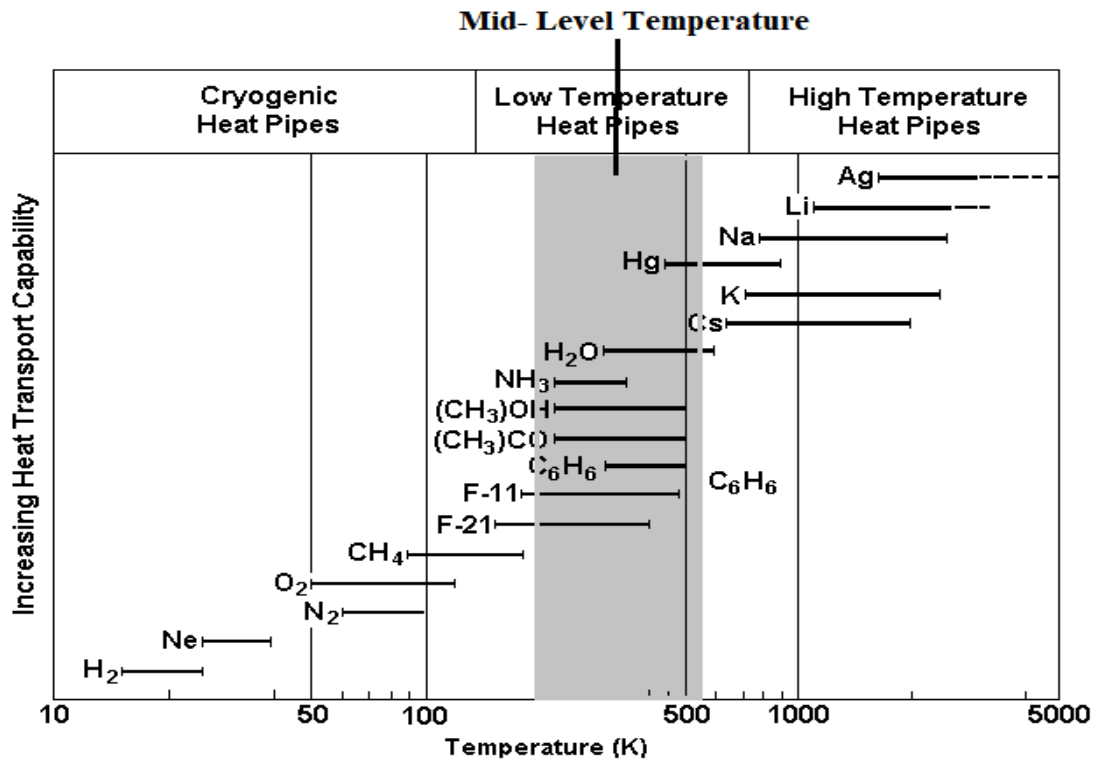
Working Fluid	Compatible Material	Incompatible Material
Water	Stainless steel, Copper, Silica, Nickel, Titanium	Aluminum, Inconel
Ammonia	Aluminium, Stainless steel, Cold rolled steel, Iron, Nickel	Copper
Methanol	Stainless steel, Iron, Copper, Brass, Silica, Nickel	Aluminum
Acetone	Aluminum, Stainless steel, Copper, Brass, Silica	
Freon-11	Aluminum	
Freon-21	Aluminum, Iron	
Freon-123	Aluminum	
Heptane	Aluminum	
Dowtherm	Stainless steel, Copper, Silica	
Lithium	Tungsten, Tantalum, Molybdenum, Niobium	Stainless steel, Nickel, Inconel, Titanium
Sodium	Stainless steel, Nickel, Inconel, Niobium	Titanium
Cesium	Titanium, Niobium	
Mercury	Stainless steel	Molybdenum, Nickel, Tantalum, Inconel, Titanium, Niobium
Lead	Tungsten, Tantalum	Stainless steel, Nickel, Inconel, Titanium, Niobium
Silver	Tungsten, Tantalum	Rhenium

Source: Adapted from Faghri (1995).

More important than the determination of the maximum operating temperature of a given working fluid is the determination of an acceptable operating temperature

range. The operating temperature range for various heat pipe working fluids as shown in the Fig. 3.3. As presented, three fairly distinct classification of working fluids have been identified: cryogenic fluids such as helium, neon, oxygen, or nitrogen; low to mid-level temperature working fluids, such as Freons, methanol, ammonia, or water; and high temperature or liquid metal working fluids, such as potassium, lithium, or sodium. Most heat pipe applications for electronic thermal control require the selection of the working fluid with boiling temperatures between 250 and 375 K. This would typically limit the selection to fluids such as ammonia, acetone, methanol and water or dielectric fluids such as Freon-11 or -113 (PETERSON, 1994).

Figure 3.3 - Operating temperature ranges of various working fluid.



Source: Peterson (1994).

Because the amount of heat transferred by a heat pipe depends on the latent heat of vaporization, the transfer of appreciable quantities of heat is possible, even for long distances. Axial heat flows of $10^8 W/m^2$ are easily reachable with sodium heat pipes. By calculating an effective thermal conductivity k_{eff} , values may reach $10^8 W/mK$ (sodium heat pipe), which is several orders of magnitude greater than the conduc-

tivity of the best conductors (IVANOVSKII et al., 1982). One of the most common applications of a heat pipe is the heat flux transformer. Using a heat pipe, high heat fluxes from a heat source can be injected over a small surface area, which is then rejected over a larger condenser surface area. Thermal flux transformation ratios greater than 10 : 1 can allow systems to employ final heat rejection with low cooling capability methods, such as natural convection or single-phase cooling (BEJAN; KRAUS, 2003)

For capillary wick limited heat pipes, which are the type most frequently found in electronic applications, the characteristics of a good working fluid are a high latent heat of vaporization, a high surface tension, a high liquid density and low liquid viscosity. Chi (1976) combined these properties into a parameter referred to as the liquid transport factor or Figure of Merit, which can be used to evaluate the effectiveness of various working fluids at specific operating temperatures. The figure of merit defined with N_1 illustrates for working fluids all the three of the operating temperature classifications described above (PETERSON, 1994).

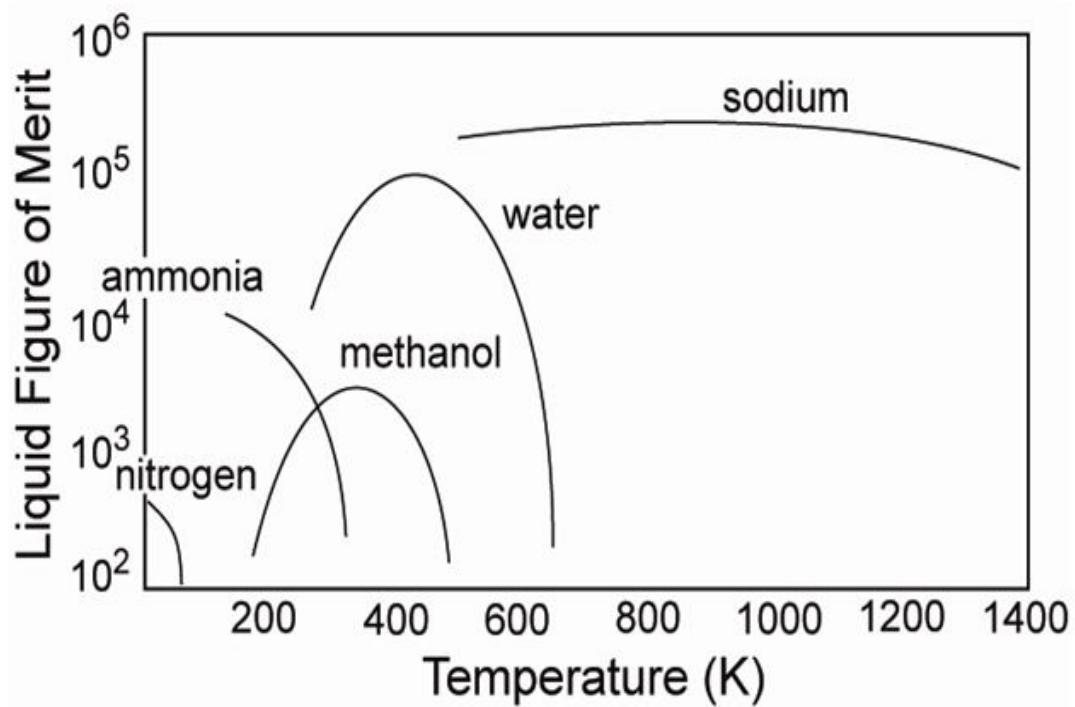
$$N_1 = \frac{\rho_l \lambda \sigma}{\mu_l} \quad (3.1)$$

Where ρ_l , λ , σ , μ_l are thermodynamics properties of the working fluid. As shown in the Fig. 3.4, sodium provides the highest liquid figure of merit over a wide range of temperatures but is typically inappropriate at temperature less than 500 K. In the low or mid-level temperature range, similar to that anticipated for use in electronic thermal control systems, water appears to have the highest figure of merit and for many applications may be the most suitable working fluid beyond excellent thermophysical properties such as heat of vaporization and surface tension, while also having the benefit of being safe and handle at minimum costs. Below the freezing point of water and above 200 K, ammonia is an excellent working fluid and is used widely in spacecraft and instrument control applications in the most near-room temperature (200-350 K) range. However, care should be taken to exposures to ammonia in the liquid and vapor states. The figure of merit or merit number defined in equation 3.1 can be utilized to evaluate the transport capacity of various fluid alternatives as a function of operating temperature (PETERSON, 1994).

One obvious feature is the superiority of water with its high latent heat vaporization and surface tension, compared with all organic fluids, such as acetone and

the alcohols. The final fluid selected is, of course, also based on cost, availability, compatibility and other factors (KEW; REAY, 2006).

Figure 3.4 - Figure of Merit for various working fluids.



Source: Peterson (1994).

3.2.2 Wick Structures

The wick structure has two functions in heat pipe operation: It is both the vehicle and the mechanism through which the working fluid returns from the condenser to the evaporator and it ensures that the working fluid is evenly distributed circumferentially over the entire evaporator surface (PETERSON, 1994). Often these two functions require wicks of different forms particularly where the condensate has to return a distance of, say, 1 m, in 0 gravity. Where a wick is retained in a "gravity-assisted" heat pipe, the role may be to enhance heat transfer and to circumferentially distribute liquid (KEW; REAY, 2006). While small pores are needed at the liquid vapor interface to develop high capillary pressures, large pores are preferred within the wick so that the movement of the liquid is not restricted too greatly. For this reason, many different types of wick structures (Fig. 3.5) have been developed in

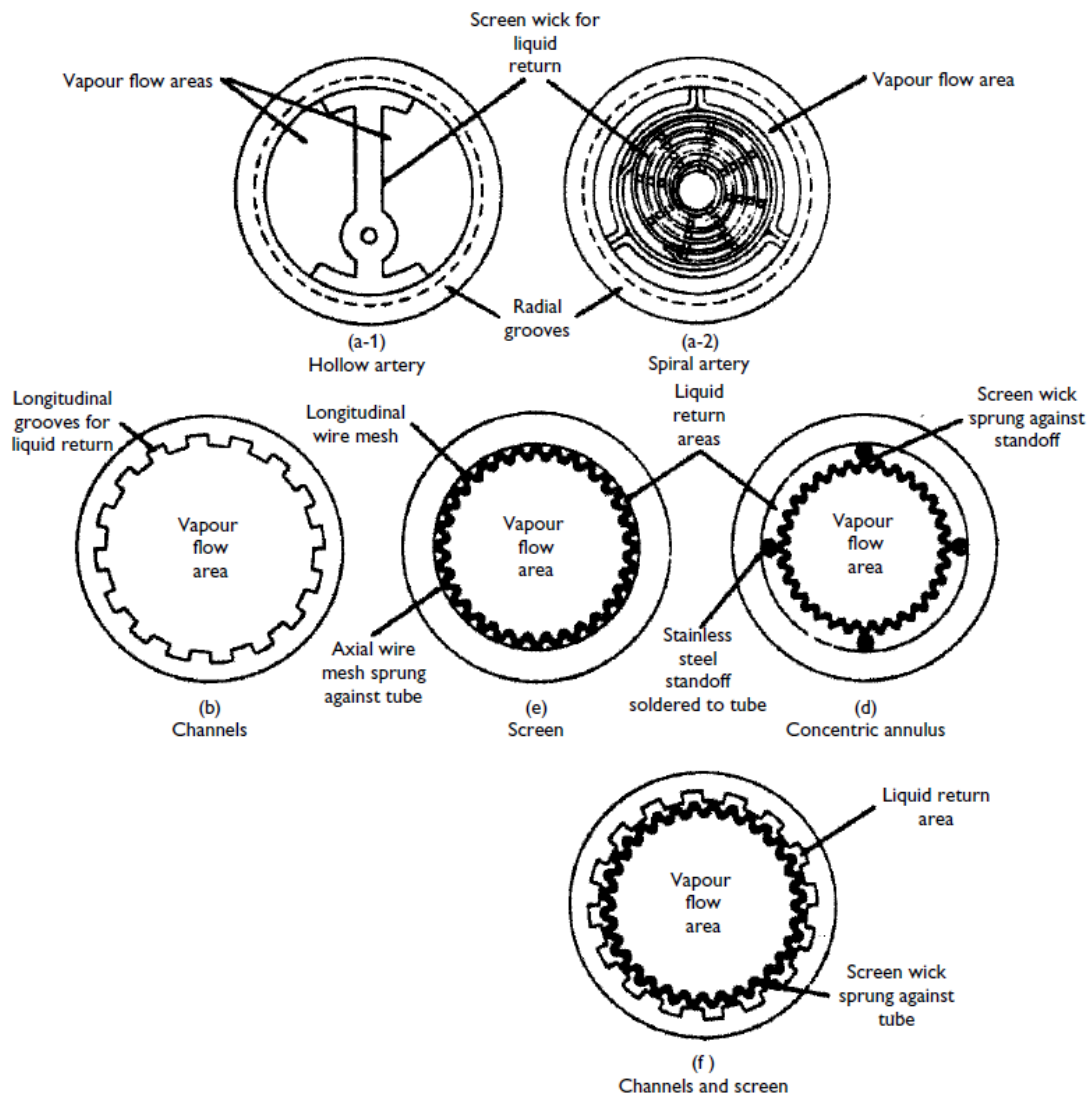
order to optimize the performance of the capillary heat pipe. The types of wick structures can be divided into two categories: homogeneous and composite wicks. Homogeneous wicks have the benefit of being relatively simple to design, manufacture and install. Composite wicks, however, can significantly increase the capillary limit of the heat pipe, but have the drawback of higher manufacturing costs. When selecting a wick structure for a particular application, one must keep in mind the benefits and drawbacks of each type of wick. There are three properties of wicks that are important in heat pipe design (FAGHRI, 2014; FAGHRI, 1995):

- Minimum capillary radius: This parameter should be small if a large capillary pressure difference is required, such as in terrestrial operation for a long heat pipe with the evaporator above the condenser, or in cases where a high heat transport capability is needed.
- Permeability: Permeability is a measure of the wick resistance to axial liquid flow. This parameter should be large in order to have a small liquid pressure drop, and therefore, higher heat transport capability.
- Effective thermal conductivity: A large value for this parameter gives a small temperature drop across the wick, which is a favorable condition in heat pipe design.

A high thermal conductivity and permeability, and a low minimum capillary radius are somewhat contradictory properties in most wick designs. For example, a homogeneous wick may have a small minimum capillary radius and a large effective thermal conductivity, but have a small permeability. Therefore, the designer must always make trade-offs between these competing factors to obtain an optimal wick design (FAGHRI, 2014; FAGHRI, 1995).

The maximum capillary pressure generated by a wick increases with decreasing pore size. The wick permeability, another desirable feature, increases with decreasing pore size, however. For homogeneous wicks, there is an optimum pore size, which is a compromise. There are three main types in this context. Low-performance wicks in horizontal and gravity-assisted heat pipes should permit maximum liquid flow rate by having a comparatively large pore size, as with 100 or 150 mesh. Where pumping capability is required against gravity, small pores are needed, the use of non-homogeneous or arterial wicks aided by small pore structures for axial liquid flow (KEW; REAY, 2006).

Figure 3.5 - Different types of wick structure.



Source: Kew e Reay (2006).

Another feature of the wick, which must be optimised is its thickness. The heat transport capability of the heat pipe is raised by increasing the wick thickness. However, the increased radial thermal resistance of the wick created by this would work against increased capability and would lower the allowable maximum evaporator heat flux. The overall thermal resistance at the evaporator also depends on the conductivity of the working fluid in the wick. Other necessary properties of the wick are compatibility with the working fluid, and wettability. It should be easily formed to mould into the wall shape of the heat pipe and should preferably be of a form that enables repeatable performance to be obtained (KEW; REAY, 2006).

3.2.3 Wick material and form

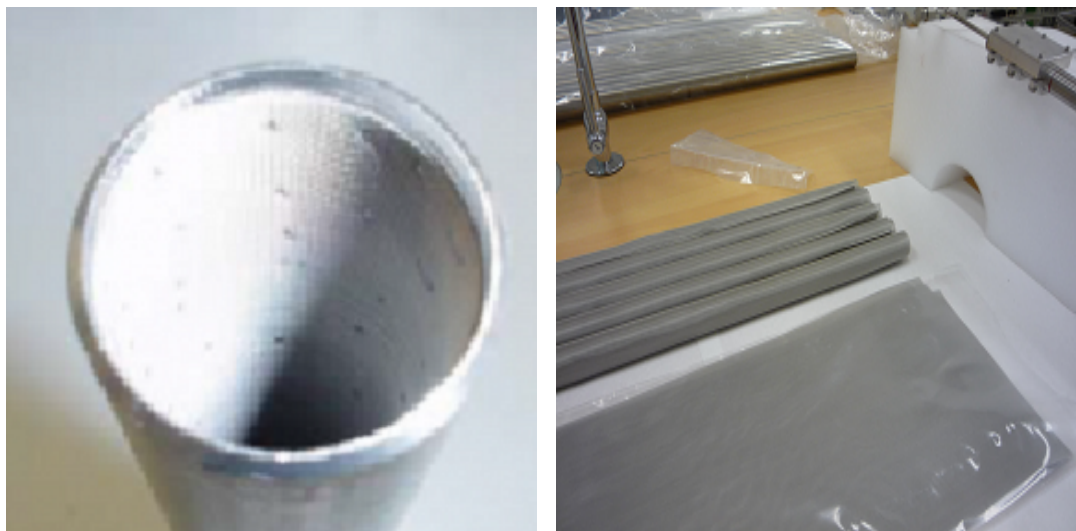
Several Basic materials are used in the construction of heat pipe wick structure. The most commonly used material is a metal fabric or screen, which is made of woven metal wires. Metal screens are manufactured with different wire diameters, pore sizes, and materials, such as copper, stainless steel, nickel, bronze, and titanium. Metal powders are also used as basic material for wicks by a process called sintering, where the powder is placed between the inner heat pipe wall and a mandrel. Metal foams are sintered metal powders, but an additional material is added which is burned away during the sintering process. Circumferential and axial grooves are also included here as basic materials used in wicks, even though they are not truly materials per se, since they are machined in the pipe wall (FAGHRI, 1995).

3.2.3.1 Wire mesh

Consists of a single or several layers of a metal cloth sprung against the inner heat pipe wall. The characteristics of the wrapped screen wick can be changed by varying the number of pores per unit area, the number of wraps, and the tightness of the wraps. While this wick has qualities such as a high capillary pressure and high permeability, the effective thermal conductivity is usually low due to the poor contact between the screen and the heat pipe wall, and between the separate layers of the screen (FAGHRI, 1995).

The number and form of materials that have been tested as wicks in heat pipes is very large. The most common form of wick is a woven wire mesh (Fig. 3.6(a)) or twill which can be made of many metals. Stainless steel (Fig. 3.6(b)), monel and copper are woven to produce meshes having very small pore size. Aluminium is available, but because of difficulties in producing and weaving fine aluminium wires, the requirements of small pore wicks cannot be met. Stainless steel is the easiest material to handle in mesh form. It can be rolled and retains its shape well, particularly when a coarse mesh is used. The inherent springiness in the coarse meshes assists in retaining the wick against the heat pipe wall, in some cases obviating the need for any other form of wick location. In heat pipes where a 400 mesh is used, a coarse 100 mesh layer located at the inner radius can hold the finer mesh in shape (KEW; REAY, 2006).

Figure 3.6 - (a) Wire mesh heat pipe, (b) Stainless steel wire mesh.



(a)

(b)

Source: Author.

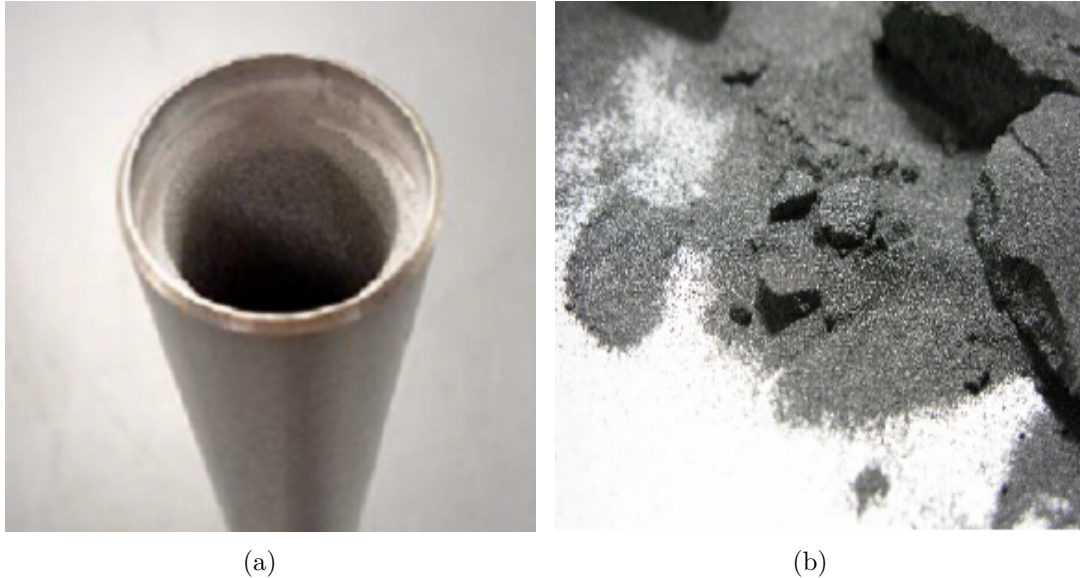
Stainless steel can also be diffusion bonded, giving strong permanent wick structure attached to the heat pipe wall. The spot welding of wicks is a convenient technique for preserving shape for attaching the wick to the wall in cases where the heat pipe diameter is sufficiently large to permit insertion of an electrode. The manufacture of heat pipes for thermal control of the chips in laptop computers and the like conventionally involves wicked copper heat pipes. Here copper or nickel mesh may be employed instead of stainless steel, depending upon the choice of the working fluid (KEW; REAY, 2006).

3.2.3.2 Sintering

A similar structure having an intimate contact with the heat pipe wall is a sintered wick (Fig. 3.7(a)). Sintering is often used to produce metallic filters, and many components of machines are now produced by this process as opposed to die casting or moulding. The sintered wick eliminates the problem of having a low thermal conductivity while maintaining a high capillary pressure, because the process involves bonding together a large number of particles in the form of a packed metal powder (Fig. 3.7(b)) to the inner wall of the heat pipe. That results in intimate contact between the wick and the wall, and between the individual metal spheres that comprises the powder. Unfortunately, the resulting permeability of the sintered metal powder wick is low, which causes a large liquid pressure drop in the condensate

(FAGHRI, 1995).

Figure 3.7 - (a) Sintered wick heat pipe, (b) Sintered metal powder.



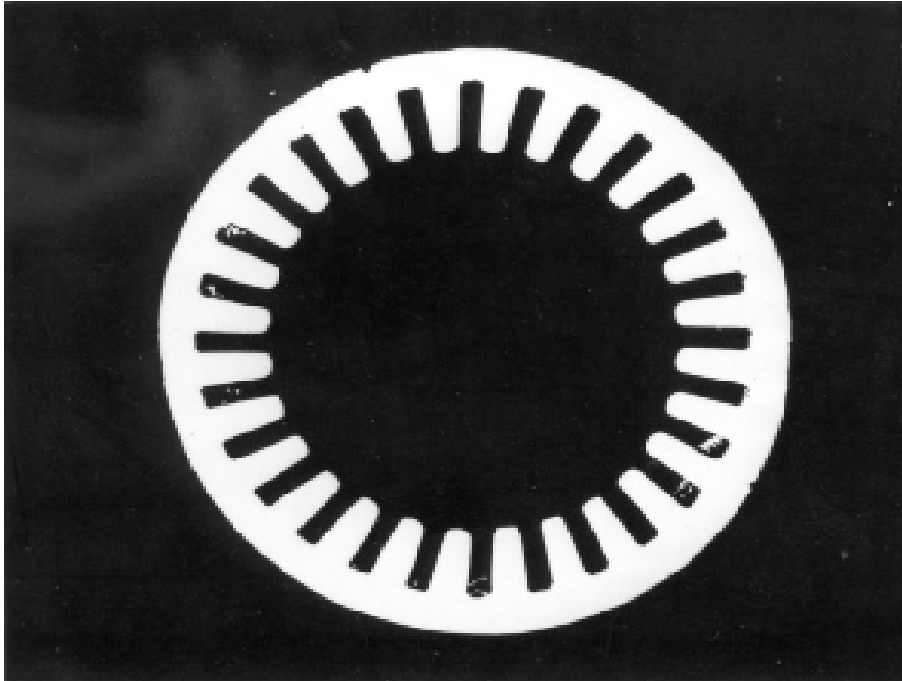
Source: Author.

The pore size of the wick thus formed can be arranged to suit by selecting powders having a particular size. The simplest way of making wicks by this method is to sinter the powder in the tube that will form the final heat pipe. This has the advantage that the wick is also sintered to the tube wall and thus makes a stronger structure (KEW; REAY, 2006). During sintering for wick construction, the powder should be sintered at temperatures between half its melting point and close to melting. Higher sintering temperature will result in better mechanical strength. Different materials require different sintering atmospheres, for example nickel powder should be sintered at a reducing atmosphere to restore the surface of the particles (LI et al., 2012).

3.2.3.3 Grooves

An axial groove wick can eliminate the problems of low thermal conductivity and low permeability encountered in the wire mesh and the sintered metal powder wick. It consists simply of grooves machined along the axial direction on the inner wall of the heat pipe. The grooves act as fins in direct contact with the condensate, so the heat transfer coefficients are large. Problems associated with the axial groove wick include liquid-vapour interaction, and low capillary pressure, which results in

Figure 3.8 - Grooved wick in a copper tube.



Source: Kew e Reay (2006).

an inability to operate against gravity (FAGHRI, 1995).

Several theoretical, experimental and optimisation approaches on improving heat and mass transfer performance have been investigated. The types of grooves that have been studied vary from triangular, rectangular, trapezoidal and "Ω" shaped grooves (ZHANG et al., 2009). A grooved system is widely used in spacecraft applications but it is unable to support significant capillary heads in earth gravity. The simplest way of producing longitudinal grooves in the wall of the heat pipe is by extrusion or by broaching. Aluminium is the most satisfactory material for extruding, where grooves may be comparatively narrow in width, but process a greater depth. An example of a copper grooved heat pipe wick is presented in Fig. 3.8. The external cross section of the heat pipe can also be adapted for particular applications. If the heat pipe is to be mounted on a plate, a flat surface may be incorporated on the wall of the heat pipe to give better thermal contact with the plate (KEW; REAY, 2006).

3.2.4 The Container

The function of the container is to isolate the working fluid from the outside environment. It has, therefore, to be leak-proof, to maintain the pressure differential across its wall and to enable the transfer of heat to take place into and from the

working fluid. Selection of the container material depends on several factors. These are as follows (KEW; REAY, 2006):

- Compatibility (both with working fluid and the external environment).
- Strength-to-weight ratio.
- Thermal conductivity.
- Ease of fabrication, including weldability, machineability and ductility.
- Porosity.
- Wettability.

A high strength-to-weight ratio is more important in spacecraft applications, and the material should be non-porous to prevent the diffusion of gas into the heat pipe. A high thermal conductivity ensures minimum temperature drop between the heat source and the wick (KEW; REAY, 2006).

As mentioned previously, formation of NCGs typically limits the operational lifetime of heat pipes. Degradation or contamination of the container can lead to chemical reactions with the working fluid and, hence, generation of NCGs. These chemical reactions have a whole host of other potential problems, including the formation of corrosive films, which tend to increase the thermal resistance and decrease the surface tension and wetting angle; pitting of the internal surface of the container material, which may result in the formation and development of enhanced nucleation sites and hence premature boiling of the working fluid; and corrosion on the internal surface of the heat pipe, which may lead to increased thermal resistance and, hence, increased overall resistance of the heat pipe (PETERSON, 1994).

Of the many materials available for the container, three are far most common in use, namely copper, aluminium and stainless steel. Copper is eminently satisfactory for heat pipes operating between 0 °C and 200 °C in applications such as electronics cooling. Aluminium is less common as a material in commercially available heat pipes but has received a great deal of attention in aerospace applications, because of its obvious weight advantages. Stainless steel unfortunately cannot generally be used as a container material with water where a long life is required, owing to gas generation problems (KEW; REAY, 2006).

3.2.5 Cleaning of container and wick

The presence of contaminants either in solid, liquid or gaseous state may be detrimental to heat pipe performance. The non-condensable gas tends to be accumulated in the condenser section with consequent loss of heat pipe conductance. In some cases, depending upon the design and operating conditions, the presence of gas may not be serious and may go completely unnoticed. Solids and liquids may be dissolved in the working fluid adversely affecting fluid properties, such as surface tension, wetting angle, and viscosity. Solid particles also tend to plug the wick. Solid particles of limited solubility may be precipitated in the evaporator section resulting in blockage of the fluid circulation (CHI, 1976). For this reason, all the materials used in a heat pipe must be clean.

Cleanliness achieves two objectives. It ensures that the working flow will wet the materials and that no foreign matter is present which could hinder capillary action or create incompatibilities. The cleaning procedure depends upon the material used, the process undergone in manufacturing and locating the wick, and the requirements of the working fluid, some of which wet more readily than others. In the case of wick/wall assemblies produced by processes such as sintering or diffusion bonding, carried out under an inert gas or vacuum, the components are cleaned during the bonding process, and provided that the time between this process and final assembly is short, no further cleaning may be necessary (KEW; REAY, 2006). There are numerous references available that describe various cleaning procedures for a wide variety of combinations. A majority of these combinations contain the same basic procedures: initial cleaning to remove any debris, metal filings, and so on; a chemical cleaning process to remove any water, oils, or films on the container or wick materials; a series of final rinse process to remove any remaining solvent or chemical etchant; and in some cases a vacuum bakeout procedure in which the heat pipe is heated and evacuated to remove any dissolved gases (PETERSON, 1994).

The order of these procedures varies in practice and several process may be carried out in combination. The excess cleaner has to be removed from the part by rinsing or evaporation between process. The selection of an appropriate cleaning method depends on a number of factors: the type and quantity of contaminations, the base metal components, and the degree of cleaning required. The following discussion should assist in the design of cleaning procedures for several common metals, e.g., aluminum, copper, and stainless steel, used in heat pipe applications (CHI, 1976).

4 HEAT TRANSFER AND FLUID FLOW THEORY

4.1 Introduction

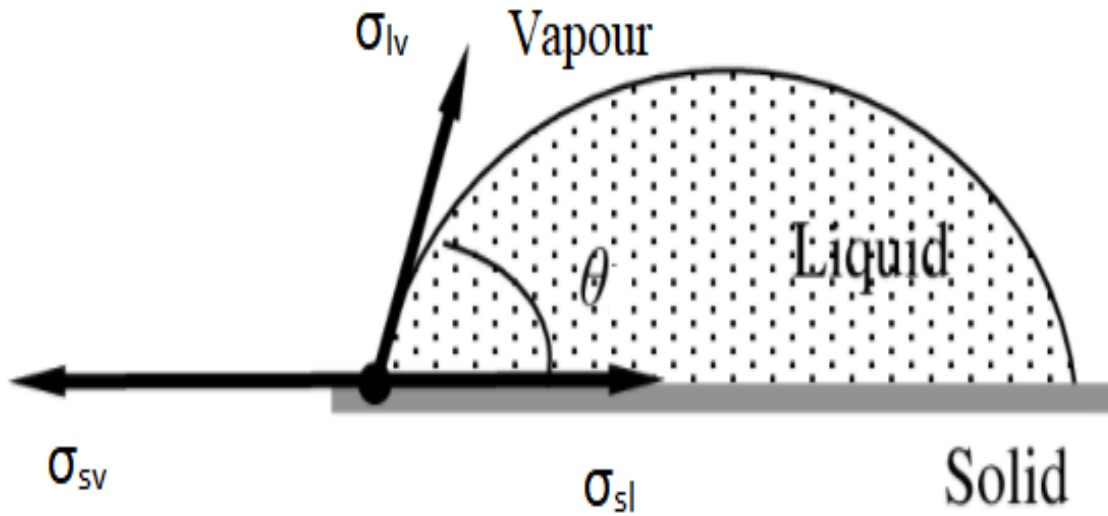
The purpose of this chapter is to discuss various interfacial phenomena, such as capillarity and disjoining pressure, and their impact on the pressure and temperature differences generated in a heat pipe wick structure. Capillarity can be defined as the macroscopic motion or flow of liquid resulting from the surface free energy and forces generated within the pore structures of the wick at the surface of the liquid. These driving forces are manifested by a pressure differential across the length of the heat pipe wick with the direction of flow determined by the direction of decreasing capillary pressure potential. The pressure difference which causes the capillary flow is due to the variations in curvature and/or the surface tension at the liquid interfaces in the different regions of the heat pipe. The pressure difference is also due to the body forces, hydrodynamic forces, phase change interactions, and disjoining pressure losses. (FAGHRI, 1995).

4.2 Surface tension and capillarity

In order to analyze and understand the operation of a heat pipe, it is first necessary to understand the phenomena that govern the behavior of the various interfaces, particularly those occurring at the liquid-vapour interface. Figure 4.2 illustrates a single droplet at rest on a solid surface surrounded by pure vapour. The point at which the three phases meet is called the contact line. If the droplet volume is fixed, that is, there is no vaporization or condensation, then increasing the contact angle will decrease the solid-liquid interface area. Likewise, decreasing the contact angle will allow the liquid to spread, forming a thin film and thereby increasing the solid-liquid interfacial area. As the limit of $\theta \rightarrow 0$, the liquid spreads over the entire available surface, forming a thin film (CAREY, 1992; PETERSON, 1994).

Previously, when discussing the surface tension, only the surface tension existing between the liquid and vapour phases of a substance, σ_{lv} , was considered. In reality there are three surface tensions that exist: one between the liquid and the vapour, σ_{lv} ; one between the solid and the liquid, σ_{sl} ; and one between the solid and the vapour, σ_{sv} . Returning to the previous force balance, it is clear that the addition of forces in the horizontal direction must be equal to zero for the droplet to be in static equilibrium, hence,

Figure 4.1 - Interfacial tensions acting on a contact line.



Source: Carey (1992).

$$\sigma_{sv} = \sigma_{sl} + \sigma_{lv} \cos \theta \quad (4.1)$$

which, although it is sometimes referred to as Neumann's formula, is more often called Young's equations.

Molecules in a liquid attract one another. A molecule in a liquid will be attracted by the surrounding molecules and, on average, a molecule in the bulk of the fluid will not experience any resultant force. In the case of a molecule near the surface of a liquid, the forces of attraction will no longer balance out and the molecule will experience a resultant force inwards. Because of this effect, the liquid will tend to take up a shape having minimum surface area, in the case of a free falling drop in vacuum this would be a sphere. Due to this spontaneous tendency to contract, a liquid surface behaves rather like a rubber membrane under tension. In order to increase the surface area, work must be done on the liquid. The work or energy required to increase the surface area can be obtained from the following relation, which is also the definition of surface tension

$$\sigma = \left(\frac{\partial E}{\partial S} \right)_{T,p,n_i} \quad (4.2)$$

when E is the surface free energy, S is the surface area, and n_i is the number of moles for the i th component for multicomponent system. Equation 4.2 is valid for solid-liquid, solid-vapour, liquid-vapour, and liquid-liquid interfaces (KEW; REAY, 2006; FAGHRI, 1995). Where the forces are attractive, the liquid is said to 'wet' the solid. The angle of contact made by the liquid surface with the solid is known as the contact angle, θ . For wetting, θ will lie between 0 and $\pi/2$ rad and for nonwetting liquids, $\theta > \pi/2$. The condition for wetting to occur is that the total surface energy is reduced by wetting (CHI, 1976).

$$\sigma_{sl} + \sigma_{lv} < \sigma_{sv} \quad (4.3)$$

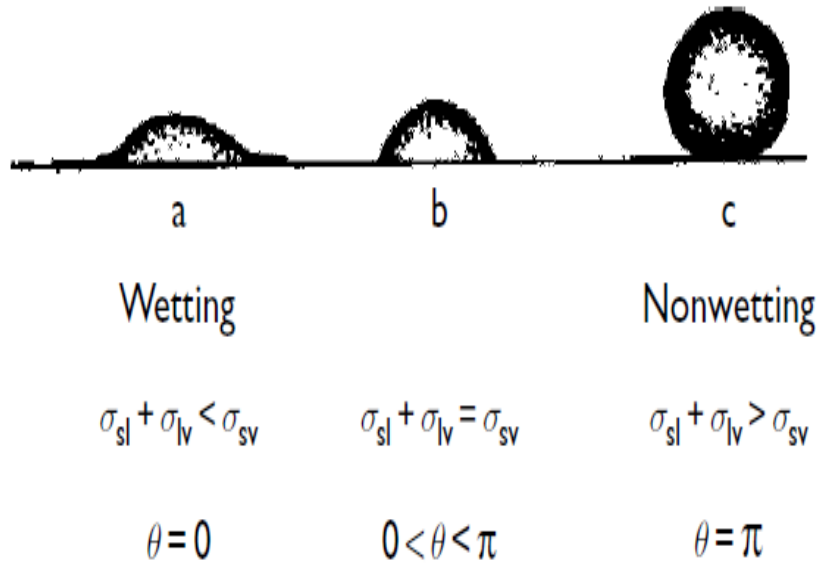
where the subscripts, s , l and v refer to solid, liquid and vapour phases, respectively, as shown in Fig. 4.2(a). Wetting will not occur if $\sigma_{sl} + \sigma_{lv} > \sigma_{sv}$ as on Fig. 4.2(c), while the intermediate condition of partial wetting $\sigma_{sl} + \sigma_{lv} = \sigma_{sv}$ is illustrated in Fig. 4.2(b).

From this expression, the surface tension can be described as a fundamental quantity which characterizes the surface properties of a given liquid. Additionally, the surface tension is referred to as free energy per unit area or force per unit length. Surface tension exists at all phase interfaces: i.e., solid, liquid and vapour. Therefore, the shape that the liquid assumes is determined by the combination of the interfacial forces of the three phases (FAGHRI, 1995).

The term capillarity as related to heat pipes is defined as the flow of a liquid under the influence of its own surface and interfacial forces. The capillary pressure difference causing flow is generated by the differences in curvature along the liquid-vapour interface and the existence of the surface tension. The three basic factors that determine the driving potential are surface tension, the contact angle and the geometry of the solid surface at the three phase boundary line (FAGHRI, 1995).

Operation of the heat pipe in its simplest form involves the evaporation of the liquid in the heated end of the heat pipe. This evaporative process leads to the formation

Figure 4.2 - Wetting and nonwetting contact.

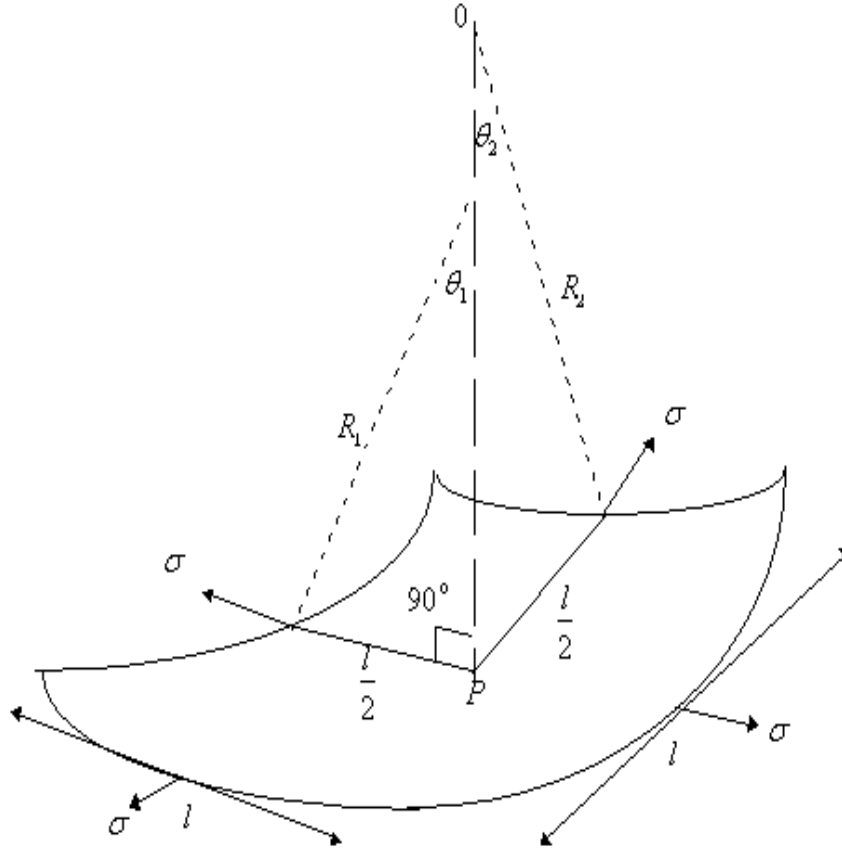


Source: Kew e Reay (2006).

of or increase in the curvature of the concave meniscus in the wick pores. As a result of surface tension forces, a capillary pressure P_c develops in the meniscus which acts against the surface tension forces. Thus, the capillary pressure can be determined by examining the radius of curvature of the meniscus (FAGHRI, 1995). When a meniscus is formed at the liquid-vapour interface, as shown in Fig. 4.2, the capillary pressure defined as $(P_v - P_l)$ can be calculated by the Laplace and Young equation,

$$\Delta P_c = \sigma \left(\frac{1}{R_1} + \frac{1}{R_2} \right) \quad (4.4)$$

Figure 4.3 - Geometry of meniscus at liquid-vapour interface.



Source: Chi (1976).

in which R_1 and R_2 are the principal radius of curvature of the meniscus and σ is the surface tension coefficient of the liquid. Limitations to use of the Laplace and Young equation are typically that the liquid-vapor interface is static, interfacial mass fluxes (evaporation) are low, and disjoining pressure effects are negligible. For cases of very thin films where disjoining pressure effects must be included to provide a physically correct and accurate prediction of the capillary pressure across an interface, a review of techniques has been provided by Wayner (1999). In particular, we are interested in finding the maximum value of $(1/R_1 + 1/R_2)$ for various types of wick structures, and hence, the maximum capillary pressure $\Delta P_{c,max}$. For convenience, it is common practice in heat pipe applications to write out Eq. 4.4 as follows:

$$\Delta P_{c,max} = \frac{2\sigma}{r_c} \cos \theta \quad (4.5)$$

Where θ is the contact angle and is dependent on the fluid-wick pair used. The contact angle is a measure of the degree of wettability of the liquid on the wick structure, where $\theta = 0^\circ$ relates to a perfectly wetting system. Carey (1992) provides a detailed discussion on parameters affecting wettability. For this expression to be maximized, the wetting angle must be zero (i.e., the liquid wets the wick perfectly). Thus, the maximum capillary pressure with a perfectly wetting fluid will be.

$$\Delta P_{c,max} = \frac{2\sigma}{r_c} \quad (4.6)$$

The effective capillary radius, r_c , in this equation is defined such that $2/r_c$ is equal to the maximum possible value of $(1/R_1 + 1/R_2)$ for different wick structures. For wick pores of simple geometry, at the liquid-vapour interface, the values of the effective capillary radius can often be determined theoretically. For pores of complex geometry, these values have to be determined experimentally. The r_c for screen wicks is expected to be equal to half of the spacing between the wires. However, because of the staggering of the wires and the interference among adjacent layers of the screen, so far it has not been possible to determine the effective radius for screen wicks by theoretical considerations. Experimental data from tests on single-layer screens seem to suggest that r_c is equal to half of the sum of the wire diameter d and the spacing ω instead of being equal to only half of the spacing. For the multilayer screens, no generalized data are yet available. However, the effect of intermeshing should reduce the effective capillary radius. It appears that the effective radius for screen wicks can be calculated, conservatively, by the equation (CHI, 1976)

$$r_c = \frac{\omega + d}{2} = \frac{1}{2N} \quad (4.7)$$

where N is the mesh number defined as number of wires per unit length. The number of openings per unit length is called the mesh number, and is given by (FAGHRI, 1995).

$$N = 1/(d + W) \quad (4.8)$$

where d is the wire diameter and W is the width of the openings. The Eq. 4.8 is used for Eq. 4.14 by Marcus (MARCUS, 1972) for porosity of metal screen wicks.

4.3 Liquid pressure drop

The liquid pressure gradient is the result of the combined effect of both viscous and inertial forces. The increase in the pressure gradient in the evaporator section is nonlinear, due to the mass injection of the working fluid into the vapour stream with the pressure in the liquid increasing along the length of the heat pipe moving from the evaporator toward the condenser (PETERSON, 1994).

In the analysis of the liquid flow in the wick structure, it is generally assumed that the liquid flow is steady two-dimensional incompressible laminar flow with negligible body forces. The fluid and the wick structure are assumed to be in local equilibrium, and the wick is assumed to be isotropic and homogeneous. The steady state conservation equations for mass, momentum, and energy in the wick region are as follows (FAGHRI, 1995).

Continuity:

$$\frac{\partial u_l}{\partial x} + \frac{\partial v_l}{\partial y} = 0 \quad (4.9)$$

Momentum in the x-direction:

$$\rho_l \left(u_l \frac{\partial u_l}{\partial x} + v_l \frac{\partial u_l}{\partial y} \right) = \mu_l \left(\frac{\partial^2 u_l}{\partial x^2} + \frac{\partial^2 u_l}{\partial y^2} \right) - \frac{\partial P_l}{\partial x} - \frac{\mu_l u_l \epsilon}{K} \quad (4.10)$$

Momentum in the y-direction:

$$\rho_l \left(u_l \frac{\partial v_l}{\partial x} + v_l \frac{\partial v_l}{\partial y} \right) = \mu_l \left(\frac{\partial^2 v_l}{\partial x^2} + \frac{\partial^2 v_l}{\partial y^2} \right) - \frac{\partial P_l}{\partial y} - \frac{\mu_l v_l \epsilon}{K} \quad (4.11)$$

Energy:

$$\rho_l C_{p,l} \left(u_l \frac{\partial T_l}{\partial x} + v_l \frac{\partial T_l}{\partial y} \right) = k_{eff} \left(\frac{\partial^2 T_l}{\partial x^2} + \frac{\partial^2 T_l}{\partial y^2} \right) \quad (4.12)$$

where ϵ is the wick porosity, and K is the permeability of the wick structure. The permeability is a property of the porous material which characterizes its ability to

transmit liquid under the action of an applied pressure gradient. Marcus (1972) has described a method for calculation of the permeability of wrapped, screened wicks. This expression, which is a modified form of the Blake-Kozeny equation, can be expressed as (PETERSON, 1994):

$$K = \frac{d^2 \epsilon^3}{122(1 - \epsilon)^2} \quad (4.13)$$

In this expression, d is the wire diameter and ϵ is the porosity, which can be determined as

$$\epsilon = 1 - \frac{1}{4} \pi S N d \quad (4.14)$$

where N is the mesh number and S is the crimping factor (approximately 1.05) (CHI, 1976).

For most heat pipes, the wick structures are very thin, so the liquid flow in the wick can be simplified to one-dimensional axial flow. Also, the liquid velocity and gradient in the axial direction is very small. Therefore, Eqs. (4.9) - (4.11) can be simplified to

$$0 = -\frac{dP_l}{dx} - \frac{\mu_l u_l}{K} \quad (4.15)$$

Rearranging Eq. 4.15, and noting that $\dot{m} = u_l A_w \rho_l$, where A_w is the wick cross-sectional area, we have:

$$\frac{dP_l}{dx} = -\frac{\mu_l \dot{m}}{\rho_l A_w K} \quad (4.16)$$

The equation above is Darcy's law for liquid flow in porous medium. Although Eqs. (4.9) - (4.11) give a more general description of the liquid flow in the wick structure,

Eq. 4.16 is more practical in the heat pipe design process (FAGHRI, 1995).

4.4 Effective thermal conductivity of wick structures

With the heat transported by a heat pipe being mainly conducted through the wick structure due to the low liquid velocity in the wick, the choice of the wick is important since its effective thermal conductivity will dictate the maximum wick structure. The effective thermal conductivity of the wick is dependent on both the solid wick material and the working fluid. For liquid metal heat pipes, the high conductivity of the working fluid provides high effective conductivity, even for relatively thick wicks. For low conductivity fluids, the effective thermal conductivity is heavily dependent on the design of the wick (FAGHRI, 1995).

The metal screen wick is the most commonly used wick structure due to its simplicity of installation. A solution for the effective thermal conductivity of a square array of uniform cylinders have been correlated, respectively, by the equation (CHI, 1976).

$$k_{eff} = \frac{k_l[(k_l + k_s) - (1 - \epsilon)(k_l - k_s)]}{[(k_l + k_s) + (1 - \epsilon)(k_l - k_s)]} \quad (4.17)$$

Equation 4.17 is used extensively for metal screen wicks. Since the porosity of metal screen wicks varies significantly.

4.5 Vapour pressure drop

The variation in vapour pressure is mainly the result of the viscous pressure drop occurring along the vapour flow path. However, in the evaporator region, the viscous present drop may be coupled with the momentum change required to accelerate the vapour molecules escaping from the liquid meniscus, which further decreases the pressure. In the adiabatic section of the heat pipe, the vapour pressure gradient is typically linear and results only from the viscous friction occurring between the flowing vapour and the pipe walls and wick structure. In the condenser region, the inertial effects caused by the deceleration of the vapour molecules can be recovered (although not completely) because of the decreasing mass flow rate caused by condensation of some of the vapour (PETERSON, 1994).

While calculation of the liquid pressure drop occurring in the wick structure of a heat pipe is relatively straightforward, calculation of the vapour pressure gradient

is significantly more difficult. As mentioned previously, the pressure gradient in the vapor passage is not only a function of the viscous pressure drop but also may be significantly influenced by the inertial effects resulting from the addition and rejection of mass in the evaporator and condenser, respectively, and by the compressibility of the vapour phase. A mass balance on a section of the adiabatic region of the heat pipe ensures continued operation, the liquid mass flow rate and vapour mass flow rate must be equal. Because of the large difference in the density of these two phases, the vapour velocity must be significantly higher than the velocity of the liquid phase. For this reason, in addition to the pressure gradient resulting from frictional drag, the pressure gradient due to variations in the dynamic pressure must also be considered even in one-dimensional flow (PETERSON, 1994). Chi (1976) found that upon integration of the vapor pressure gradient, the dynamic pressure effects cancel. The result is the expression

$$\frac{dP_v}{dx} = \left(\frac{C(f_v Re_v)\mu_v \dot{m}}{2(r_{h,v})^2 A_v \rho_v} \right) \quad (4.18)$$

where $r_{h,v}$ is the hydraulic radius of the vapour space and C is a constant that depends on the Mach number.

During steady-state operation, the liquid mass flow rate at any axial position, \dot{m}_l , must be equal to the vapour mass flow rate \dot{m}_v , and while the liquid flow regimes is always laminar, the vapour flow may be either laminar or turbulent. It is therefore necessary to determine the vapour flow regime as a function of the heat flux. This can be accomplished by evaluating the local axial Reynolds number in the vapour, defined as (PETERSON, 1994):

$$Re_v = \frac{2(r_{h,v})Q}{A_v \mu_v \lambda} \quad (4.19)$$

In addition, it is necessary to determinate if the flow should be treated as compressible or incompressible by evaluating the local Mach number, define as (PETERSON, 1994)

$$M_v = \frac{Q}{A_v \rho_v \lambda (R_v T_v \gamma_v)^{1/2}} \quad (4.20)$$

where R_v is the gas constant, T_v is the vapour temperature, and γ_v is the ratio of specific heats, which is equal to 1.4 for diatomic vapour (CHI, 1976).

Previous investigations summarized by Kraus e Bar-Cohen (1983) have demonstrated that the following combinations of these conditions can be used with reasonable accuracy:

$$\begin{aligned} Re_v < 2300 & \quad M_v < 0.2 \\ (f_v Re_V) = 16 & \quad C = 1.0 \end{aligned} \quad (4.21)$$

$$\begin{aligned} Re_v < 2300 & \quad M_v > 0.2 \\ (f_v Re_V) = 16 & \quad C = \left[1 + \left(\frac{\gamma_v - 1}{2}\right) Ma_v^2\right]^{-1/2} \end{aligned} \quad (4.22)$$

$$\begin{aligned} Re_v > 2300 & \quad M_v < 0.2 \\ (f_v Re_V) = 0.038 \left(\frac{2(r_{h,v})Q}{A_v \mu_v \lambda}\right)^{3/4} & \quad C = 1.0 \end{aligned} \quad (4.23)$$

The equations used to evaluate both the Reynolds number and the mach number are functions of the heat capacity, it is first necessary to assume the conditions of the vapour flow (PETERSON, 1994).

4.6 Normal hydrostatic pressure

The hydrostatic pressure gradient occurring in heat pipes is due to gravitational or body forces within the vapour and liquid phases. For heat pipes with the evaporator located below the condenser, the gravitational body forces would result in a linearly increasing contribution to the pressure in the liquid phase and a linearly decreasing contribution to the pressure in the vapour phase. It is also important to observe the effect of the gravitational body forces on the location of the dry point within the

cross-sectional configuration of the heat pipe. Because some hydrostatic pressure gradient exists in a heat pipe, even one operating in a horizontal orientation, the first point to experience dry-out in the wicking structure would typically occur at the end of the evaporator furthest from condenser and at the highest elevation. The normal hydrostatic pressure drop can be expressed as (PETERSON, 1994)

$$\Delta P_{\perp} = \rho_l g d_v \cos \psi \quad (4.24)$$

where ρ_l is the density of the liquid, g is the gravitational acceleration, d_v is the diameter of the vapour portion of the heat pipe, and ψ is the angle the heat pipe makes with respect to the horizontal.

4.7 Axial hydrostatic pressure

The axial hydrostatic pressure drop results from the component of the body force acting along the longitudinal axis. It can be expressed as

$$\Delta P_{\parallel} = \rho_l g L \sin \psi \quad (4.25)$$

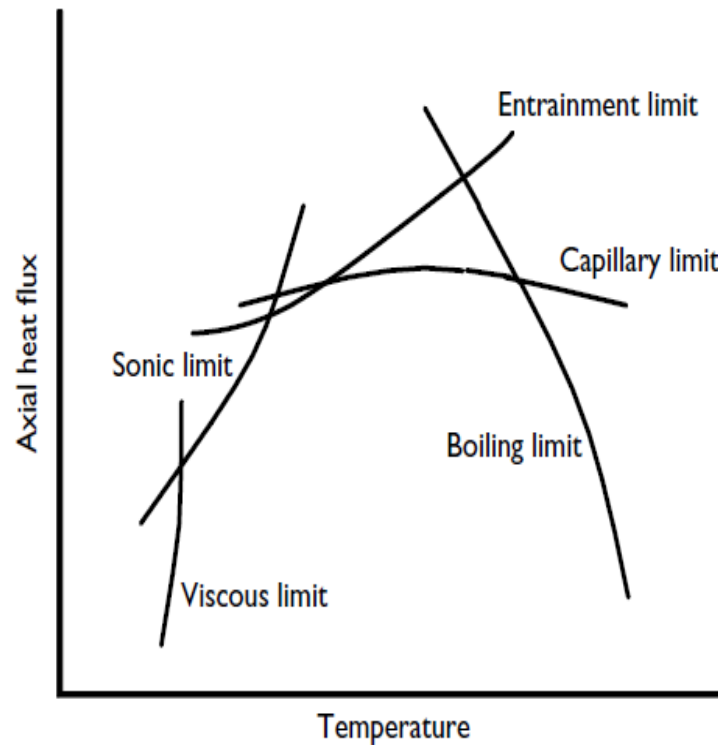
where L is the overall length of heat pipe. In a gravitational environment, the axial hydrostatic pressure term may either assist or hinder the capillary pumping process depending upon whether the tilt of the heat pipe promotes or hinders the flow of liquid back to the evaporator (i.e., the evaporator lies either below or above the condenser). In zero-gravity environment, both this term and the normal hydrostatic pressure drop term can be neglected because of the absence of body forces (PETERSON, 1994).

4.8 Operating limits

Although heat pipes are very efficient heat transfer devices, they are subject to a number of heat transfer limitations. These limitations that determine the maximum heat transfer rate and the type of limitation that restricts the operation of the heat pipe can be determined by which limitation has the lowest value at a specific heat pipe working temperature. The possible limitations on maximum axial heat transfer rate are shown schematically in Fig. 4.4 as a function of heat pipe working

temperature (FAGHRI, 1995).

Figure 4.4 - Limitations to heat transport in a heat pipe.



Source: Kew e Reay (2006).

Limitations to heat transport arise mainly from the ability of the wick to return condensate to the evaporator, and from thermodynamic barriers encountered in the flow of the vapour (FAGHRI, 1995). These limitations can be divided in two primary categories: limits that result in heat pipe failure and limits that do not. For the limitations resulting in heat pipe failure, all are characterized by insufficient liquid flow to the evaporator for a given heat input, thus resulting in dryout of the evaporator wick structure. However, limitations not resulting in heat pipe failure do require that the heat pipe operate at an increased temperature for an increase heat input. The two categories and basic phenomena for each limit may be summarized as follows (BEJAN; KRAUS, 2003).

Limitations - Failure

- Capillary limit: The capillary limit relates to the fundamental phenomenon governing heat pipe operation which is a development of capillary pres-

sure differences across the liquid-vapor interfaces in the evaporator and condenser. When the driving capillary pressure is insufficient to provide adequate liquid flow from the condenser to the evaporator, dryout of the evaporator wick will occur. Generally, the capillary limit is the primary maximum heat transport limitation of a heat pipe.

- **Boiling limit:** The boiling limit occurs when the applied evaporator heat flux is sufficient to cause nucleate boiling in the evaporator wick. This creates vapor bubbles that partially block the liquid return and can lead to evaporator wick dryout. The boiling limit is sometimes referred to as the heat flux limit.
- **Entrainment limit:** The entrainment limit refers to the case of high shear forces developed as the vapor passes in the counterflow direction over the liquid saturated wick, where the liquid may be entrained by the vapor and returned to the condenser. That results in an insufficient liquid flow through the wick structure.

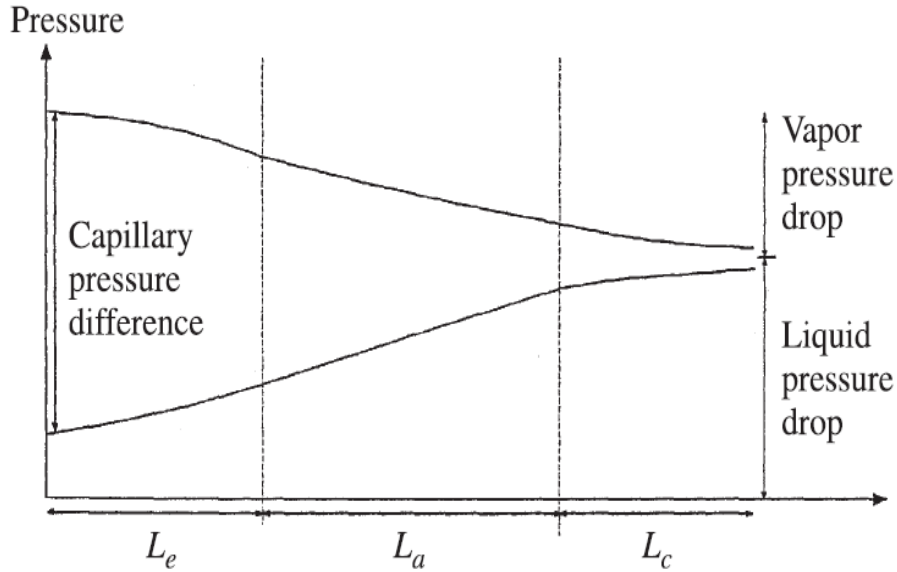
Limitations - Nonfailure

- **Viscous limit:** The viscous limit occurs in low operating temperatures, where the saturation vapor pressure may be of the same order of magnitude as the pressure drop required to drive the vapor flow in the heat pipe. The result is in an insufficient pressure available to drive the vapor. The viscous limit is sometimes called the vapor pressure limit.
- **Sonic limit:** The sonic limit is due to the fact that at low vapor densities, the corresponding mass flow rate in the heat pipe may result in very high vapor velocities, and the occurrence of choked flow in the vapor passage may be possible.

4.8.1 Capillary limitation on heat transport capability

Although heat pipe performance and operation are strongly dependent on the shape, working fluid, and wick structure, the fundamental phenomenon that governs the operation of these devices arises from the difference in the capillary pressure across the liquid-vapour interfaces in the evaporator and condenser regions. The combined effect of this vaporization and condensation results in a meniscus radius of curvature that varies along the axial length of the heat pipe. The point at which the meniscus

Figure 4.5 - Liquid and Vapour pressure distributions in a heat pipe.



Source: Peterson (1994).

has a minimum radius of curvature is referred to as the "dry" point and usually occurs in the evaporator at the furthest point from the condenser region. The "wet" point occurs at that point where the vapour pressure and liquid pressure are approximately equal or where the radius of curvature is at a maximum (PETERSON, 1994). The capillary pressure gradient across a liquid-vapour interface is equal to the pressure difference between the liquid and vapour phases at any given axial position. The Figure 4.5 illustrates the relationship between the static liquid and static vapour pressures in an operating heat pipe (PETERSON, 1994).

For a heat pipe to function properly, the net capillary pressure difference between the wet and dry points, must be greater than the summation of all the pressure losses occurring throughout the liquid and vapour flow paths. This relationship, referred to as the capillary limitation, can be expressed mathematically as (PETERSON, 1994)

$$\Delta P_{c,max} \geq \int_{L_{eff}} \frac{dP_l}{dx} dx + \int_{L_{eff}} \frac{dP_v}{dx} dx + \Delta P_+ + \Delta P_{||} \quad (4.26)$$

where $\Delta P_{c,max}$ = maximum capillary pressure difference generated within capillary wicking structure between wet and dry point, ΔP_+ = normal hydrostatic pressure drop, and $\Delta P_{||}$ = axial hydrostatic pressure drop.

Assuming one-dimensional flow and that the wet point is the end of the condenser yields

$$\int_{L_{eff}} \frac{dP_l}{dx} dx = \Delta P_l = \left(\frac{\mu_l}{K A_w \rho_l \lambda} \right) L_{eff} Q_{c,max} \quad (4.27)$$

$$\int_{L_{eff}} \frac{dP_v}{dx} dx = \Delta P_v = \left(\frac{C(f_v Re_v) \mu_l}{2(r_{h,v})^2 A_v \rho_v \lambda} \right) L_{eff} Q_{c,max} \quad (4.28)$$

where ΔP_v = pressure drops occurring in vapour phase, ΔP_l = pressure drops occurring in liquid phase and L_{eff} is the effective heat pipe length, defined as

$$L_{eff} = 0.5L_e + L_a + 0.5L_c \quad (4.29)$$

The maximum axial heat transfer the heat pipe can transport prior to reaching the capillary limit, assumption of laminar and incompressible flow, in this case is

$$Q_{c,max} = \frac{(Q_{c,max} L_{eff})}{L_{eff}} \quad (4.30)$$

and the Equation 4.26 can be expressed as:

$$\frac{2\sigma}{r_c} \geq \left(\frac{\mu_l}{K A_w \rho_l \lambda} + \frac{C(f_v Re_v) \mu_v}{2(r_{h,v})^2 A_v \rho_v \lambda} \right) (Q_{c,max} L_{eff}) + \rho_l g d_v \cos \psi + \rho_l g L \sin \psi \quad (4.31)$$

4.8.2 Viscous limitation

At very low operating temperatures, the vapour pressure difference between the evaporator and the condenser regions of a heat pipe may be extremely small. In some cases, the viscous forces within the vapour region may actually be larger than the pressure gradients caused by the imposed temperature field. When this occurs,

the pressure gradients within vapour region may not be sufficient to generate flow and the vapour may stagnate. This no-flow or low flow condition in the vapour portion of a heat pipe is referred to as viscous limitations. Because the vapour pressures typically must be very low for this to occur, the viscous limit is most often observed in cryogenic heat pipes, heat pipes with extremely long condenser regions, or heat pipes undergoing startup from a frozen state (PETERSON, 1994).

Busse (1973) provided an analytical investigation of the viscous limit. The model first assumed an isothermal ideal gas for the vapor and that the vapor pressure at the condenser end was equal to zero, which provides the absolute limit for the condenser pressure. Using these assumptions, a one-dimensional model of the vapor flow assuming laminar flow conditions was developed and expressed as

$$Q_v = \frac{A_v r_0^2 \lambda \rho_v P_v}{16 \mu_v L_{eff}} \quad (4.32)$$

where P_v and ρ_v are the vapor pressure and density at the evaporator end of the heat pipe. The values predicted by this expression were compared with the results of previous experimental investigations and were shown to agree well (BEJAN; KRAUS, 2003; PETERSON, 1994).

4.8.3 Sonic limitation

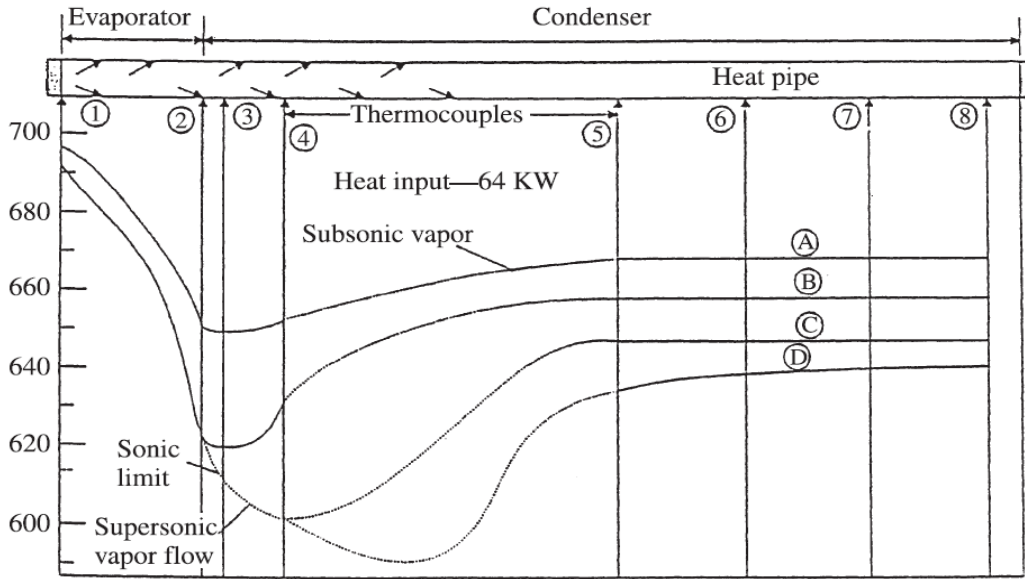
The evaporator and condenser sections of a heat pipe represent a vapor flow channel with mass addition and extraction due to the evaporation and condensation, respectively. The vapor velocity increases along the evaporator and reaches a maximum at the end of the evaporator section. The limitation of such a flow system is similar to a converging diverging nozzle with a constant mass flow rate, where the evaporator exit corresponds to the throat of the nozzle. Therefore, one expects that the vapor velocity at that point cannot exceed the local speed of sound. This choked flow condition is called the sonic limitation. The sonic limit usually occurs either during heat pipe startup or during steady state operation when the heat transfer coefficient at the condenser is high (FAGHRI, 1995; FAGHRI, 2014).

The sonic limit is typically experienced in liquid metal heat pipes during startup or low-temperature operation due to the associated very low vapor densities in this condition. This may result in choked, or sonic, vapor flow. For most heat pipes oper-

ating at room temperature or cryogenic temperatures, the sonic limit is typically not a factor, except in the case of very small vapor channel diameters. With the increase of the vapor velocities, inertial, or dynamic, pressure effects must be included. It is important to note that in cases where inertial effect of the vapor flow is significant, the heat pipe may no longer operate in a nearly isothermal case, resulting in a significantly increased temperature gradient along the heat pipe. In cases of heat pipe operation where the inertial effects of the vapor flow must be included, an analogy between heat pipe operation and compressible flow in a converging diverging nozzle can be made. In a converging diverging nozzle, the mass flow rate is constant and the vapor velocity varies due to the varying cross-sectional area. However, in heat pipes, the area is typically constant and the vapor velocity varies due to mass addition (evaporation) and mass rejection (condensation) along the heat pipe (BEJAN; KRAUS, 2003; PETERSON, 1994). These flow characteristics of heat pipes have been demonstrated experimentally by Kemme (1969) in a sodium heat pipe. The results of this test are shown in Figure 4.6 on a plot of temperature versus the heat pipe length.

Curve A demonstrates a subsonic flow condition with a slight temperature recovery in the condenser. The temperature decreased along the evaporator section, as the vapour stream was accelerated, due to mass addition caused by evaporation. When the condenser temperature was lowered (curve B) by increasing the heat rejection rate, the evaporator temperature was also lowered, the vapour velocity at the exit became sonic, and critical and choked flow conditions existed. Further increasing the heat rejection rate only lowered the condenser temperature because the heat transfer of that section could not be increased due to existence of choked flow. The change in condenser temperature had no effect upon the evaporator temperature because the vapour was moving at the speed of sound at the evaporator exit and changes in condenser conditions could not be transmitted upstream to the evaporator section (CHI, 1976).

Figure 4.6 - Temperature as a function of axial position.



Source: Peterson (1994).

Levy (LEVY, 1968) developed a closed-form expression for the sonic limit derived from one-dimensional vapor flow theory. This analysis assumed that the frictional effects may be neglected; thus inertial effects dominate, and the vapor behaves as a perfect gas. Combining these assumptions with the energy and momentum equations results in expressions for the temperature and pressure ratios. Substituting the local Mach number and relating the axial heat flux to the density and velocity, the relationship between the static and stagnation temperatures and pressure can be rewritten as (PETERSON, 1994)

$$\frac{T_0}{T_v} = 1 + \frac{\gamma_v - 1}{2} M_v^2 \quad (4.33)$$

and

$$\frac{P_0}{P_v} = 1 + \frac{\gamma_v}{2} M_v^2 \quad (4.34)$$

where the subscripts 0 and v indicate the stagnation and static states of the va-

por, respectively. Combining the temperature and pressure ratios with the ideal gas law yields an expression for the density ratio that, when combined with the two expressions given, yields an equation for the axial heat flux in terms of the physical properties, geometrical dimensions, and Mach numbers. The recognition that the Mach number should be equal to unity at sonic velocities yields an expression for the maximum axial heat transport (PETERSON, 1994).

$$Q_s = A_v \rho_v \lambda \left[\frac{\gamma_v R_v T_v}{2(\gamma_v + 1)} \right]^{1/2} \quad (4.35)$$

an alternative approach has been presented by Busse (1973). Using one dimensional laminar flow, the momentum equation yield.

$$\frac{dp}{dx} = \frac{d}{dx} \rho v^2 \quad (4.36)$$

Integrating this expression, applying a non-slip boundary condition, combining with the continuity equation and assuming that the vapor behaves as an ideal gas yields an expression for the maximum heat transport capacity as a function of the thermophysical and geometric properties.

$$Q = \lambda \left(\frac{\rho_v P_v}{A} \right)^{1/2} \left[\frac{P}{P_v} \left(1 - \frac{P}{P_v} \right) \right]^{1/2} \quad (4.37)$$

Setting the first derivative $dQ/dP = 0$ yields a relationship for the sonic limit of (PETERSON, 1994)

$$Q_s = 0.474 \lambda A_v (\rho_v P_v)^{1/2} \quad (4.38)$$

where ρ_v and P_v are the vapour density and pressure at the end of the evaporator. The greatest difficulty in determining the sonic limit is determining these two quantities along with the inlet pressure to the condenser. As is apparent in equation

4.38, these values may have a significant effect on the vapour velocity and can cause large variations in the existence or location of the choked flow condition.

4.8.4 Entrainment limitation

Since the vapour and liquid move in apposite directions in a heat pipe, a shear force exists at the liquid-vapour interface. If the vapour velocity is sufficiently high, a limit can be reached at which liquid will be torn out from the surface of the wick and entrained in the vapour, inhibiting the return of liquid to the evaporator. Once entrainment begins, there is a sudden substantial increase in fluid circulation until the liquid return system cannot accommodate the increased flow. When this occurs, abrupt dryout of the wick at the evaporator results. The phenomenon of entrainment was detected in heat pipe tests by monitoring the sounds made by liquid droplets striking the condenser end of the heat pipe and through the abrupt overheating of the evaporator. The most common approach to estimate the entrainment limit in heat pipes is to use a Weber number criterion. [Cotter \(1968\)](#) presented one of the first methods to determine the entrainment limit. This method utilized the Weber number, defined as the ratio of the viscous shear force to the forces resulting from the surface tension ([BEJAN; KRAUS, 2003](#); [PETERSON, 1994](#)).

$$We = \frac{2r_{h,w}\rho_v V_v^2}{\sigma} \quad (4.39)$$

By relating the vapor velocity and the heat transport capacity to the axial heat flux as

$$v_v = \frac{Q}{A_v \rho_v \lambda} \quad (4.40)$$

and assuming that to prevent entrainment of liquid droplets in the vapor flow, the Weber number must be less than unity, the maximum transport capacity based on entrainment can be written as

$$Q_e = A_v \lambda \left(\frac{\sigma \rho_v}{2r_{h,w}} \right)^{1/2} \quad (4.41)$$

where $r_{h,w}$ is the hydraulic radius of the wick structure. Since the initial development of this expression, numerous investigations of entrainment in heat pipes have been conducted.

4.8.5 Boiling limitation

At higher heat fluxes, nucleate boiling may occur in the wick structure, which may allow vapor to become trapped in the wick, thus blocking liquid return and resulting in evaporator dryout. This phenomenon, referred to as the boiling limit, differs from other limitations discussed previously, as it depends on the radial or circumferential heat flux applied to the evaporator, as opposed to the axial heat flux or total thermal power transported by the heat pipe (BEJAN; KRAUS, 2003). Determination of the heat flux or boiling limit is based on nucleate boiling theory and is comprised of two separate phenomena: bubble formation and the subsequent growth or collapse of the bubbles. Bubble formation is governed by the size (and number) of nucleation sites on a solid surface and the temperature difference between the heat pipe wall and the working fluid. The temperature difference, or superheat, governs the formation of bubbles and can typically be defined in terms of the maximum heat flux as (PETERSON, 1994)

$$Q = \left(\frac{k_{eff}}{T_w} \right) \Delta T_c \quad (4.42)$$

where k_{eff} is the effective thermal conductivity of the liquid-wick combination presented in Equation 4.17 and ΔT_c is the critical superheat, defined by Marcus (1972) as

$$\Delta T_c = \left(\frac{T_{sat}}{\lambda \rho_v} \right) \left(\frac{2\sigma}{r_n} - \Delta P_{c,max} \right) \quad (4.43)$$

where T_{sat} is the saturation temperature of the fluid and r_n is the critical nucleation site radius which, according to Kew e Reay (2006), ranges from 2.54×10^{-5} to 2.54×10^{-7} m for conventional metallic heat pipe case materials. The growth or collapse of a given bubble once established on a flat or planar surface is dependent on the liquid temperature and corresponding pressure difference across the liquid-vapor interface caused by the vapor pressure and surface tension of the liquid. By performing a

pressure balance on any given bubble and using the Clausius-Clapeyron equation to relate the temperature and pressure, an expression for the heat flux beyond which bubble growth will occur may be developed (CHI, 1976) and expressed as (PETERSON, 1994)

$$Q_b = \left(\frac{2\pi L_e k_{eff} T_v}{\lambda \rho_v \ln(r_i/r_v)} \right) \left(\frac{2\sigma}{r_n} - \Delta P_{c,max} \right) \quad (4.44)$$

where r_i is the inner radius of the heat pipe wall, and r_n is again the nucleation site radius.

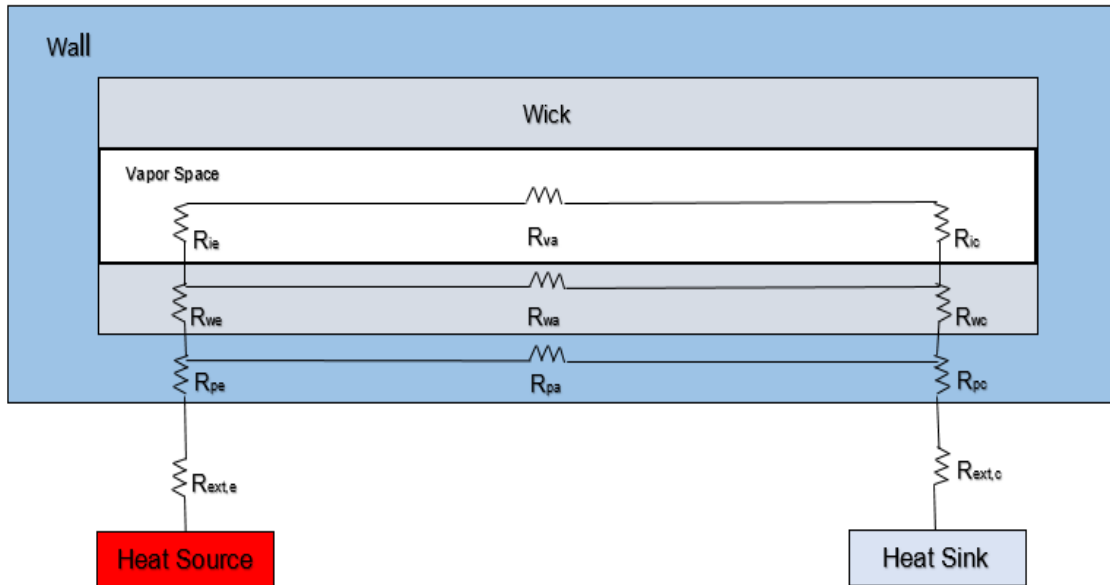
4.9 Heat pipe thermal resistance

The overall temperature difference between the heat sink and the heat source is an important characteristic for thermal control systems utilizing heat pipes. As the heat pipe is typically referred to as an overall structure of very high effective thermal conductivity, an electrical resistance analogy similar to that found in conduction heat transfer analysis is used. As the heat transfer occurs from the heat source to the heat sink, each part of the heat pipe can be separated into an individual thermal resistance. The combined resistances provide a mechanism to model the overall thermal resistance and the temperature drop from heat sink to heat source associated with the given heat input. Figure 4.7 illustrates the electrothermal analog for a simple cylindrical heat pipe. As shown, the overall thermal resistance is comprised of nine different resistances arranged in a series-parallel combination (PETERSON, 1994).

There are two other resistances shown in Fig. 4.7 that play a very important role in the design of heat pipes for electronic applications. These are the external, or contact, resistances occurring between the heat source and the heat pipe evaporator, $R_{ext,e}$, and the contact resistance occurring between the heat sink and the condenser, $R_{ext,c}$. In many applications, the combination of these two resistances will be of the same order of magnitude as the overall heat resistance (PETERSON, 1994).

Several simplifications can be made, because of the comparative magnitudes of the resistance of the vapour space and axial resistance of the pipe wall and the liquid-wick combinations, the axial resistance of both the pipe wall and the liquid-wick combination may be treated as open circuits and neglected. The comparative resistances, the liquid-vapour interfaces resistances, and the axial vapour resistance can,

Figure 4.7 - Overall thermal resistance of a heat pipe.



Source: Peterson (1994).

in most situations, be assumed to be negligible (CHI, 1976; PETERSON, 1994).

The radial resistances at the pipe wall can be computed from Fourier's law of heat conduction, for our purpose states that the flow of heat Q as a result of temperature difference, $(T_e - T_c)$, can be calculated by

$$Q = \frac{T_e - T_c}{R} \quad (4.45)$$

where R is the thermal resistance, which is defined by (Eq. 4.46) as for cylindrical heat pipes.

$$R_{p,e} = \frac{\ln(d_0/d_i)}{2\pi L_e k_p} \quad (4.46)$$

The most complicated and perhaps least understood of the resistances is the resistance of the liquid-wick combination. An expression for the equivalent thermal resistance in the evaporator of a heat pipe is:

$$R_{w,e} = \frac{\ln(d_i/d_v)}{2\pi L_e k_{eff}} \quad (4.47)$$

Expressions for the condenser would be similar.

The thermal resistance of the vapour flow, R_v is determined by [Chi \(1976\)](#)

$$R_v = \frac{\pi r_0^2 T_v F_v (1/6L_e + L_a + 1/6L_c)}{\rho_v \lambda} \quad (4.48)$$

where F_v is the vapour frictional coefficient and can be expressed by the Eq. [4.49](#) below:

$$F_v = \frac{(f_v Re_v) \mu_v}{2r_{h,v}^2 A_v \rho_v \lambda} \quad (4.49)$$

Considering some simplifications, [Chi \(1976\)](#) and [Peterson \(1994\)](#) developed a simplified analytical equation to predict the approximate overall thermal resistance for a cylindrical heat pipe as follows:

$$R_T = R_{p,e} + R_{w,e} + R_v + R_{p,c} + R_{w,c} \quad (4.50)$$

Summing all individual resistances [4.50](#) and the comparative magnitudes of the axial resistance of the pipe wall and liquid-wick combinations treated as open circuits may be neglected. The thermal conductance of the heat pipe is then estimated as:

$$G = \frac{1}{R_T} \quad (4.51)$$

The experimental results point to possible variations from heat pipe manufacturing standpoint, which affects heat pipe operation. Considering that the heat pipes were

manually manufactured, an adjustment factor was taken into account in the thermal conductance results in such a way that it can lead to a more accurate analysis of these possible variations. The adjustment factor is defined as follows

$$Factor = \frac{G_e}{G_{global}} \quad (4.52)$$

$$G_{global} = \alpha \frac{Q}{T_e - T_a} \quad (4.53)$$

where α is coefficient for global thermal conductance and can be varied from 0.5 until 3.5.

The calculated thermal conductance used in this study for each power applied to the heat pipe can be defined as:

$$G_C = \frac{1}{R_T} * Factor \quad (4.54)$$

With the consideration of the thermal conductance, it is expected that the calculated thermal conductance (theoretical) presents the same trends of the ones obtained experimentally. The calculated thermal conductances (theoretical), by the analysis of thermal resistances, do not consider important characteristics of an experiment, such as mounting characteristics for each heat pipe, volume of fluid filling each heat pipe, differences in the mesh of the porous structure inserted into each heat pipe, or even in the folding of the mesh for closing each heat pipe, etc. Therefore, adjustment factors for the thermal conductance calculated (theoretical) were considered for a better comparison with the results of the calculated and experimental thermal conductances.

The experimental results described in this study are based on the thermal conductance concept defined as follows:

$$G_E = \frac{Q}{T_e - T_c} \quad (4.55)$$

The errors found between G_E and G_C were determined by the equation below:

$$Error = \left(\frac{G_E - G_C}{G_E} \right) 100 \quad (4.56)$$

4.10 Uncertainties Analysis

The uncertainties on the experimental results were performed according to Moffat (1988). For tests regarding heat transfer, Moffat (1988) suggests that an uncertainty analysis must be performed by single-sample. Then, the effect of each measurement uncertainty on the calculated result if only that one measurement was in error, it would be

$$\Delta f_{x_i} = \frac{\partial f}{\partial x_i} \Delta x_i \quad (4.57)$$

The partial derivative of f with respect to x_i is the sensitivity coefficient for the result f , with respect to the measurement x_i . Although, when several independent variables are used in the function f , the individual terms are combined by root-sum-square method, as follows

$$\Delta f_{x_i} = \left[\sum_{i=1}^{\infty} \left(\frac{\partial f}{\partial x_i} \Delta x_i \right)^2 \right]^{1/2} \quad (4.58)$$

where this is the basic equation of single-sample uncertainty analysis. The accuracy of the thermocouples, voltage and amperage readings were approximately 0.3°C , 0.1V and 0.025A , respectively. The uncertainties of the applied voltage, electric current and the evaporator and condenser sections temperatures are considered in the evaluation of the thermal conductance uncertainty (Eq. 4.59), which yields

$$\Delta G = \left[\left(\frac{\partial G}{\partial V} \Delta V \right)^2 + \left(\frac{\partial G}{\partial I} \Delta I \right)^2 + \left(\frac{\partial G}{\partial T_e} \Delta T_e \right)^2 + \left(\frac{\partial G}{\partial T_c} \Delta T_c \right)^2 \right]^{1/2} \quad (4.59)$$

The overall uncertainty analysis given by Eq. 4.59 aims to present the cumulative errors generated during the evaluation of the experimental tests and their results, in order to assist a proper analysis for the better understanding of the heat pipes thermal behaviour.

5 EXPERIMENTAL PROGRAM

5.1 Introduction

Among the most used working fluids applied for heat pipes operating at mid-level temperatures, water has been chosen. This choice is due to its more favorable properties, such as high latent heat of vaporization, high surface tension, high thermal conductivity, good thermal stability and low viscosity. As water presents itself in the liquid phase at atmospheric conditions, its insertion in the heat pipe is a much simpler process when compared to other fluids. The selection of the working fluid must also be based on thermodynamic considerations, which are concerned with the various limitations to heat flow occurring within the heat pipe (KEW; REAY, 2006).

One of the most important goals in the industrial and aerospace areas is the two-phase capillary pumping system for thermal control. Depending on the application, thermal control devices such as heat pipes must be designed and fabricated respecting the characteristics of each application. Knowing the importance of the application of the technology of heat pipes in several segments, this study presents an experimental and development regarding the thermal performance of heat pipes using water as the working fluid, operating with power 25W, 50W, 75W, 100W and 125W and also power cycles, in the following inclination (tilt) angles: 0°, 30°, 60° and 90°. The maximum heat transport at mid-level temperature applications is limited by the capillary pressure that can be generated by the wick structure (FAGHRI, 1995). Therefore, capillary pressure and liquid pressure drop, vapour and liquid pressure drops were calculated for temperatures up to 160°C, which is the approximate temperature at which the heat pipes reached temperature stabilization at the highest power (125W) used in the experiments. For this investigation, 6 heat pipes were built similarly basically using 3 layers of each screen mesh selected, each heat pipe were built by using less conductive container (stainless steel) comparing to higher conductive container (copper), with 100, 200 and 400 mesh for stainless-steel heat pipes and with 100, 200 mesh for copper heat pipes.

5.2 Heat pipe design

The operation of a heat pipe is easily understood by using a cylindrical geometry. The components of a heat pipe are a sealed container, a wick structure, and a small amount of working fluid which is in equilibrium with its own vapor. The length of the heat pipe is divided into three parts: evaporator section, adiabatic section and condenser section. Heat applied to the evaporator section by an external source is

conducted through the pipe wall and wick structure, where it vaporizes the working fluid. The resulting vapor pressure drives the vapor through the adiabatic section to the condenser, where the vapor condenses, releasing its latent heat of vaporization to the provided heat sink (FAGHRI, 1995; PETERSON, 1994). The material selection and compatibility between wick and container as well as the working fluid are major factors in the design of heat pipes. Both copper heat pipes and stainless steel heat pipes present a good material compatibility level with water (KEW; REAY, 2006). For this study each heat pipe was designed with the characteristics as presented by Tab. 5.1 for heat pipes designed to use stainless steel and by Tab. 5.2 for heat pipes designed to use copper.

Methods of selecting heat pipes working fluid, wick structures, wick materials, and container materials have been developed in the chapter two. The procedure used to choose the geometric characteristics to determine the container and wick details so that the pipe will operate as specified is presented below:

- Pipe diameter was the first to be determined so that the vapour velocity is not excessive;
- Mechanical design was used to determine the container details;
- Wick details were designed considering the capillary limit;
- Other heat transport limits, i.e., entrainment and boiling limits, were checked to ensure that the pipe will operate within all limits.

Although heat pipes can be made of different cross-sectional shapes, the round shape is the most common configuration. Round tubes and pipes of many materials are readily available, and they are the most efficient configuration from the stress point of view. The size of the pipe diameter necessary for a given application should be determined so that vapour velocity is not excessive. Control of vapour velocity is required since at high Mach number the flow compressibility of vapour contributes to a large axial temperature gradient. For the heat pipes designed for this study its maximum Mach number in the vapour flow passage does not exceed 0.2. Under this condition, the vapour is considered incompressible and the axial temperature gradient negligibly small.

Table 5.1 - Characteristics of heat pipes HP1, HP2 and HP3

Characteristics of Experimental HP - Stainless steel			
	HP1	HP2	HP3
Evaporator/Adiabatic/Condenser/Total length, m	0.25/0.90/0.35/1.50		
Working fluid	Water		
Tube material	316L - Stainless steel		
Screen mesh material	316L - Stainless steel		
Outside diameter, m	0.0191		
Inside diameter, m	0.0135		
Screen mesh number	100	200	400
Number of screen mesh layer	3		
Wick porosity, %	0.68	0.64	0.61
Wick permeability, m^2	2.4E-10	5.1E-11	1.1E-11
Mean pore radius, m	1.27E-04	6.35E-05	3.18E-05
Liquid pressure drop, $N/m^2 - 160^\circ C$	5.81E+02	1.34E+03	2.82E+03
Vapour pressure drop, $N/m^2 - 160^\circ C$	4.28E+01	1.96E+01	8.47E+00
Normal pressure, $N/m^2 - 160^\circ C$	1.12E+02	1.15E+02	1.17E+02
Capillary pressure, $N/m^2 - 160^\circ C$	7.36E+02	1.47E+03	2.94E+03
Operating temperature range, $^\circ C$	24 - 160		
Operating power, W	25-125		

Source: Author.

Table 5.2 - Characteristics of heat pipes HP4, HP5 and HP6

Characteristics of Experimental HP - Copper			
	HP4	HP5	HP6
Evaporator/Adiabatic/Condenser/Total length, m	0.25/0.90/0.35/1.50		
Working fluid	Water		
Tube material	Copper		
Screen mesh material	Copper		316L - SS
Outside diameter, m	0.0191		
Inside diameter, m	0.01657		
Screen mesh number	100	200	200
Number of screen mesh layer	3		
Wick porosity, %	0.68	0.64	0.64
Wick permeability, m^2	2.4E-10	5.1E-11	5.1E-11
Mean pore radius, m	1.27E-04	6.35E-05	6.35E-05
Liquid pressure drop, $N/m^2 - 160^\circ C$	5.92E+02	1.33E+03	1.33E+03
Vapour pressure drop, $N/m^2 - 160^\circ C$	6,85E+00	1.59E+00	1.59E+00
Normal pressure, $N/m^2 - 160^\circ C$	1.37E+02	1.42E+02	1.42E+02
Capillary pressure, $N/m^2 - 160^\circ C$	7.36E+02	1.47E+03	2.94E+03
Operating temperature range, $^\circ C$	24 - 160		
Operating power, W	25-125		

Source: Author.

5.3 Limits for the heat pipes

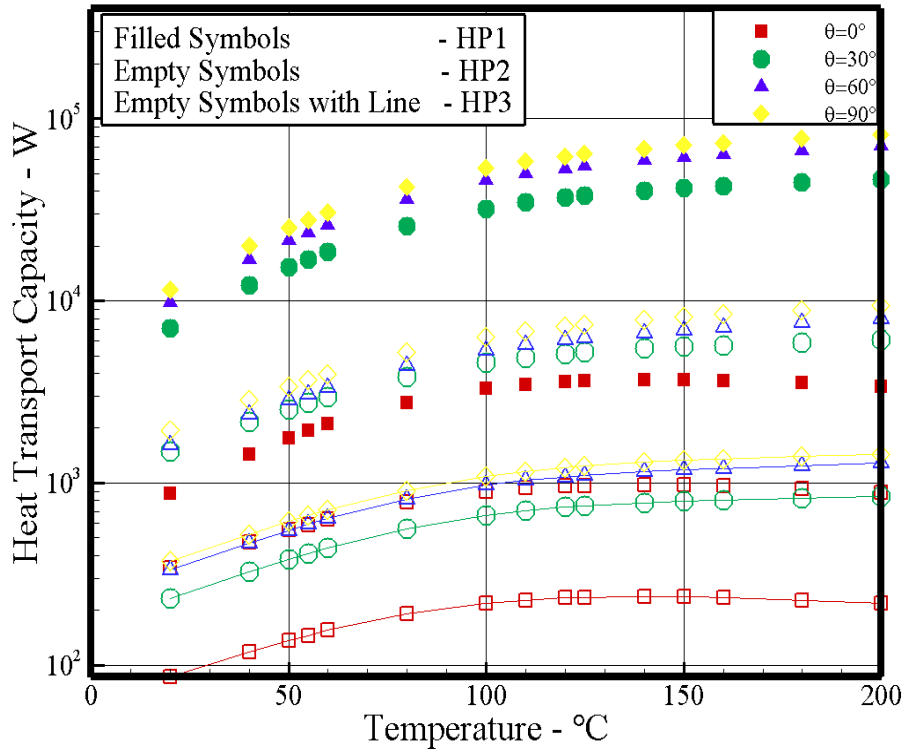
The methods and procedures for calculating the various operational limits of heat pipe have been presented in the previous Chapter. These procedures can be used to determine the performance limits and operational characteristics for a specific heat pipe as a function of the operating temperature. The type of limitation restricting the heat pipe transport capability of a heat pipe is determined by which limitation has the lowest value at the temperature under consideration. The magnitude of these different limitations is in turn dependent upon various properties of the working fluid, the wick structures, and the heat pipe dimensions. In other words, the rate of heat transport through a heat pipe is subject to a number of operating limits. Physical phenomena that might limit heat transport in heat pipes are due to capillary, sonic, viscous, entrainment and boiling. The heat transfer limitation can be any of the above limitations depending on the size and shape of the pipe, working fluid, wick structure, and operating temperature. The lowest limit among the five constraints defines the maximum heat transport limitation of a heat pipe at a given temperature.

Typically this procedure begins with estimation of the capillary limit, because the equations used to evaluate both the Reynolds number and the Mach number are functions of the heat transport capacity. The maximum heat transport capacity can be determined by substituting the values of the individual pressure drop and solving for the axial heat transfer. Once this values have been obtained, the axial heat transfer can be substituted into the expressions for the vapour Reynolds number and the Mach number to determine the accuracy of the original assumptions.

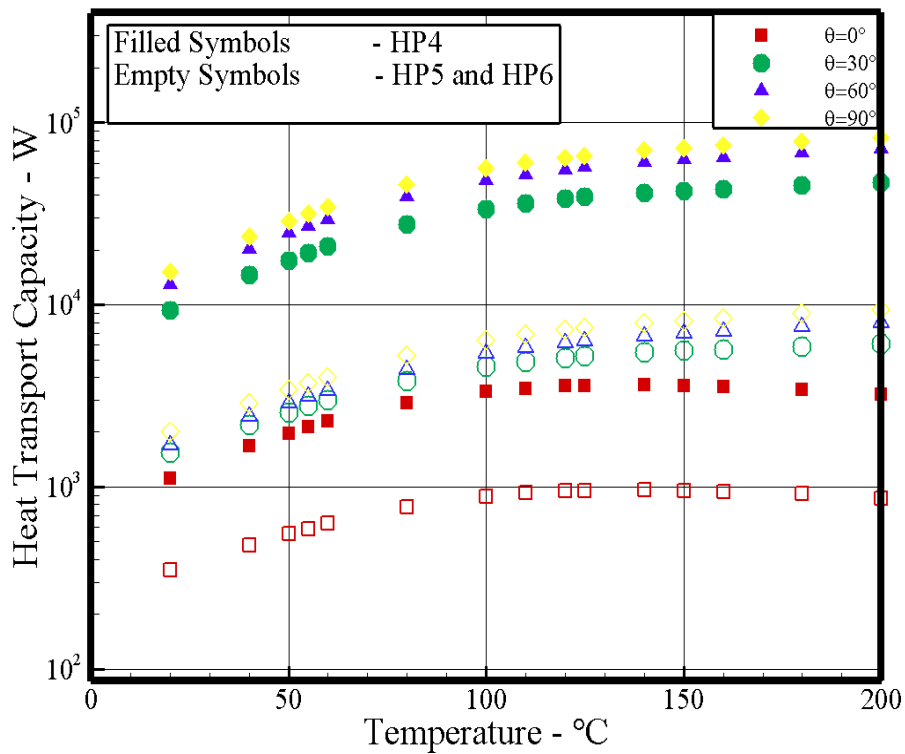
Wallin (2012) studied three working fluids, for the same operating temperature, and they have been evaluated with regard to the operation limitations. Water (used in this study) is best for most of the limits compared to methanol and acetone. Especially the capillary limit that is a measurement for the performance. The choice is therefore water as working fluid.

The heat pipe designer can calculate or compute the value of each of the operational limits as a function of temperature. The effects of tilt angle (evaporator elevated below the condenser) on the heat pipe performance with different mesh are presented in Fig. 5.1 where is illustrated the effects that the gravitational environment can have on capillary limit of heat pipes, but this is only one of the several limits encountered during the design and operation of heat pipes.

Figure 5.1 - Tilt angle on the heat pipes (a) HP1, HP2 and HP3, (b) HP4, HP5 and HP6



(a)

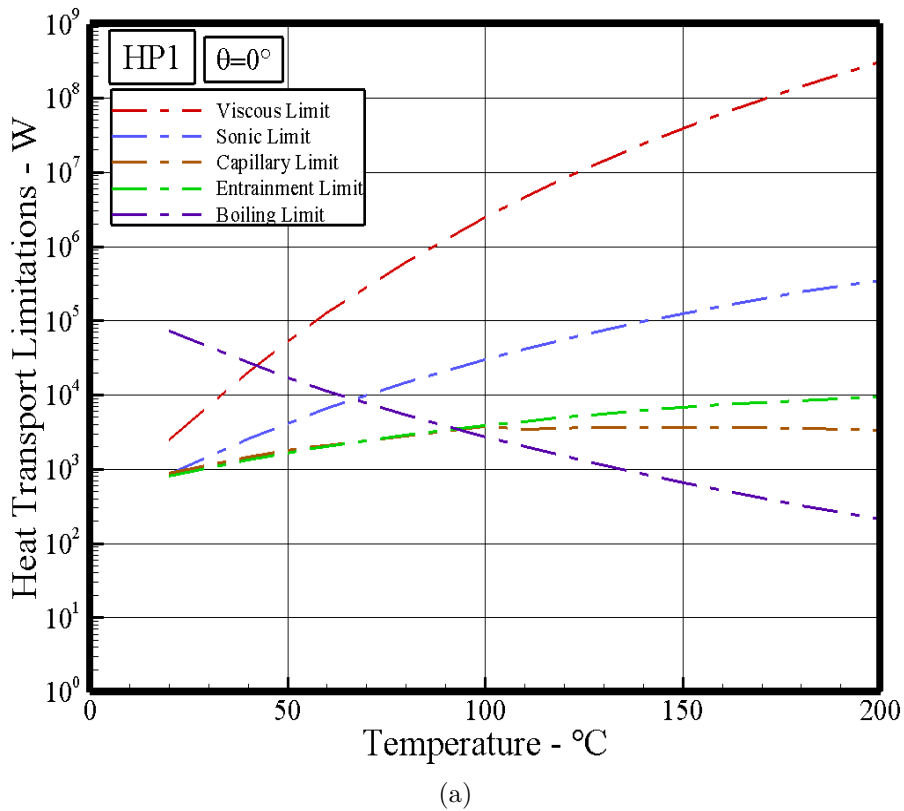


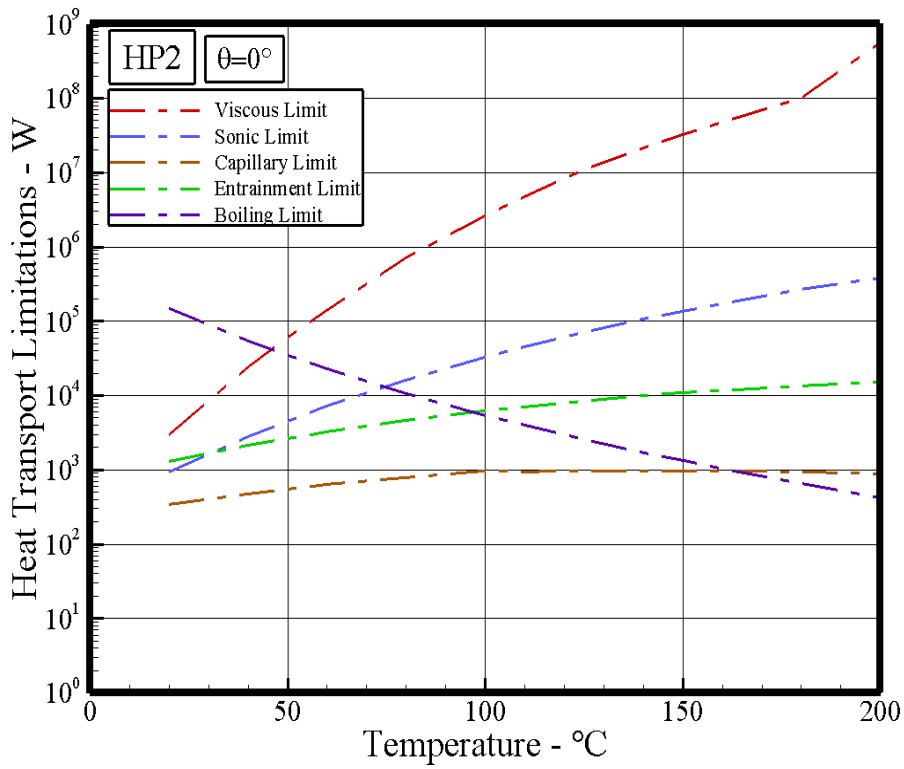
(b)

Source: Author.

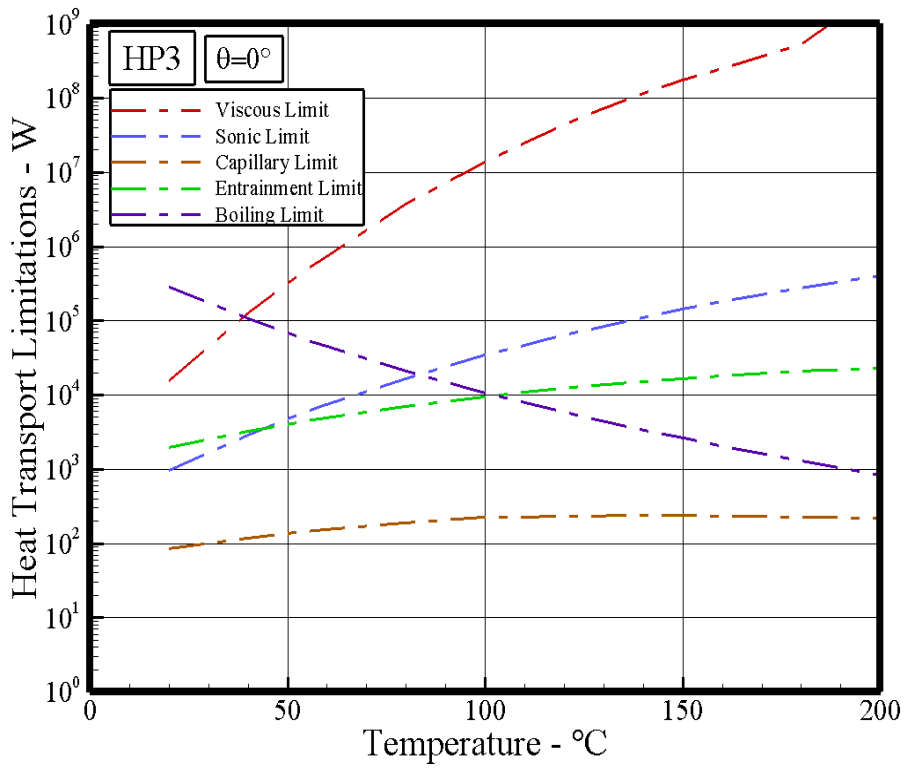
The individual performance limits defined and described in previous Chapter are presented in Fig. 5.2 for Stainless steel and Fig. 5.3 for copper in order to verify the potential of presenting any operation issues for the temperature range and power applied. This operational range defines the combination of temperature and axial transport capacities at which the heat pipe will work effectively. If at a given transport power the operating temperature is such that the power lies outside of this operational range, failure due to one of the limiting conditions will result. The five limits can be represented graphically as a function of the operating temperature, this configuration are capillary and boiling limited over the entire temperature range for the HP1, HP2 and HP4. The procedure for finding and estimating the maximum transport capacity as determined by the capillary limit for the HP3, HP5 and HP6 with the heat pipe operating at 0° .

Figure 5.2 - (a) HP1, (b) HP2 and (c) HP3.





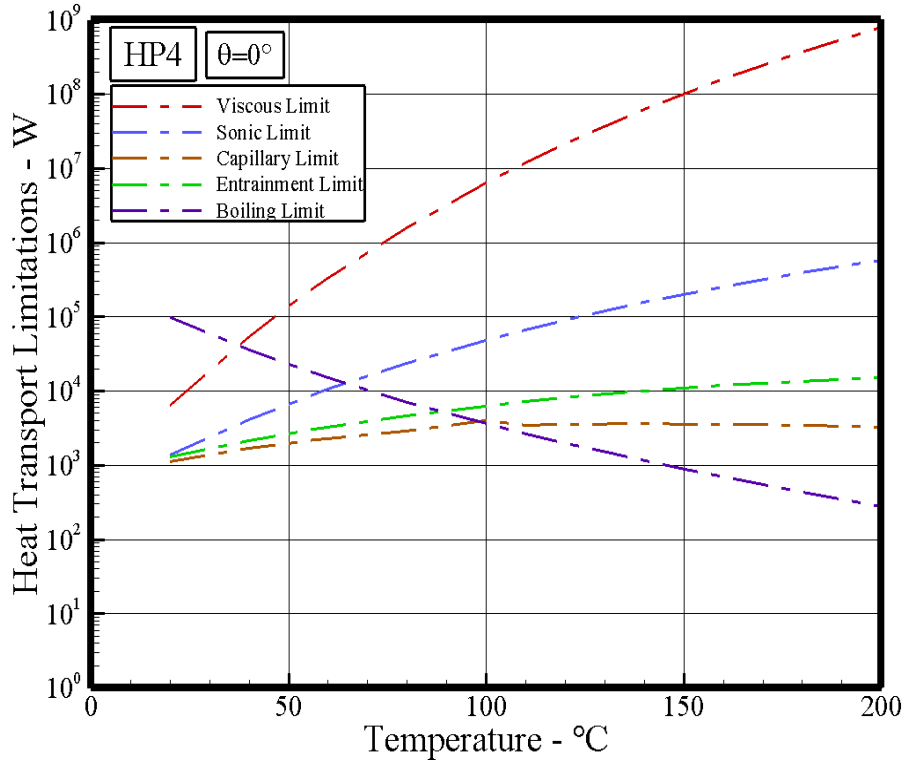
(b)



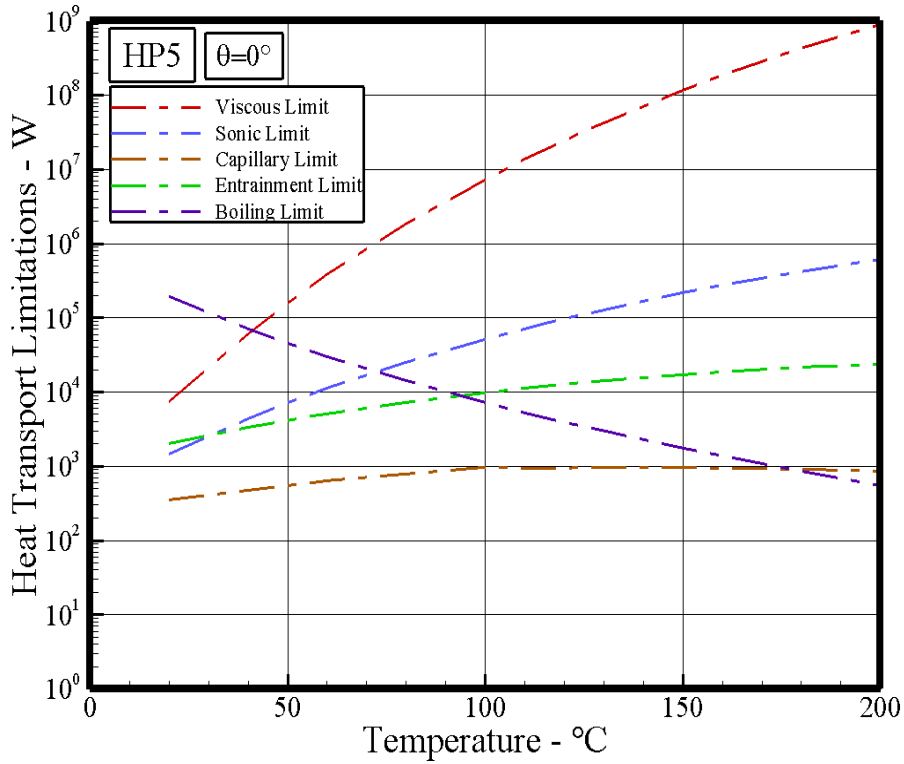
(c)

Source: Author.

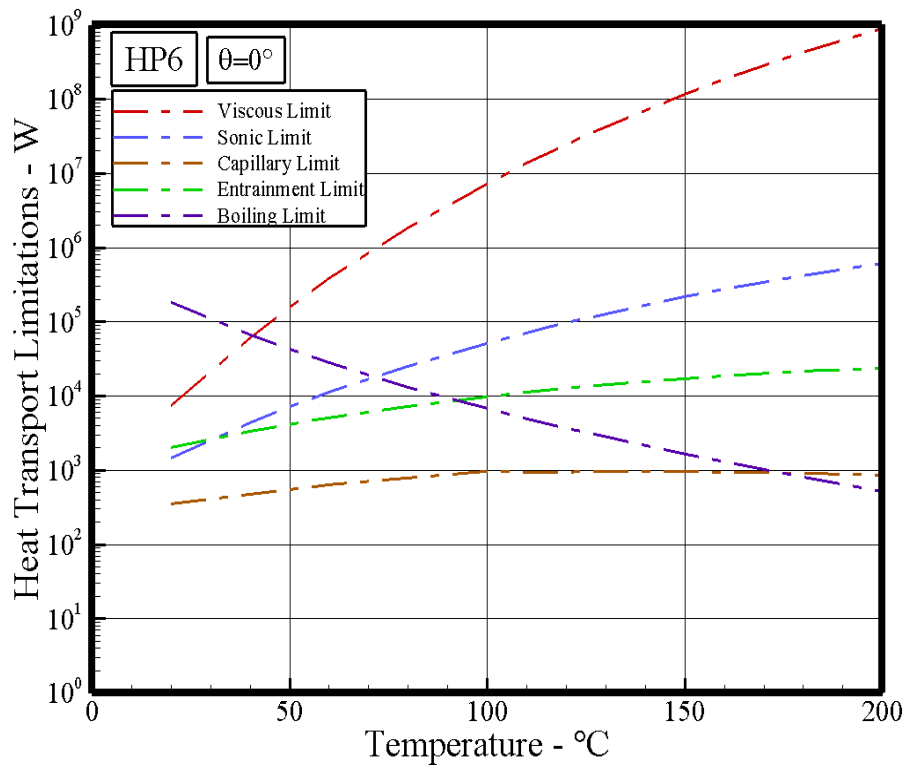
Figure 5.3 - (a) HP4, (b) HP5 and (c) HP6.



(a)



(b)



(c)

Source: Author.

5.4 Experimental Procedure

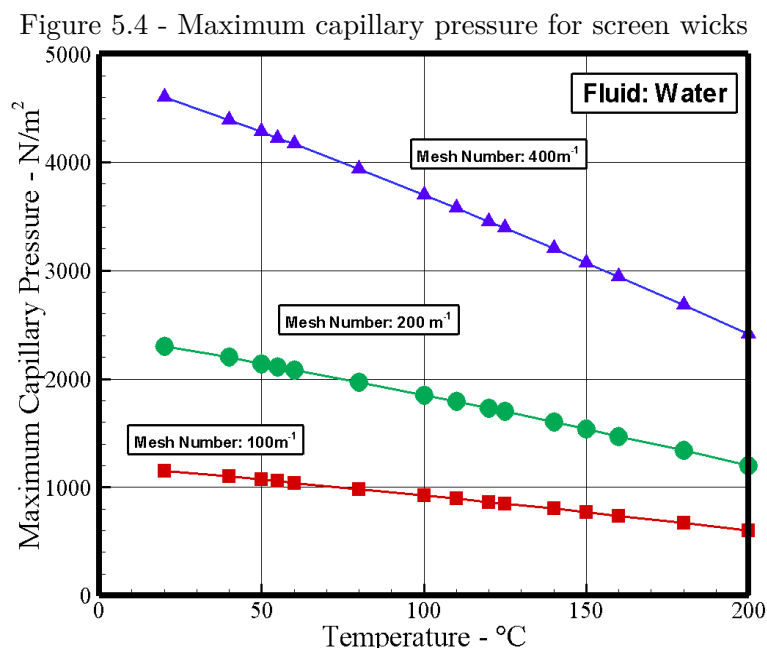
An experimental investigation was performed to verify which combinations of fluids, wick structures, wick materials, and container materials should first be selected before detailed design calculations are made. For this purpose, with the operating temperature known the selection process was made as follows:

- The working fluid was selected with the aid of Figs. 3.3 through 3.4. Working fluids with a large liquid figure of Merit transport are usually preferred.
- Appropriate wick structure was next determined. Screen wick of Fig. 3.5 was first considered for its low cost.
- Wick and container materials were then selected in order to be compatible with the working fluid. Table 3.2 shows some compatible fluid-material combinations.

5.4.1 Materials Selection

Materials were selected based on thermophysical and mechanical properties, manufacturing considerations, and supplier availability. Water was chosen as the working fluid due to its high liquid transport factor and its compatibility with container and wick materials.

Copper was selected for the container material due to its high thermal conductivity, its availability in a wide range of a standard sizes and its common use in mid level temperature heat pipes and stainless steel was selected based in its availability in a wide range of a standard sizes, and stainless steel-water heat pipes operating at mid-level temperature range represent one of the alternatives for several industry applications. Stainless steel and copper were selected in straight lengths to eliminate bending and straightening operations, thus ensuring excellent thermal contact between the wall and the wick. Stainless steel mesh (100, 200 and 400 mesh) and copper mesh (100 and 200 mesh) comprised the standard wick material, favored due to its thermal conductivity as well as its widespread use in heat pipe applications. Capillary pressures in heat pipes tend to be higher when the pores of wick structure go smaller as shown in Fig. 5.4. On the other hand, large pores are preferred for the liquid movement within the wick structure. Which means that wick structure mesh and pore dimensions aren't quite simple to be designed and indeed demand specific investigations depending on the applications.

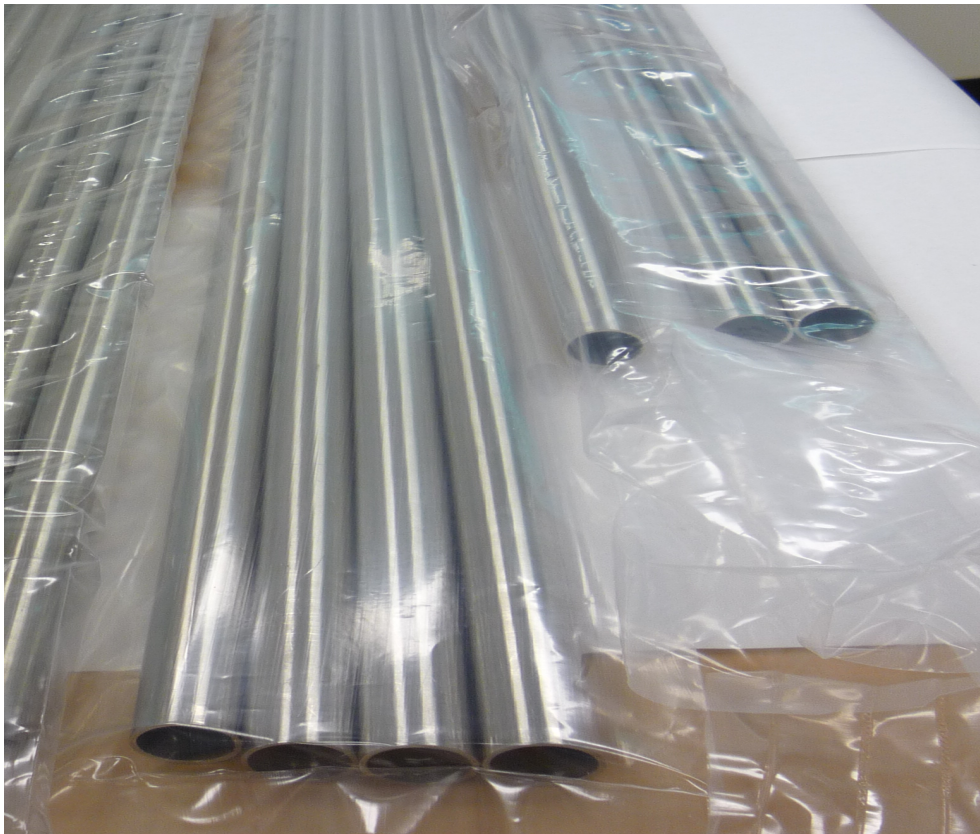


Source: Author.

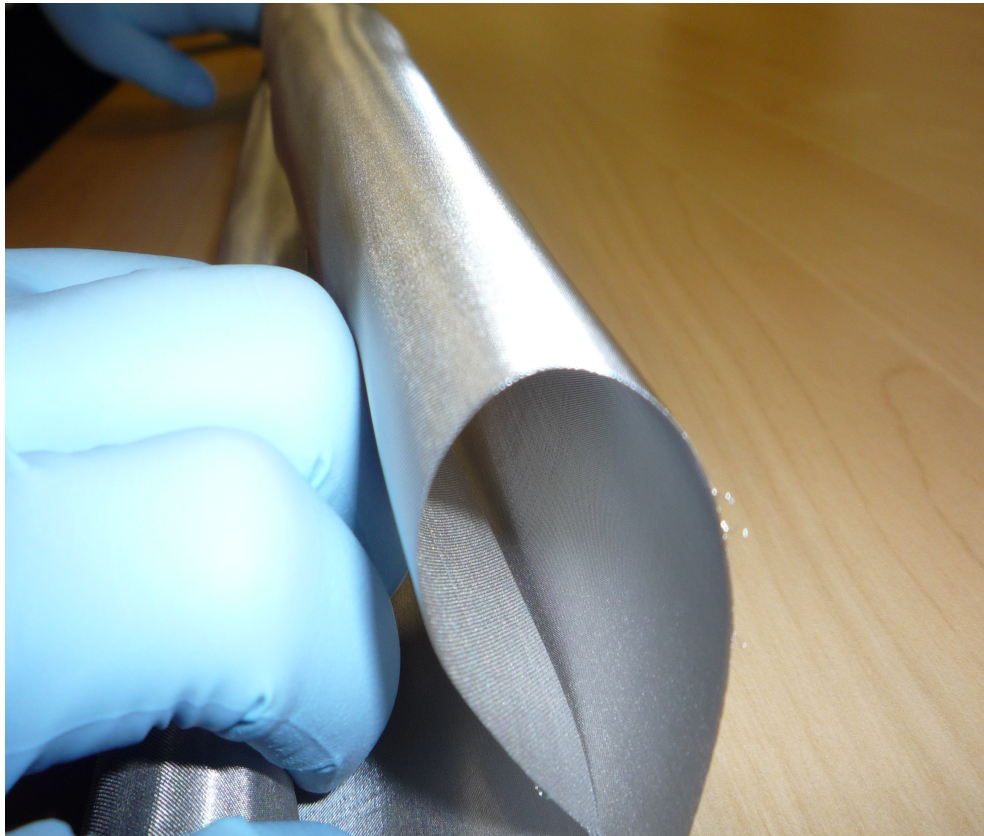
5.4.2 Cleaning and Fabrication Procedures

Fabrication issues in heat pipe construction range from techniques ensuring continuous connection of the wicking structure and maintaining adequate contact between the wick and the external case. This issues involving the fabrication and cleaning of the container and screen mesh wick used for the construction of the heat pipes were presented in Chapter 2. The fig. 5.5 illustrates the container material after the process of cleaning and the screen mesh wick before being inserted into the container.

Figure 5.5 - Container and screen mesh wick (a) Stainless steel container, (b) Stainless steel screen mesh wick



(a)



(b)

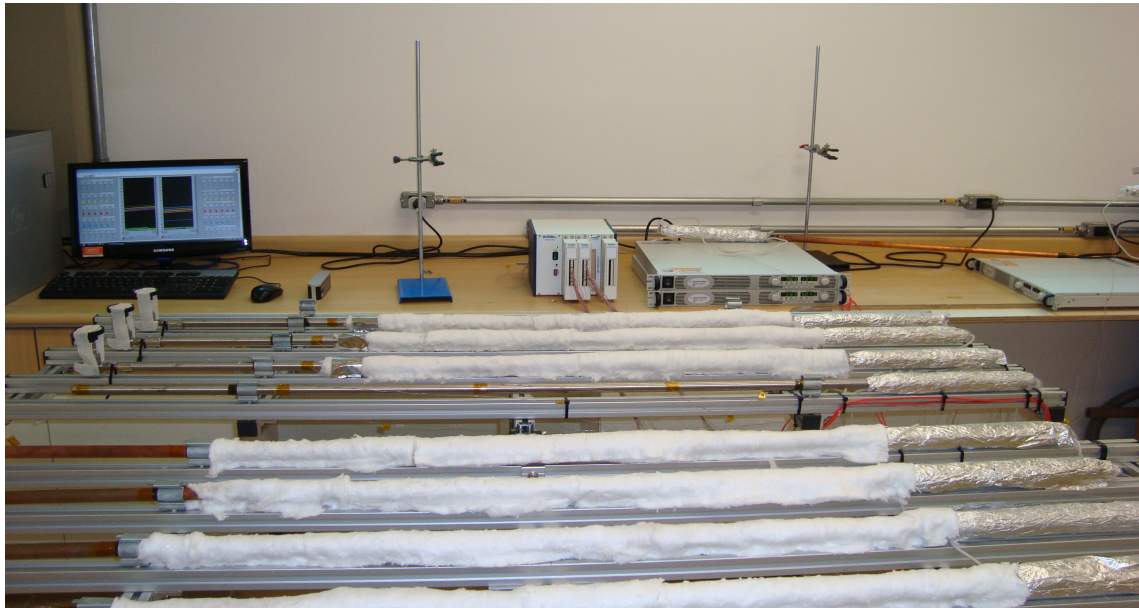
Source: Author.

One simple cleaning procedure is to use a mild acidic solution as a cleaning agent in conjunction with vigorous brushing. This should be followed by several thorough flushing and rinsing cycles with water for the copper material and the same for cleaning stainless steel materials to remove any iron or steel residue remaining from fabrication process. The wicking material has also undergone a preliminary cleaning procedure to eliminate oils, surface films, or oxide layers that may have formed during the fabrication or storage of the material. The wick was then fabricated and cut in appropriate size and shape. Once the initial shaping and cleaning process have been completed, the wicking structure can be inserted into the heat pipe container.

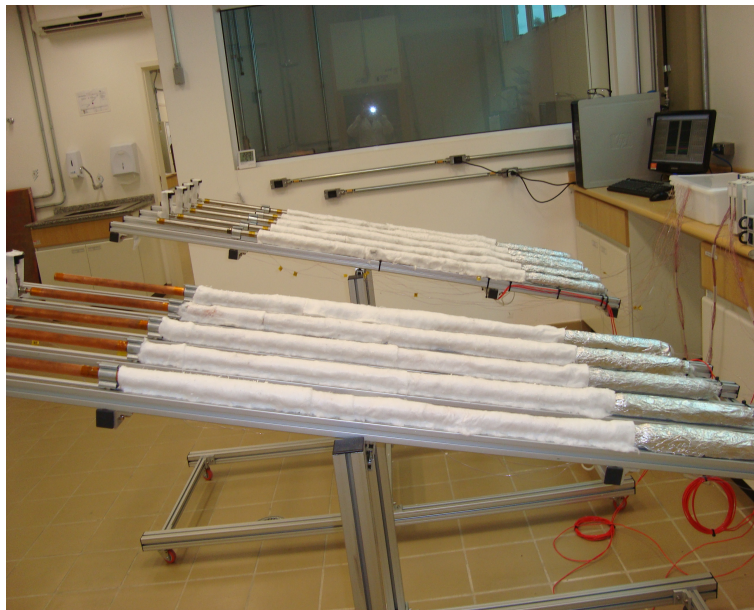
5.4.3 Test Apparatus and Instrumentation

For this experimental study, the heat pipes were built similarly to the schematics presented by Fig. 5.6 for the heat pipes operating at 0° (a) and operating at 30° , basically using 3 layers of each screen mesh. They were built according to numerical simulations performed with a proprietary computer code (RIEHL, 2002), which has

Figure 5.6 - Heat Pipes Experimental Bench (a) Experimental test rig 0°, (b) Experimental test rig 30°.



(a)



(b)

Source: Author.

been applied to several other projects over the years. The objective was to investigate the thermal behavior of each heat pipe using a less conductive container (stainless steel) comparing to higher conductive container (copper), upon applying the same wick materials.

The proposed experimental test rig comprises a test bench (see Fig. 5.6), a DC power controller (Agilent N5749A), and a National Instrument SCXI data acquisition system controlled by LabVIEW, as presented by Fig. 5.7(a). Six Omega T-type thermocouples with accuracy of $\pm 0.3^\circ\text{C}$ were used to measure the wall temperatures of each heat pipe in two locations of the evaporation, adiabatic and condenser sections (Fig. 5.7(b)).

Another thermocouple was used to measure the ambient temperature. All tests were performed under controlled room conditions, with the temperature set at $22^\circ\text{C} \pm 2^\circ\text{C}$. The condenser was open to the ambient air, exchanging heat by natural convection. Therefore, oscillations on the ambient temperature were expected due to the air conditioning on/off operation.

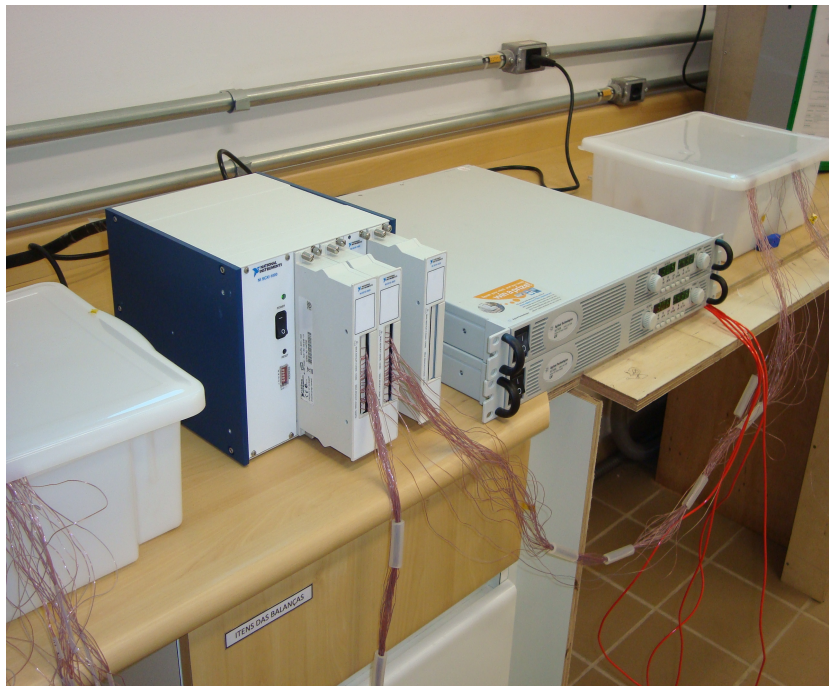
The heat source was a silicone flexible electric heater, being insulated by rock wool with the thermal conductivity of 0.04 W/mK , which was wrapped around the adiabatic section to reduce the heat loss to the surroundings. Prior to charging the heat pipes, they were properly cleaned and evacuated at a vacuum level of 10^{-5} mbar. Charging was only performed once the heat pipe was able to sustain such a vacuum level for at least 12 h. At this point, in the test procedure, it was made a pressurized verification test to determine if the joints, enclosures, and/or seams of the heat pipe case were appropriately sealed. This was best done by pressurizing the case using conventional leak testing equipment to check the case for leaks.

Deionized water was used as working fluid, which was outgassed prior to its insertion in the heat pipes, in order to guarantee that the working fluid was on its saturation condition with minimum content of dissolved gases that could be an issue for the noncondensable gas (NCG) generation. This choice is due to its more favorable properties, such as high latent heat of vaporization, high surface tension, high thermal conductivity, good thermal stability, and low viscosity. As water presents itself in the liquid phase at atmospheric conditions, its insertion in the heat pipe is a much simpler process when compared to other fluids. The selection of the working fluid must also be based on thermodynamic considerations, which are concerned with various limitations to heat flow occurring within the heat pipe (SARNO, 2012).

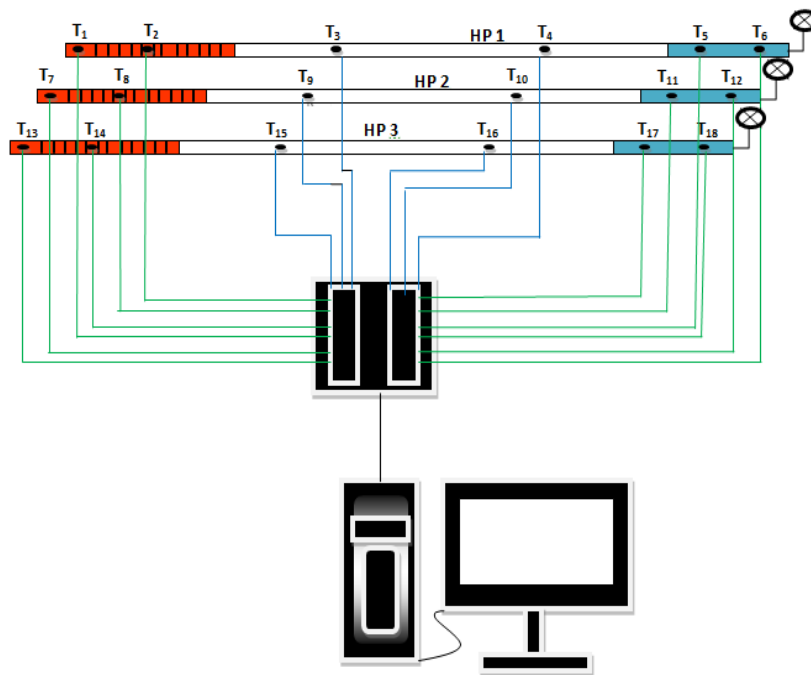
5.4.4 Aging Process

Each time heat pipes are manufactured, they need to undergo NCG testing in order to verify the manufacturing procedures involved such as cleaning, purification, charging etc. Therefore, this is a very important test that needs to be carried out

Figure 5.7 - (a) Data acquisition system and power controller, (b) Position of thermocouples on the heat pipes and data acquisition system.



(a)



(b)

Source: Author.

accordingly and without shortcuts. Once this test has been performed for a given batch of heat pipes (different models and sizes require independent NCG tests as well), the amount of NCG can be measured which is then flushed prior to the verification tests. It is clear that without doing this test sequence, NCGs will be in the heat pipes and will cause their failure by losing performance with time (RIEHL, c).

The test sequence usually accepted and established over the years of heat pipes manufacturing is as follows (RIEHL, c):

- The test is basically composed of a so-called "burn in", where a sample of a heat pipe from the same batch is submitted to a high temperature testing in order to accelerate the NCG production;
- After being charged and submitted to a bake-out procedure (3 to 4 hours in the oven at 150°C), the heat pipe is tested for performance at 20°C (when using water)
- Then, the heat pipe is installed at a rack with gravity orientation (evaporator below the condenser) and tested for 12 hours at 150°C ;
- Once this test is finished, the heat pipe is submitted for 30 days at 100°C of operation at the same orientation;
- As a final test, the heat pipe is submitted to a performance test at 20°C once again and the results are compared with the first one, in order to verify whether or not NCGs were present.

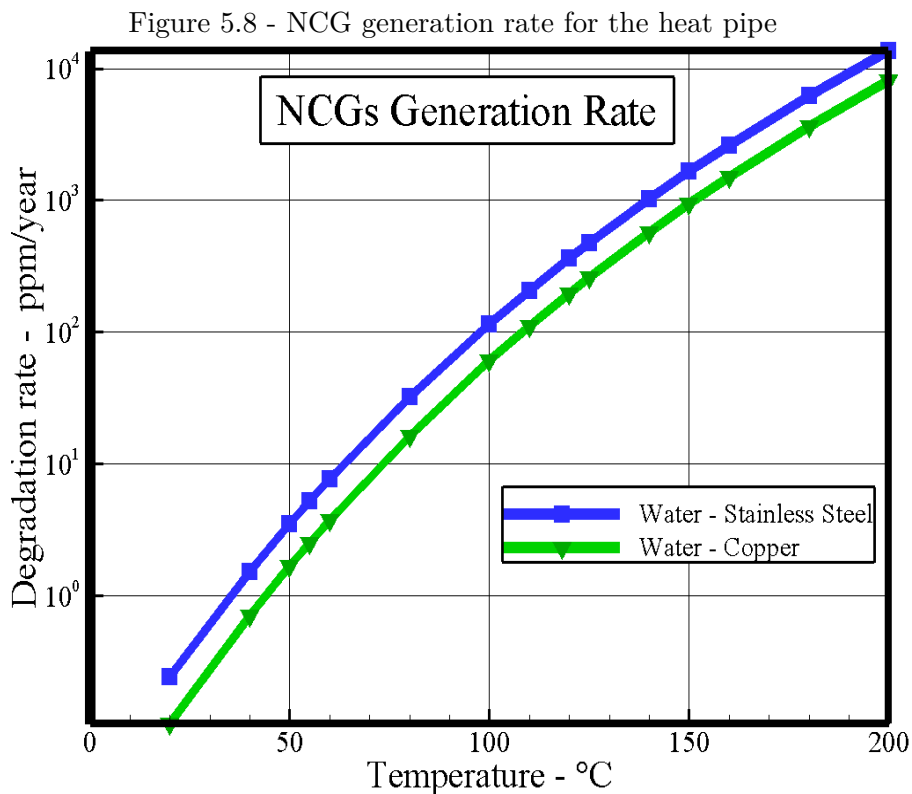
The volume of NCGs can be calculated for any working fluid and amount, which makes an important task to be considered during the manufacturing and testing of a given heat pipe batch. Although it is time consuming, such a procedure is extremely important to correct the final charge (guided by the final overall weight of the heat pipe) and to prevent malfunctioning due to excess to NCG present in the heat pipe (RIEHL, c).

Therefore, the following Arrhenius type equation (REYES et al., 1990; MUENZEL, 1978) can be applied for predicting the amount of NCG as

$$K = Ae^{\frac{-E_{act}}{RT}} \quad (5.1)$$

where K is the rate of decomposition, A is the pre-exponential factor, E_{act} is the activation energy of the reaction, R is the universal gas constant and T is the absolute temperature.

For the case of Water - Stainless Steel, $A = 0.023 \text{ s}^{-1}$ and $E_{act} = 70.000 \text{ J/mol}$ (YOSHIHARA; CAMPBELL, 1996; REYES et al., 1990) which leads to a decomposition rate at 20°C (293 K) of $7.75 \times 10^{-09} \text{ s}^{-1}$, which yields to $6.99 \times 10^{-4} \text{ ppm/day}$ and 0.244 ppm/year with a life time of approximately 14 years. For the Water - Copper, the $E_{act} = 72.000 \text{ J/mol}$ (YOSHIHARA; CAMPBELL, 1996; REYES et al., 1990) which leads to a decomposition rate at 20°C (293 K) of $3.41 \times 10^{-09} \text{ s}^{-1}$, which yields to $2.94 \times 10^{-4} \text{ ppm/day}$ and 0.107 ppm/year with a life time of approximately 18 years. The test can be accelerated once the temperature is increased, however, one should be careful regarding the maximum allowable temperature for a given working fluid in order to avoid explosions. Figure 5.8 shows the NCG generation rate for the stainless steel and copper heat pipes.



Source: Author.

5.4.5 Test Sequence for the Heat Pipes

After the heat pipes underwent the aging process to verify the NCG generation related to the manufacturing procedures, the laboratory tests could be conducted with the following procedures according to the parameters presented by Table 5.4 for power step and Table 5.5 for power cycle.

- The test bench with the heat pipes was placed in the following slopes: 0° , 30° , 60° and 90° , adjusted by a digital inclination measurement instrument in order to avoid any influence of the gravity force;
- The heat was applied to the evaporator by a controlled electric heater, being used the testing power steps and power cycles as presented by Tab. 5.3 of 25W, 50W, 75W, 100W and 125W per heat pipe;
- Heat was applied to each heat pipe to observe, at first, the start-up effect. Once the temperatures for the start-up power have reached stability (presenting variation of $\pm 1^\circ\text{C}$ during the last (20 minutes), the power was changed according to the testing profile, following the sequence to temperature stabilization. Once all power levels were tested, the power was switched off and waited for temperature equalization with the ambient.
- The first tests were conducted for the power step with inclinations from 0° to 90° , to verify the temperature stabilization under each power. After the tests with the power step were finished and the results verified, the tests were conducted out with the heat pipes operating with the power cycle where the objective with the power cycles investigation was to verify whether the heat pipes present a dry-out tendency in the evaporator, which could affect their performance and operation. The tests always starting with cycle 1 until cycle 5 for heat pipes operating the 0° to 90° . The duration of the experimental tests for this study was about 223 hours.

Table 5.3 - Applied power

Power Step	25W - 50W - 75W - 100W - 125W
Cycle 1	50W - 100W - 75W - 125W - 25W
Cycle 2	125W - 50W - 100W - 25W - 75W
Cycle 3	100W - 25W - 50W - 75W - 125W
Cycle 4	75W - 125W - 25W - 100W - 50W
Cycle 5	25W - 75W - 125W - 50W - 100W

Source: Author.

Table 5.4 - Schedule of tests realized with the heat pipes: power step

		Date	Test Time			Date	Test Time
Stainless Steel	0°	27Jan2011	8h37min	Copper	0°	27Jan2011	8h37min
	30°	19Jan2011	9h45min		30°	19Jan2011	9h45min
	60°	20Jan2011	9h53min		60°	20Jan2011	9h53min
	90°	25Jan2011	6h27min		90°	25Jan2011	6h27min

Source: Author.

Table 5.5 - Schedule of tests realized with the heat pipes: power cycles

Stainless Steel				Copper			
		Date	Test Time			Date	Test Time
0°	Cycle 1	24Mar2011	10h20min	0°	Cycle 1	24Mar2011	10h20min
	Cycle 2	06Apr2011	10h06min		Cycle 2	06Apr2011	10h06min
	Cycle 3	07Apr2011	10h13min		Cycle 3	07Apr2011	10h13min
	Cycle 4	12Apr2011	10h17min		Cycle 4	12Apr2011	10h17min
	Cycle 5	13Apr2011	10h10min		Cycle 5	13Apr2011	10h10min
		Date	Test Time			Date	Test Time
30°	Cycle 1	14Apr2011	10h07min	30°	Cycle 1	14Apr2011	10h07min
	Cycle 2	19Apr2011	10h05min		Cycle 2	19Apr2011	10h05min
	Cycle 3	25Apr2011	10h20min		Cycle 3	25Apr2011	10h20min
	Cycle 4	04Jul2011	08h08min		Cycle 4	04Jul2011	08h08min
	Cycle 5	05Jul2011	08h14min		Cycle 5	05Jul2011	08h14min
		Date	Test Time			Date	Test Time
60°	Cycle 1	06Jul2011	08h34min	60°	Cycle 1	06Jul2011	08h34min
	Cycle 2	07Jul2011	09h24min		Cycle 2	07Jul2011	09h24min
	Cycle 3	08Jul2011	08h50min		Cycle 3	08Jul2011	08h50min
	Cycle 4	11Jul2011	09h09min		Cycle 4	11Jul2011	09h09min
	Cycle 5	13Jul2011	09h04min		Cycle 5	13Jul2011	09h04min
		Date	Test Time			Date	Test Time
90°	Cycle 1	14Jul2011	09h18min	90°	Cycle 1	14Jul2011	09h18min
	Cycle 2	15Jul2011	09h01min		Cycle 2	15Jul2011	09h01min
	Cycle 3	18Jul2011	08h53min		Cycle 3	18Jul2011	08h53min
	Cycle 4	20Jul2011	09h40min		Cycle 4	20Jul2011	09h40min
	Cycle 5	21Jul2011	08h28min		Cycle 5	21Jul2011	08h28min

Source: Author.

6 EXPERIMENTAL RESULTS AND DISCUSSION

In this study, the heat transfer characteristics of heat pipes with screen mesh wick were analyzed. The wall temperature heat pipe at different positions was measured. The average wall temperature of the heat pipes at their evaporator, adiabatic and condenser sections at different heat inputs were acquired in order to verify their thermal performance, specially when operating in cycles. With the conducted tests, it was possible to verify the temperature along the heat pipes length in order to obtain their profiles, be able to calculate the temperature difference between the evaporator and the condenser in order to obtain the lowest temperature difference between the ends of the heat pipes and calculate the thermal conductance for all heat pipes for different inclinations. The objective with the power cycles investigation was to verify whether the heat pipes presented a dry-out tendency in the evaporator, which could affect their performance and operation.

6.1 Stainless Steel Heat Pipes - 0° of inclination

6.1.1 The effects of input heat

The effect input on the thermal performance of the heat pipe was examined by charging the system with 62.5 ml of water and slowly increasing the heat input. This corresponds to roughly 30% of the total volume of the heat pipe. This amount of fluid is enough to saturate the entire evaporator section. The first results are presented for the heat pipes operating without inclination, so that they could all be verified at the same operating condition. The oscillations observed during the start-up process can be considered normal when water is used as working fluid, also the effects regarding the meniscus formation and equilibrium between the evaporation and condensation process must be generated in the interface. Once the equilibrium is established, the heat pipes reaches a more stable operation with small or even without oscillations of applied heat to the evaporator.

The temperature profiles to evaluate their thermal performance for all power levels are shown by Fig. 6.1. Typically, the temperature of the outer wall of a heat pipe's adiabatic section is selected as the parameter to study the response time since it shows the status of the heat pipe. This temperature is also used as the saturated vapor temperature to determine the operating pressure of the heat pipe.

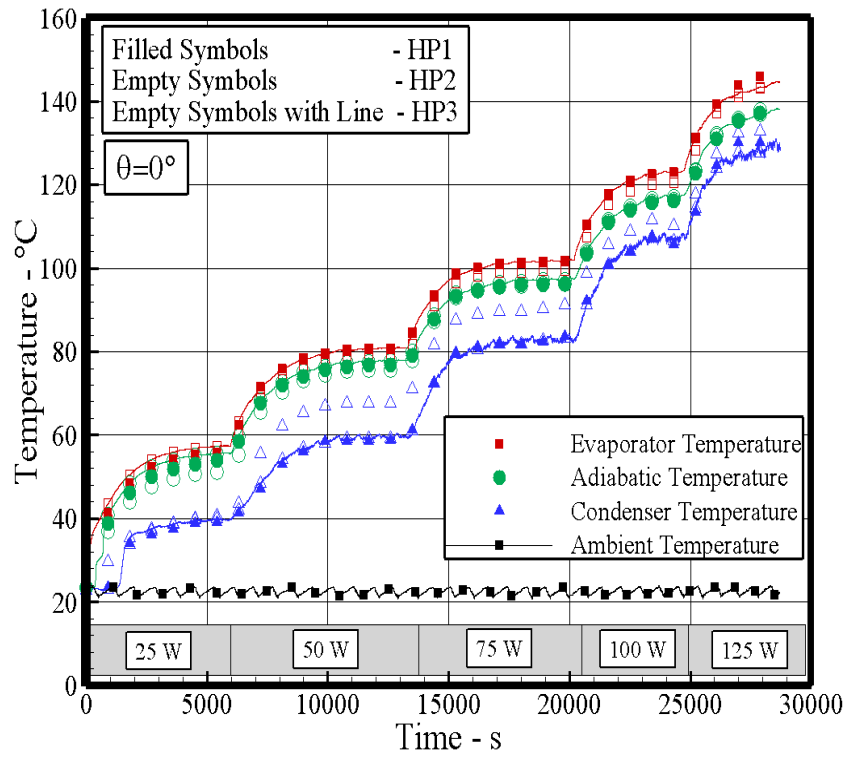
First, to verify the operation functionality of the heat pipes the power step test was realized (Fig 6.1(a)). This test was carried out to evaluate the temperatures reached

at each power applied at the moment of the start-up and of temperature stabilization, to obtain an initial analysis regarding their heat pipe transport capacity, and observe the behaviour of the evaporator in the change of each power step applied. As the heat flux increases in the evaporator wall and the liquid (porous structure) that is in contact with the evaporator wall can progressively overheat and form bubbles at the nucleation sites. These bubbles can carry energy to the surface by latent heat of vaporization. With increasing heat flux, a critical value can be reached and dry-out of the porous structure that will potentially interrupt the operation of heat pipes. After the test with the power step, tests were carried out with the power cycles (Fig. 6.1(b)) for analysis of thermal performance of heat pipes. It was possible to verify the temperatures along the heat pipes to obtain the temperature profile for Cycle 2, being this one the most critical one, where the heat pipes have had their start-ups with the highest power of 125 W.

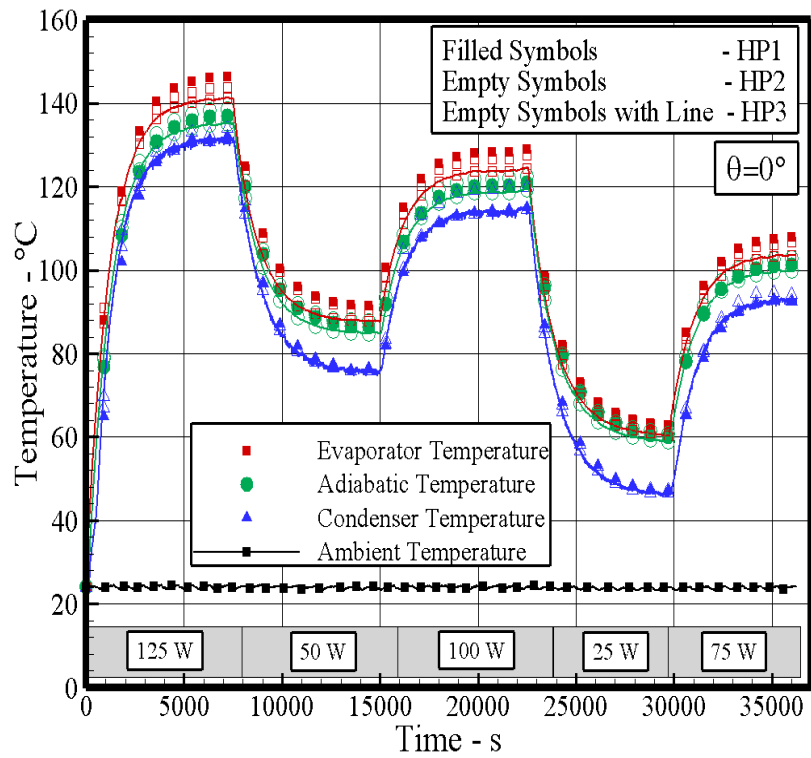
The largest temperature difference between the evaporator and the condenser of approximately 23.35°C was presented for HP3 at 50W of applied power, when operating in power steps. The lowest temperature difference was 6.5°C for the HP2 operating at 125W when the heat pipes were operating at power cycle 2. The HP2 showed in all tests a smaller temperature difference between the evaporator and the condenser when compared to HP1 and HP3, for the highest applied power (125W). The small temperature difference between the two section is the results of the effects of axial conduction in both the wall and wick regions. The wall surface temperature at the evaporator is higher than the vapour temperature since the heat must be conducted through the heat pipe wall and wick to the wick-vapour interface. At the condenser, a lower temperature is observed at the outer surface as heat must be rejected from the wick-vapour interface to the heat sink.

The temperature difference decreased with increasing power in all the tests performed. For power cycle (for power of 100 and 125 W) the HP2 obtained the smallest temperature difference between the evaporator and the condenser due to the behavior of the fluid in the evaporation section. For the same power applied, and for the same heat pipes, different stabilization temperatures were obtained due to the greater or smaller amount of liquid in different parts of the evaporator, at the beginning of each performed test.

Figure 6.1 - Temperature profiles of HP1, HP2 and HP3: (a) Power Step, (b) Power Cycles by Table 5.3.



(a)



(b)

Source: Author.

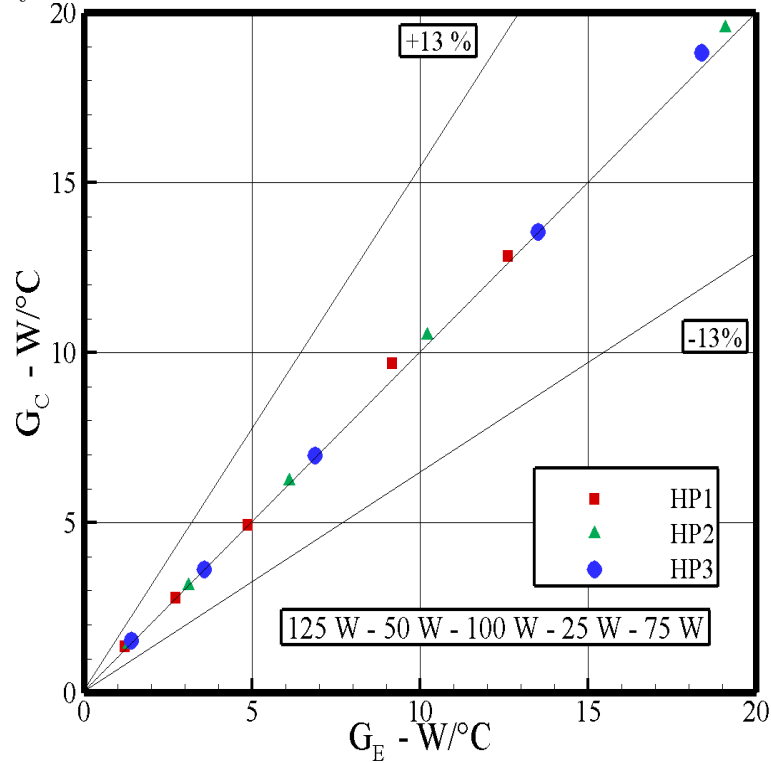
For the improved analysis, the experimental thermal conductance of the heat pipe was calculated by Eq. 4.55 and compared with the calculated thermal conductance (Eq. 4.54), which considers an adjustment given by the variable factor that involves the uncontrolled variables that are inherent to the manufacturing processes of the heat pipes. The calculated thermal conductance was introduced in the thermal resistance analysis (Eq. 4.51) along with the adjustment factor (Eq. 4.53) for each applied power, and the results of this comparison are presented by Fig. 6.5. The results show a good correlation between the experimental and calculated results, which demonstrated that the adjustment factor was effective in consideration of the differences present during the heat pipes manufacturing processes. The proposed calculated thermal conductance, with the adjustment factor, correctly predicted the increase in thermal conductance with the increase in the heat input and the same has been validated experimentally.

The highest experimental thermal conductance obtained with the heat pipes was for the HP1 of $12.60W/^{\circ}C$, by HP2 of $19.10W/^{\circ}C$ and by HP3 of $18.40W/^{\circ}C$ for cycle 2 Fig 6.2 and $12.84W/^{\circ}C$ - HP1, $19.54W/^{\circ}C$ - HP2 and $18.80W/^{\circ}C$ - HP3 for the calculated thermal conductance (theoretical thermal conductance x adjustment factor). Therefore, upon analyzing previous (SILVA et al., 2015) and current results, similarity in the temperature and heat transfer patterns were expected. Thus, the results presented here are related to several series of tests for the sake of comparing the heat pipes performances and checking their life time reliability as well. In this specific case, the heat pipes have presented similar thermal behavior over time, as presented by the results. The heat pipes HP2 and HP3 showed better thermal performance due to smaller pore size, lower porosity and permeability and higher capillary pressure. The heat pipe HP3, by its design characteristics, presented better ability to carry heat in relation to the other heat pipes except for the powers 100 and 125 W. The theoretical thermal conductances presented results of approximately $9.6W/^{\circ}C$ for the HP1, $15.5W/^{\circ}C$ for the HP2 and $23.0W/^{\circ}C$ for the HP3.

The results of the calculated thermal conductances did not take into account the applied powers and the power cycles used at each stage of the operation. For this, a different adjustment factor was calculated for each power in each test performed (power step or power cycles) for the three heat pipes tested. Different adjustment factors were required to correlate the calculated thermal conductances to the experimental thermal conductances within the calculated experimental error. For the tests performed with the heat pipes, when operated in power steps the adjustment factor ranged from 0.13 to 0.80 for HP1, 0.10 to 0.77 for HP2 and 0.05 to 0.34 for

HP3. In the case of heat pipes operating in power cycles, the adjustment factor ranged from 0.15 to 1.34 for HP1, 0.09 to 1.25 for HP2 and 0.07 to 0.82 for HP3. The tables 6.1- 6.3 present results for the best thermal performance of the heat pipes. The results are presented for experimental thermal conductance, factor of adjustment, calculated thermal conductance and error presented by the conductances by the Eq. 4.56.

Figure 6.2 - Thermal conductance experimental x calculated for HP1, HP2 and HP3: Cycle 2 by Table 5.3.



Source: Author.

Table 6.1 - Thermal performance for the HP1 operating with power cycles - Cycle 2

Power	G_E	adjustment factor	G_C	Error
25W	1.21W/°C	0.15	1.36W/°C	±12.5%
50W	2.72W/°C	0.30	2.77W/°C	±1.9%
75W	4.87W/°C	0.52	4.92W/°C	±1.2%
100W	9.17W/°C	1.01	9.68W/°C	±5.5%
125W	12.60W/°C	1.34	12.84W/°C	4±1.7%

Source: Author.

Table 6.2 - Thermal performance for the HP2 operating with power cycles - Cycle 2

Power	G_E	adjustment factor	G_C	Error
25W	1.31W/°C	0.09	1.41W/°C	±7.3%
50W	3.10W/°C	0.20	3.14W/°C	±1.1%
75W	6.10W/°C	0.40	6.21W/°C	±1.9%
100W	10.20W/°C	0.67	10.50W/°C	±2.8%
125W	19.10W/°C	1.25	19.54W/°C	±2.4%

Source: Author.

Table 6.3 - Thermal performance for the HP3 operating with power cycles - Cycle 2

Power	G_E	adjustment factor	G_C	Error
25W	1.41W/°C	0.07	1.53W/°C	±8.4%
50W	3.57W/°C	0.16	3.62W/°C	±1.5%
75W	6.88W/°C	0.31	6.98W/°C	±1.5%
100W	13.51W/°C	1.60	13.55W/°C	±0.3%
125W	18.40W/°C	1.82	18.80W/°C	±2.3%

Source: Author.

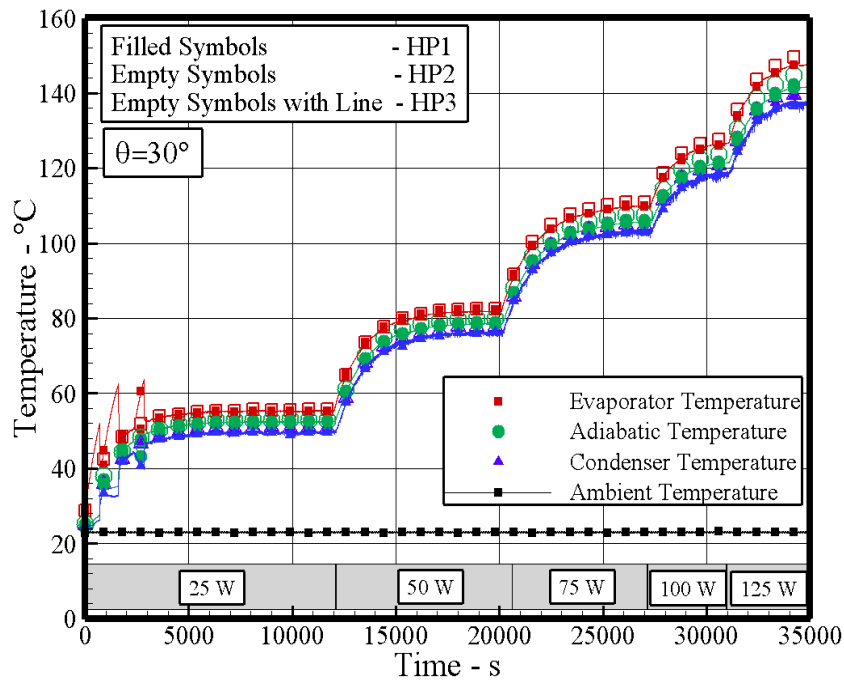
6.2 Stainless Steel Heat Pipes - 30° of inclination

6.2.1 The effects of input heat

With the conducted tests, it was possible to verify the temperature along the heat pipes operating at 30° of inclination in order to obtain their profiles and the heat transfer characteristics. However all three heat pipes presented stable operation and temperature profiles to evaluate their thermal performance for all power levels as shown by Fig. 6.3 for heat pipes operating in power steps and by Fig. 6.4 for heat pipes operating in power cycles. The oscillations observed during the start-up process can be considered normal when water is used as working fluid, also the effects regarding the meniscus formation and equilibrium between the evaporator and condenser process must be generated in the interface. Since that the equilibrium is established, the heat pipe reaches a more stable operation with small or even without oscillations of the applied heat to the evaporator. The largest temperature difference between the evaporator and the condenser of approximately 23.7°C was presented for HP1 at 75 W when operating in power cycle (cycle 5). The HP1 heat pipe showed a lower temperature difference operating at power steps. For the

power of 25 W it showed a difference of 4.8°C and for the higher power (125 W) a temperature difference of 8.3°C between the evaporator and the condenser. The lower temperature difference between the ends of the HP1 was caused mainly by the larger pore radius and higher permeability, thus the return of the liquid to the evaporator with greater ease and better capacity of heat transport for all powers tested. The HP2 obtained lower temperature difference between the ends operating with Cycle 2 of 8.3°C and HP3 presented for Cycle 1 of 8.0°C for the higher power used in the experimental tests of 125 W.

Figure 6.3 - Temperature profiles of HP1, HP2 and HP3 for power step.

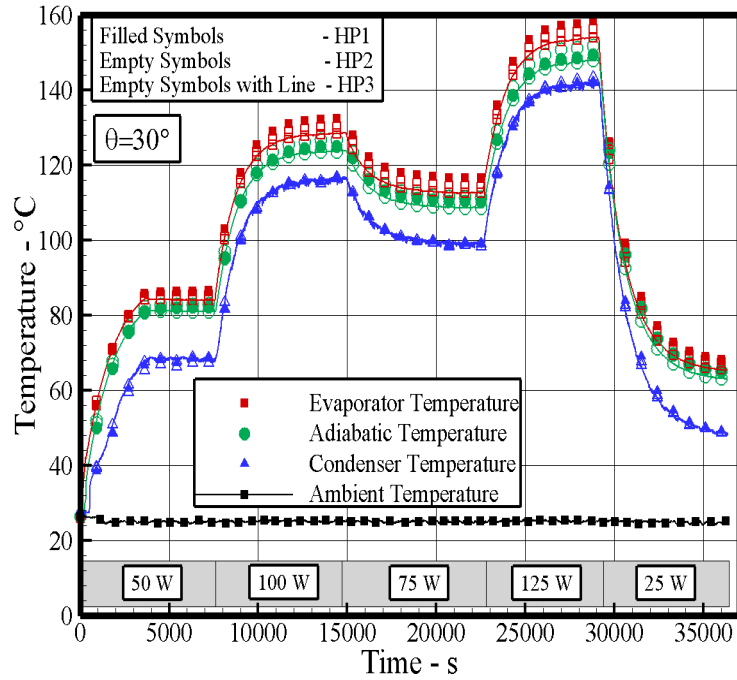


Source: Author.

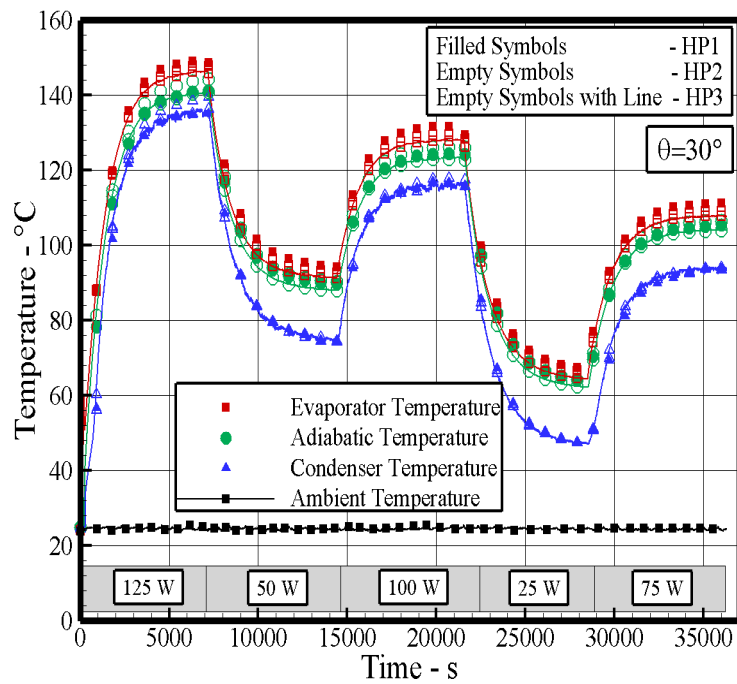
This behavior discussed above for heat pipes operating with power steps can lead us to at least two parameters that affect heat pipe operation: liquid flow resistance and capillary pumping. The liquid flow is inversely proportional to the square of mesh size in wick structure and capillary pumping pressure is inversely proportional to mesh size. Thus, by comparing HP1 that uses screen mesh number 100 to HP2 that uses screen mesh number of 200 and HP3 that uses screen mesh number of 400, the liquid flow resistance will be smaller for HP1 than liquid flow resistance in HP2 and HP3, so that the HP1 has a higher speed of liquid return from the condenser back to evaporator. In the same way, for HP2 and HP3 the liquid flow resistance is higher

than HP1 due to their smaller mesh size.

Figure 6.4 - Temperature profiles of HP1, HP2 and HP3: (a) Cycle 1 and (b) Cycle 2 by Table 5.3.



(a)

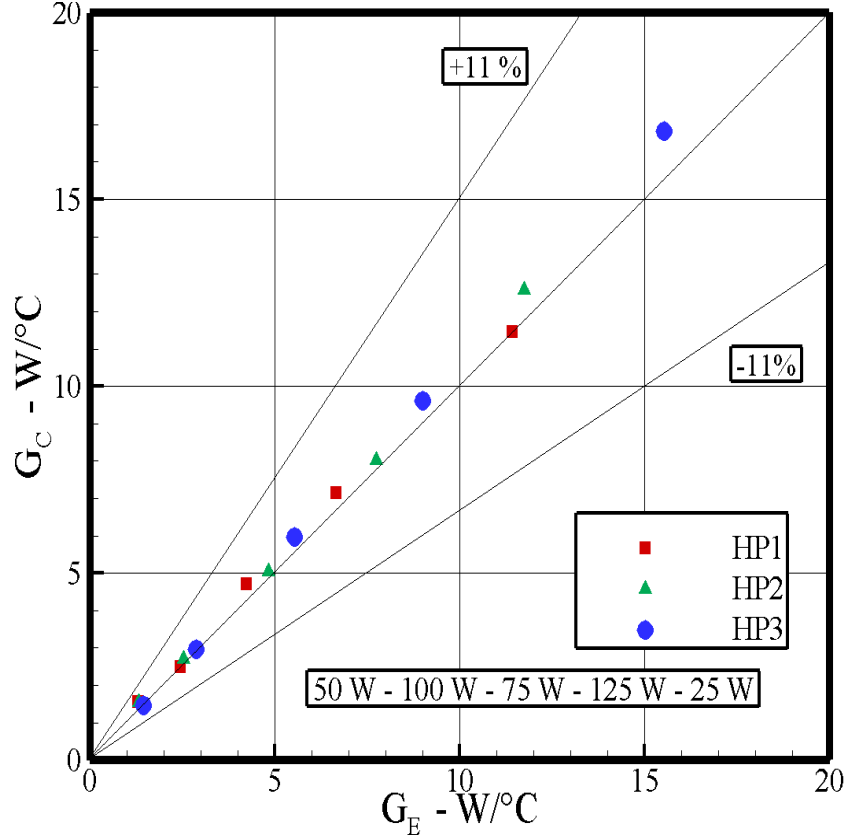


(b)

Source: Author.

The effect of the heat input on the thermal conductance is shown in Figure 6.5. The heat pipe has a smaller thermal conductance at lower heat inputs because more liquid resides in the evaporator. Additionally, as the input increases, the operating temperature and pressure of the heat pipe increases. This indicates that the vapor temperature drop along the length of the heat pipe is relatively small in comparison to the heat pipe operating temperature. The higher thermal conductance was obtained for HP3 operating with cycle 1 of $15.5W/^\circ C$ for the applied power of 125 W. The HP1 presented higher thermal conductance for all applied power levels except for power of 125 W as shown in Table 6.4 operating on power step.

Figure 6.5 - Thermal conductance experimental x calculated for HP1, HP2 and HP3: Cycle 1 by Table 5.3.



Source: Author.

For the tests performed with the heat pipes, when operated in power step the adjustment factor ranged from 0.60 to 1.56 for HP1, 0.31 to 0.90 for HP2 and 0.17 to 0.54 for HP3. In the case of heat pipes operating in power cycles, the adjustment factor ranged from 0.12 to 1.19 for HP1, 0.07 to 0.96 for HP2 and 0.06 to 0.73 for

HP3.

Table 6.4 - Thermal performance for the HP1 (power step) with the thermal conductance uncertainty of 11%

Power	G_E	adjustment factor	G_C	Error
25W	5.20W/°C	0.60	5.46W/°C	±5.0%
50W	9.10W/°C	0.97	9.16W/°C	±0.8%
75W	11.80W/°C	1.30	12.42W/°C	±5.2%
100W	14.10W/°C	1.49	14.36W/°C	±1.9%
125W	15.00W/°C	1.56	15.03W/°C	±0.2%

Source: Author.

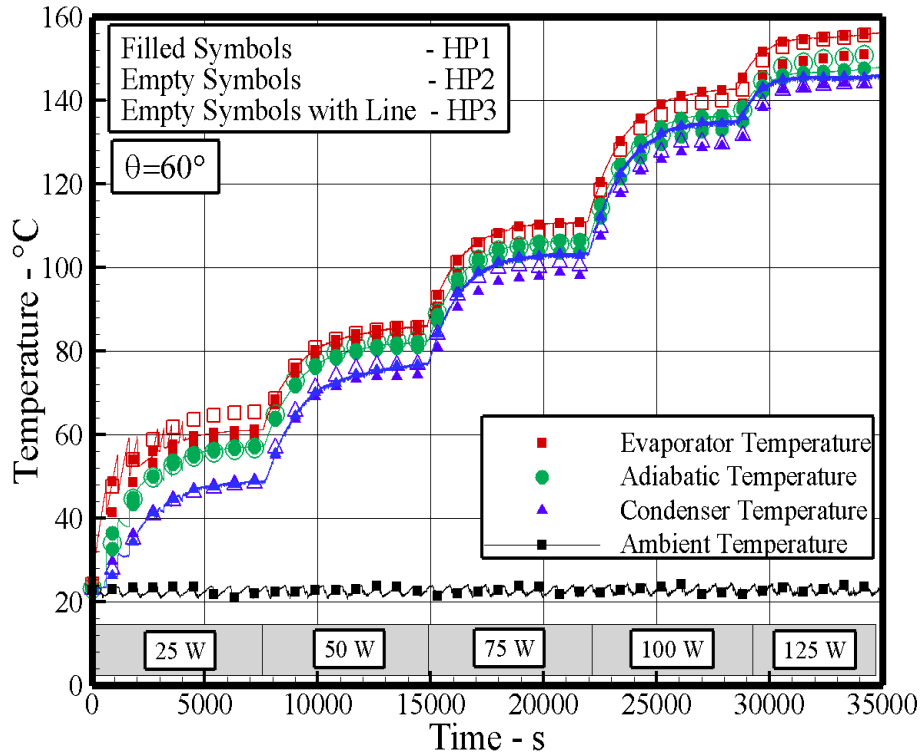
For HP1 the theoretical thermal conductance (8.0W/°C to 9.6W/°C) approached the experimental thermal conductance for the applied power of 50 W and was lower for the powers of 75W to 125W, with adjustment factors above 1.0 being required as shown in Table 6.4.

6.3 Stainless Steel Heat Pipes - 60° of inclination

6.3.1 The effects of input heat

The heat pipes operating at 60° showed oscillation during the stand-up for the powers of 25 W and 50 W in power step and power cycles. When the applied heat flux in the evaporator lead to boiling, vapor bubbles were produced in the evaporator which may have partially blocked the liquid flow coming from the condenser. The smallest temperature difference between the ends of the heat pipe was presented for HP1 operating on power step of 6.6°C for the power of 125 W. The HP2 obtained its best thermal performance when operating with cycle 1 with the temperature difference between the ends of 10.6°C and the HP3 operating in power step of 10.5°C. In the Figure 6.6 is shown the temperature profile for the heat pipes operating in power step where the lowest temperature difference between the evaporator and the condensate was obtained.

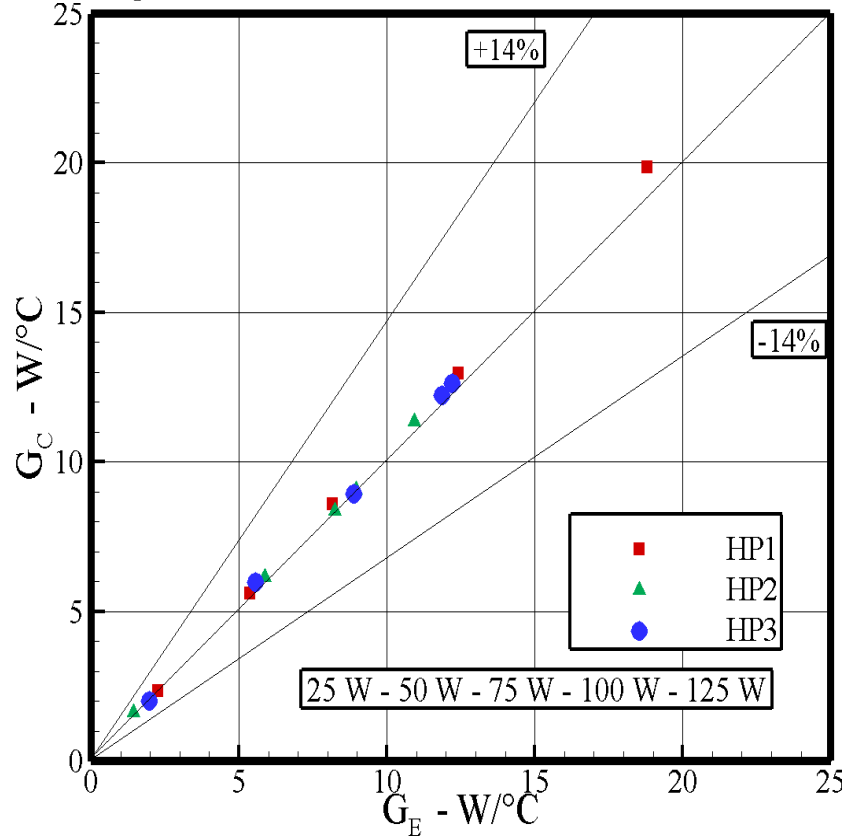
Figure 6.6 - Temperature profiles of HP1, HP2 and HP3 for power step



Source: Author.

The largest temperature difference between the evaporator and condenser of approximately 27.0°C was also presented for HP1 at 50 W when operating with cycle 3. The experimental thermal conductance obtained by the HP1 was $18.8\text{W}/^{\circ}\text{C}$ with thermal conductance uncertainty of 14% (Fig. 6.7). For HP1 operating in power step, when the heat input increases from 25 - 125 W, the temperature difference reduces from 11.1 to 6.6°C . This observation shows that further increase in heat input contribute to the increase in thermal conductance since the heat transfer limit corresponding to the power level was not reached for heat pipes operating in power step. For power cycles this does not happen for low power, for example. For power of 25 W the temperature difference between the ends of the heat pipes are higher than when applied the power of 50 W.

Figure 6.7 - Thermal conductance experimental x calculated for HP1, HP2 and HP3:
Power step.



Source: Author.

In the Table 6.5 the results for the adjustment factor for the theoretical thermal conductance are presented. For the power of 75 W the theoretical thermal conductance is close to the experimental one with shown by the adjustment factor of 0.90. The largest thermal conductance uncertainty error was 14% as shown in Figure 6.7 and the largest error obtained between the experimental and calculated thermal conductance results was 12% for the HP2 operating with cycle 2.

Table 6.5 - Thermal performance for the HP1 (power step) with the thermal conductance uncertainty of 14%

Power	G_E	adjustment factor	G_C	Error
25W	2.25W/°C	0.26	2.35W/°C	±4.3%
50W	5.37W/°C	0.59	5.60W/°C	±4.1%
75W	8.15W/°C	0.90	8.60W/°C	±5.5%
100W	12.42W/°C	1.35	12.97W/°C	±4.4%
125W	18.80W/°C	2.07	19.85W/°C	±5.6%

Source: Author.

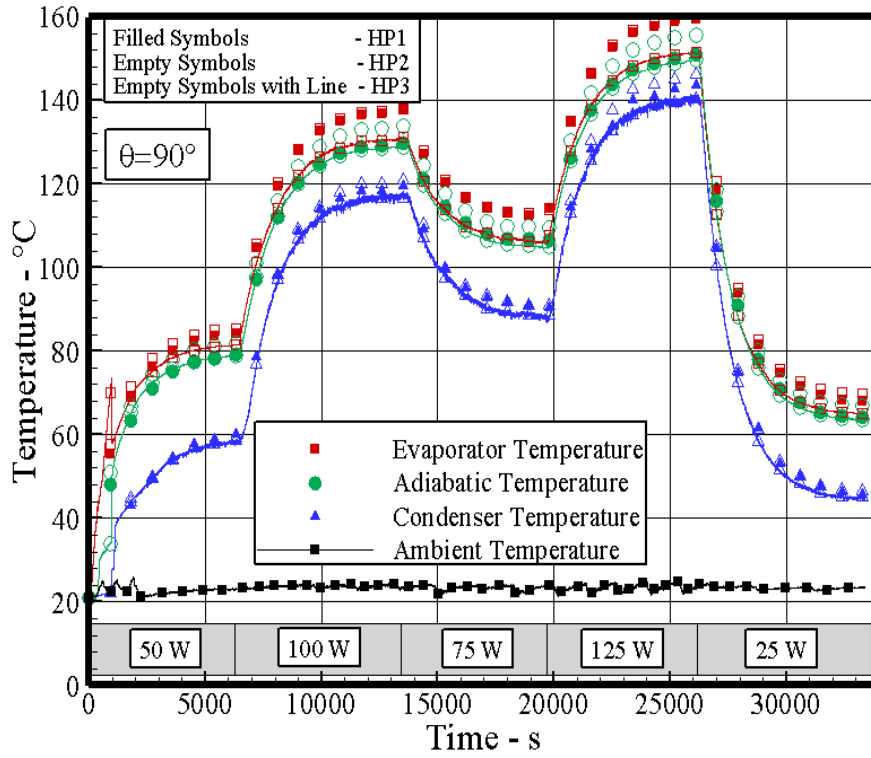
6.4 Stainless Steel Heat Pipes - 90° of inclination

6.4.1 The effects of input heat

The oscillations observed at the start-up of the heat pipes when operating at 30° were also observed when operating at 90° of inclination for power of 50 W. The heat pipes did not show drying tendency in the evaporator but when they operated at 90° they presented larger difference of temperature between the evaporator and the condenser when compared to all tested slopes. The largest temperature difference between the ends of the heat pipe was reached by the HP2 of 28.3°C operating with cycle 2 for the power of 50 W. For the power step the HP1 and HP2 heat pipes presented very close thermal performance to each other and lower when compared with the other inclinations. The temperature difference between the ends of the heat pipes was 8.3°C for the power of 100 W and the heat transport was not maintained for the power of 125 W increasing the temperature difference to 11.7°C.

For heat pipes operating in power cycles, it is shown in the figure 6.8 the temperature profile and the thermal conductance for the cycle 1 (Fig. 6.9) where it presented the best thermal performance when operating at 90°. the HP3 showed a temperature difference between the ends of the heat pipe from 8.5°C to the highest applied power (125 W) while maintaining the decrease in the temperature difference from 50 W. The experimental thermal conductance reached was 14.70W/°C with an experimental error of 11%. The Table 6.6 shows the adjustment factor for each heat pipe and the calculated thermal conductance for each power applied.

Figure 6.8 - Temperature profiles of HP1, HP2 and HP3 for cycle 1



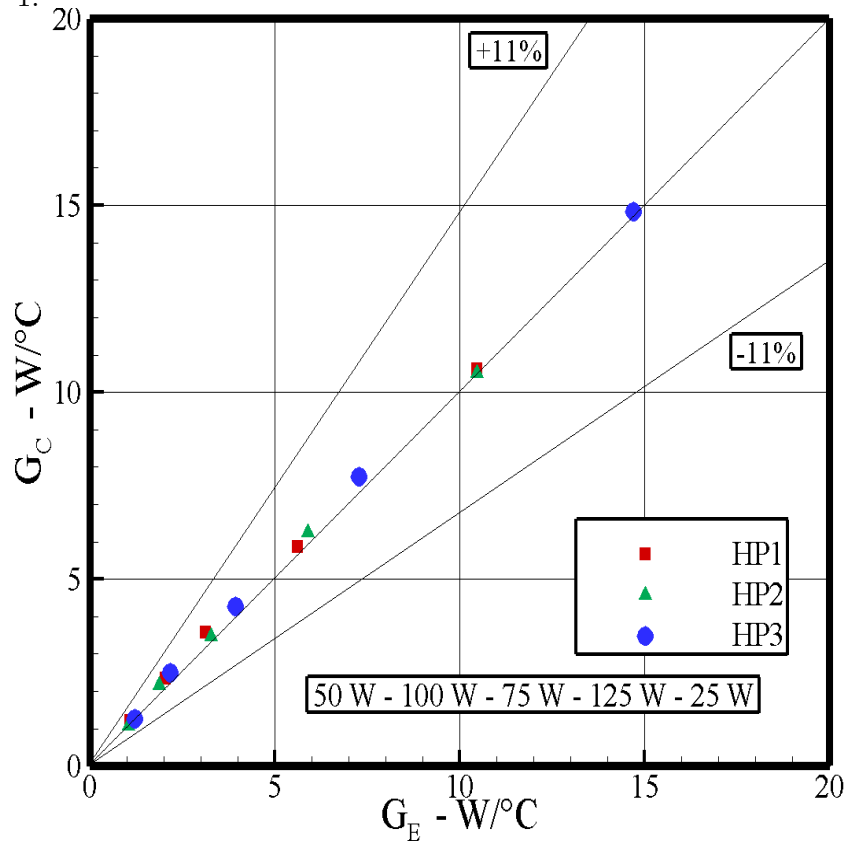
Source: Author.

Table 6.6 - Thermal performance for the HP3 (cycle 1) with the thermal conductance uncertainty of 11%

Power	G_E	adjustment factor	G_C	Error
25W	$1.20W/^\circ C$	0.05	$1.26W/^\circ C$	$\pm 5.0\%$
50W	$2.16W/^\circ C$	0.11	$2.50W/^\circ C$	$\pm 15.3\%$
75W	$3.90W/^\circ C$	0.19	$4.26W/^\circ C$	$\pm 8.3\%$
100W	$7.27W/^\circ C$	1.34	$7.73W/^\circ C$	$\pm 6.3\%$
125W	$14.70W/^\circ C$	0.65	$14.83W/^\circ C$	$\pm 0.8\%$

Source: Author.

Figure 6.9 - Thermal conductance experimental x calculated for HP1, HP2 and HP3: Cycle 1.



Source: Author.

The differences between the observed temperatures for the same heat pipes in each power level when operating in power cycles is due to the behaviour of liquid in the evaporation section. As the heat flux is increased in the evaporator, bubbles begin to form on the surface and begin to detach from the porous structure of the evaporator. At this stage, a reduction of the temperature in the evaporation section can be observed. A small temperature difference between the evaporator and the condenser ensures proper operation and steady heat transfer by the heat pipes.

Different thermal conductances were obtained experimentally due to different temperatures obtained in steady state condition for the different power level conditions applied to each test. With the progressive increase of the power step in the heat pipes, bubble formation in the porous structure of the evaporator becomes evident when the temperature of the evaporator becomes higher (more vapour), increasing the temperature difference between the evaporator and condenser. This temperature can stabilize at higher values by having an inadequate amount of liquid returning

from the condenser or continuing to increase until the dry out of the evaporator and heat pipes stop operating.

Stainless steel-water heat pipes operating at mid-level temperature range investigated in this study represent one of the alternatives for several industry and aerospace applications. They can easily be implemented as heat exchangers inside sorption and vapor-compression heat pumps, refrigerators and other types of heat transfer devices. The use of heat pipes on heat exchangers presents to be rather interesting due to their direct influence on increasing the efficiency, allowing a more compact design (SILVA; RIEHL, 2016).

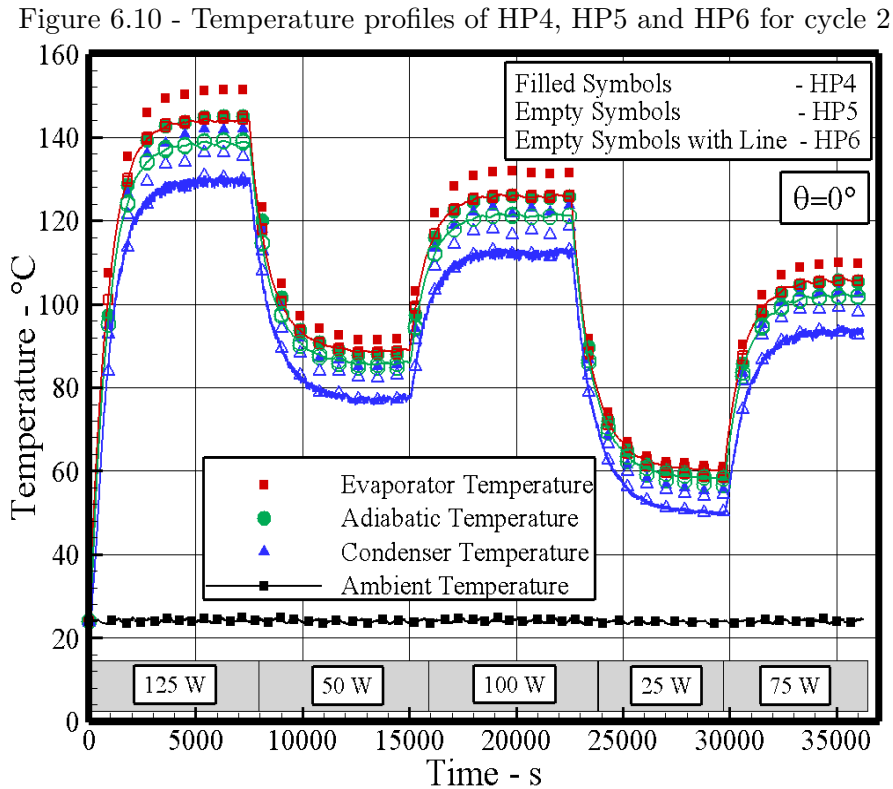
6.5 Copper Heat Pipes - 0° of inclination

6.5.1 The effects of input heat

The effect of input heat on the thermal performance of the heat pipe was examined by charging the system with 97.0 mL of water and slowly increasing the heat input. This corresponds to roughly 30% of the total volume of the heat pipe. This amount of fluid is enough to saturate the entire evaporator section. The copper heat pipes were analyzed with the same procedure used for the stainless steel heat pipes. The thermal behavior for heat pipes in relation to the start-up and the temperature difference between the evaporator and condenser in the heat pipes for each applied power level were verified for heat pipes operating in power step and power cycles. The heat pipes showed stability at start-up for each power applied. The largest temperature difference between the evaporator and condenser occurred in the heat pipe HP6 that was designed with stainless steel wire mesh. The results with power cycles tests showed no dry-out tendency in the evaporator section and presented small temperature difference between the evaporator and condenser due to the thermal conductivity of the copper (approximately 22 times higher than stainless steel). Performance tests are required to check the heat pipe failure or influence of NCGs (non-condensable gases) during their performance.

The largest temperature difference between the evaporator and the condenser of approximately 25.75°C was presented for HP6 at 100W when operating in power steps. The lowest temperature difference was 4.0°C for the HP5 operating at 25W with the heat pipes operating at power cycle 3. The HP4 showed in all the tests a smaller temperature difference between the evaporator and condenser when compared to HP5 and HP6, for all applied powers except for power of 100W with the temperature difference of 5.95°C between evaporator and condenser when operat-

ing with cycle 2 (Fig. 6.10). Such behaviour was due to the fact that HP5 was built using copper for container and wick, whilst HP6 was built using stainless steel wick resulting in higher thermal resistance for this heat pipe as stainless steel presents thermal conductivity lower than copper.

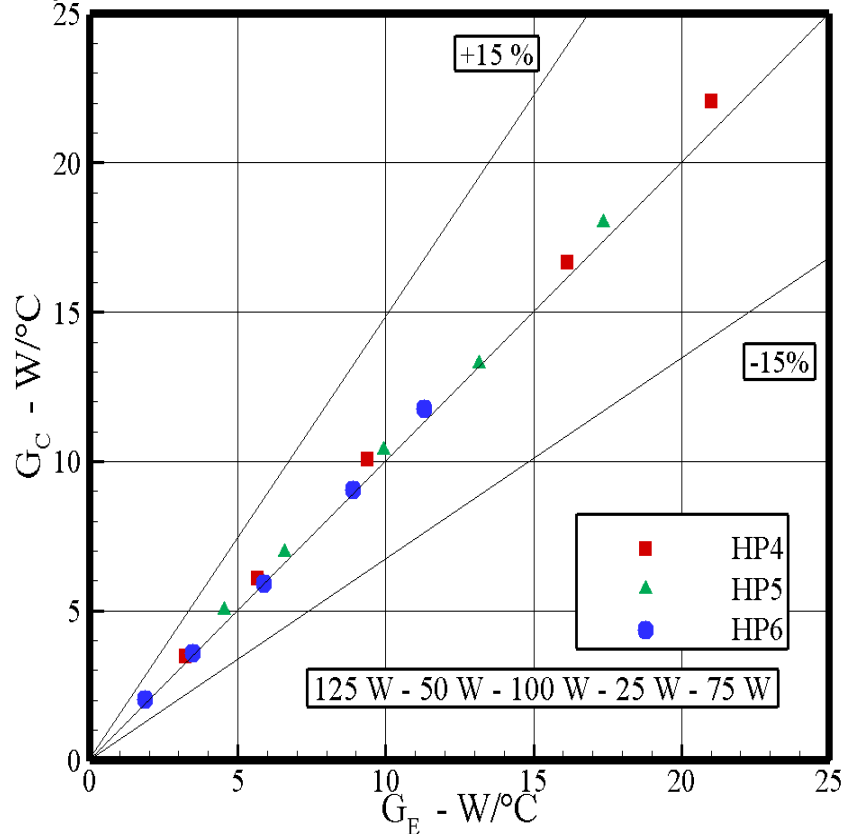


For power cycles (for power levels of 25 until 100W) the HP5 obtained the smallest temperature difference between the evaporator and condenser. For the same power applied and for the same heat pipes, different stabilization temperatures were obtained due to the greater or smaller amount of liquid in different parts of the evaporator, at the beginning of each performed test due to the behavior of the fluid in the evaporator section.

Figure 6.11 presents the results of thermal conductance obtained from Eq. 4.55 and Eq. 4.54 for a better analysis of the heat pipes thermal operation. For the results with the heat pipes operating in power steps, the HP4 presented the highest thermal conductance when compared with HP5 and HP6 and was $17.36W/°C$ due liquid flow resistance smaller and higher speed of liquid return from the condenser back to

evaporator. The HP4 presented faster start-up and without oscillations, reaching the temperature of the evaporator, adiabatic and condenser regions near the isothermal condition, when compared to HP5 and HP6 due to higher permeability and porosity, leading to faster fluid circulation at the start-up, configuring better performance when analysed by thermal conductance.

Figure 6.11 - Thermal conductance experimental x calculated for HP4, HP5 and HP6: Cycle 2.



Source: Author.

An adjustment factor was considered for the calculated thermal conductance, in order to add uncontrolled variables that are inherent to the heat pipe manufacturing process, such as: porous structure thickness, correct amount of working fluid inside the heat pipe, the mesh folding, the closing of the heat pipe and so on. The results of the thermal conductance calculated with the adjustment factor were within the experimental error for each test performed with the heat pipes.

The greatest thermal conductance uncertainty was 15% for the experimental results

with the heat pipes operating at cycle 2. The copper heat pipes obtained the highest experimental thermal conductance of $21W/^\circ C$ for the HP4 (mesh number 100 operating with cycle 2) and $22W/^\circ C$ for the calculated thermal conductance (theoretical thermal conductance x adjustment factor) (Fig. 6.11). The theoretical thermal conductances presented results of approximately $16.0W/^\circ C$ for the HP4, $31.0W/^\circ C$ for the HP5 and $24.0W/^\circ C$ for the HP6. Therefore, upon analyzing previous results for the stainless steel heat pipes and current results, similarity in the temperature and heat transfer patterns were expected. The results presented here are related to several series of tests for the sake of comparing the heat pipes performances and check their life time reliability as well. In this specific case, the heat pipes presented similar thermal behaviour over the time, as presented by the results.

The table 6.7 presents results for the best thermal performance of the heat pipes. The results are presented for experimental thermal conductance, factor of adjustment, calculated thermal conductance and experimental error presented by the conductances by the Eq. 4.56.

Table 6.7 - Thermal performance for the HP4 (cycle 2) with the thermal conductance uncertainty of 15%

Power	G_E	adjustment factor	G_C	Error
25W	$3.22W/^\circ C$	0.22	$3.48W/^\circ C$	$\pm 7.3\%$
50W	$5.68W/^\circ C$	0.38	$6.08W/^\circ C$	$\pm 6.6\%$
75W	$9.37W/^\circ C$	0.62	$10.06W/^\circ C$	$\pm 6.8\%$
100W	$16.13W/^\circ C$	1.02	$16.65W/^\circ C$	$\pm 3.2\%$
125W	$21.00W/^\circ C$	1.35	$22.05W/^\circ C$	$\pm 4.7\%$

Source: Author.

6.6 Copper Heat Pipes - 30° of inclination

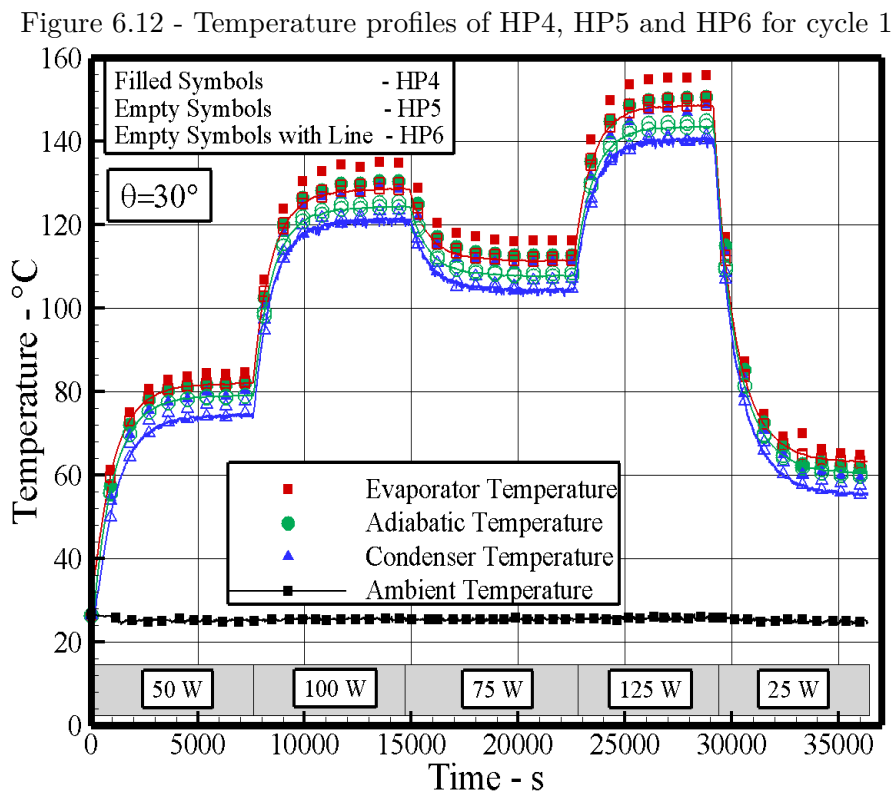
6.6.1 The effects of input heat

The three heat pipes presented stable behavior, for both transient and steady-state conditions, when they operated using the power levels in power steps and power cycles. During the experimental tests and analysis of the results the heat pipes presented no dry-out tendency in the evaporator section. Heat pipes operating at $30^\circ C$ presented start-up without oscillations of temperatures, confirming better performance when analyzing the thermal conductance results.

The copper heat pipes presented better thermal performance when operated with the cycle 1. Very small temperature difference between the evaporator and the condenser were observed for this power cycle when compared with all the slopes tested, which is because of the role of gravity helping the liquid back to the evaporator.

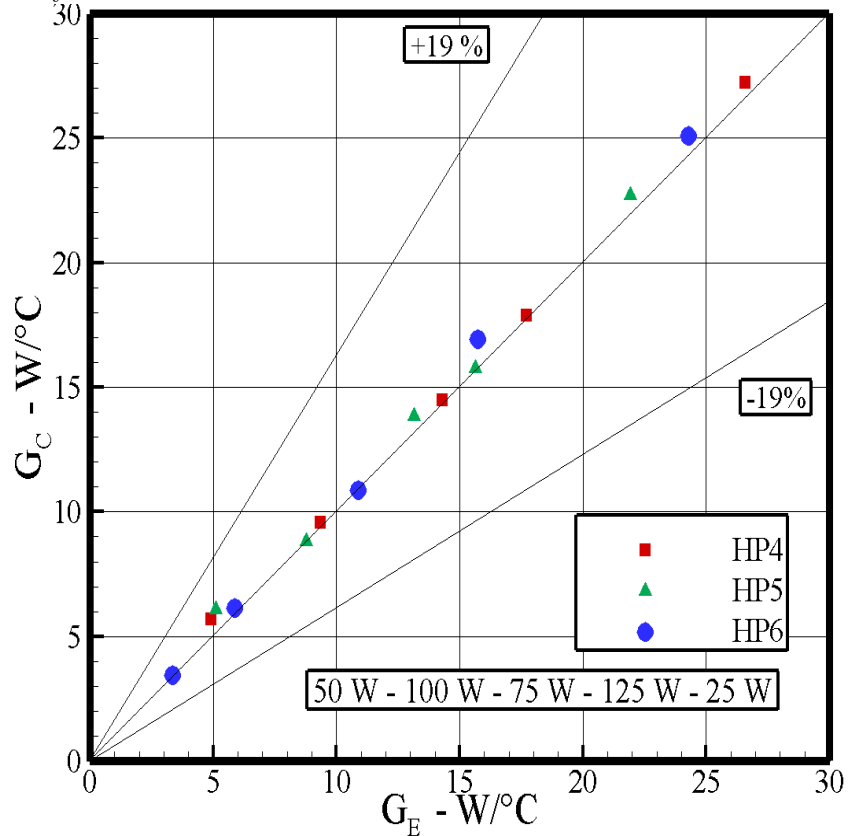
Considering the heat pipes operating in power step the highest temperature difference between the ends was obtained for the HP5 heat pipe of 11.5°C . The heat pipe started operation with a temperature difference of 6.3°C for the power level of 25 W and increasing the temperature difference to the power level of 125W. For the heat pipes operating in power cycles the highest temperature difference was obtained by HP6 of 17.5°C .

The largest temperature difference between the ends of the heat pipe was observed for the HP6 of 8.5°C due to stainless steel mesh wick for the applied power of 50 W. The HP4 heat pipe presented better thermal performance with temperature difference between the ends of less than 5.7°C for all tested powers. The Figure 6.12 shows the temperature profile for the heat sinks operating with cycle 1.



The Figure 6.13 shows the results for the thermal conductance. Considering the best thermal performance the results for cycle 1 are presented. The highest thermal conductance was obtained from $26.6W/^\circ C$ for HP4, $21.9W/^\circ C$ for HP5 and $24.3W/^\circ C$ for HP6 with uncertainty experimental study of 19%.

Figure 6.13 - Thermal conductance experimental x calculated for HP4, HP5 and HP6: Cycle 1.



Source: Author.

The higher thermal conductivity for HP4 was due to the smaller pore radius, higher permeability and porosity facilitating the return of the fluid to the evaporator with the help of gravity. The Table 6.8 presents results for the adjustment factor for each heat pipe and the calculated thermal conductance for each power applied and experimental error presented by the conductances by the Eq. 4.56

Table 6.8 - Thermal performance for the HP4 (cycle 1) with the thermal conductance uncertainty of 19%

Power	G_E	adjustment factor	G_C	Error
25W	4.90W/°C	0.36	5.70W/°C	±14.1%
50W	9.34W/°C	0.60	9.56W/°C	±2.3%
75W	14.28W/°C	0.89	14.49W/°C	±1.4%
100W	17.69W/°C	1.10	17.88W/°C	±1.0%
125W	26.59W/°C	1.63	27.20W/°C	±2.2%

Source: Author.

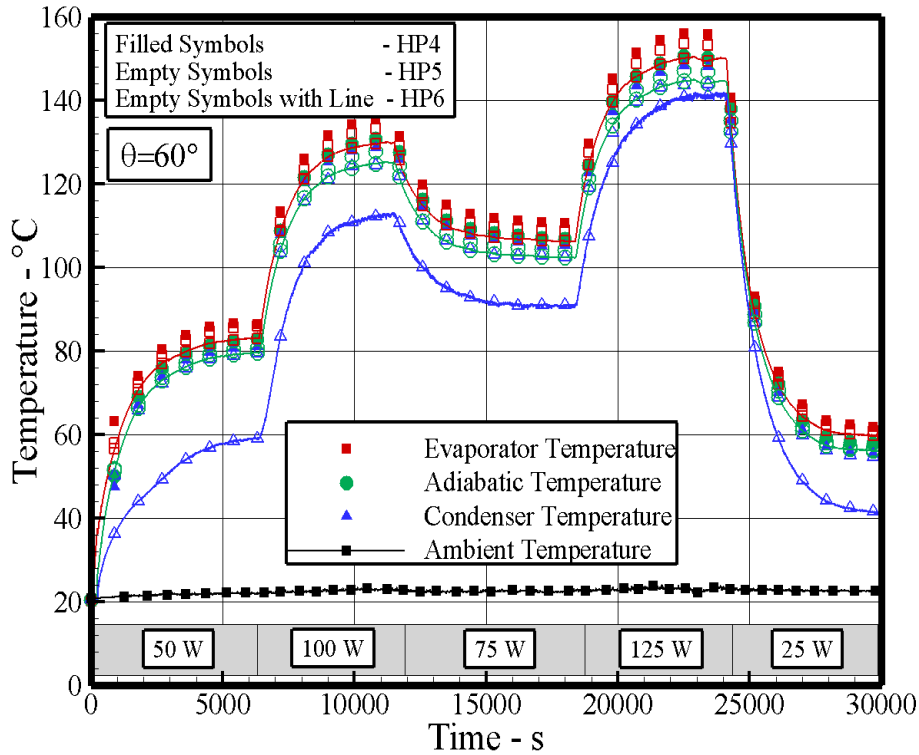
6.7 Copper Heat Pipes - 60° of inclination

6.7.1 The effects of input heat

With the conducted tests the results for heat pipes operating at 60° of inclination were presented and it was possible to verify the temperature along the heat pipes in order to obtain temperature profiles. As expected, there was an increase in the temperature with the highest power applied to the evaporator. However, all three heat pipes presented stable operation for both transient and steady-state conditions. The Figure. 6.14 presents the temperature profiles for all heat pipes, to evaluate their thermal performances during all power levels.

As a result, the temperature difference between the evaporator and the condenser of heat pipe also increases linearly with heat inputs when operating in power step. The smallest temperature difference between the ends of the heat pipes was 7.7°C for HP4 operating with cycle 1, 9.2°C for HP5 operating with cycle 2 and 6.9°C for HP6 operating with cycle 4 (both for 125W). For the heat pipes operating in power step the smaller temperature difference between the evaporator and the condenser was obtained by the HP4 of 4.3°C for the power of 50 W and the biggest temperature difference was obtained by the HP5 of 10.0°C.

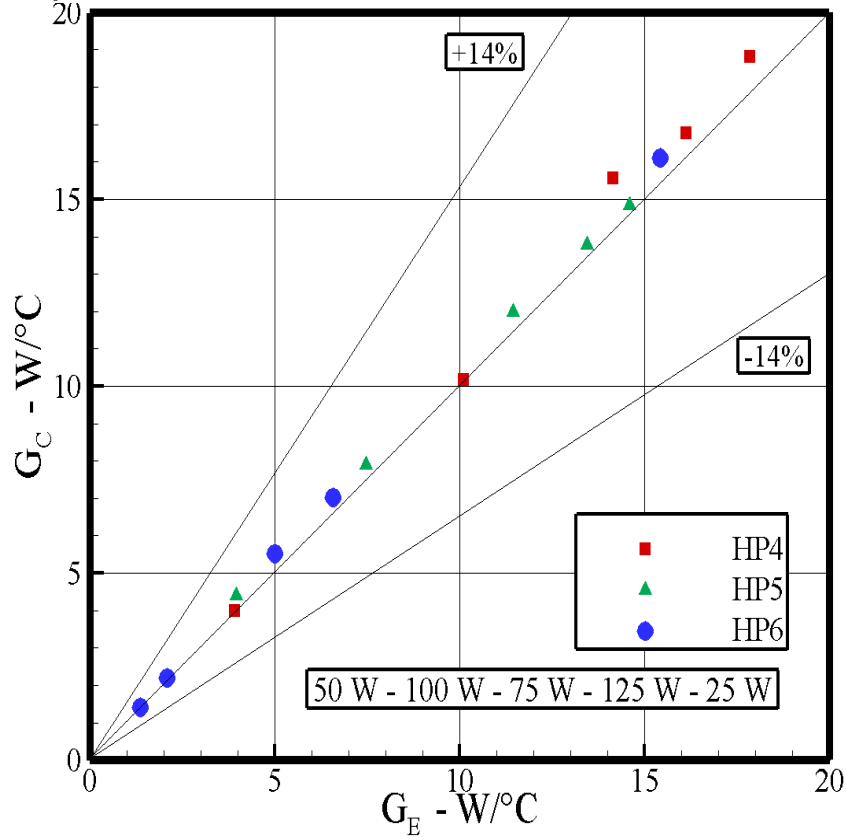
Figure 6.14 - Temperature profiles of HP4, HP5 and HP6 for cycle 1



For a better analysis of the thermal performance of the heat pipes operating with the slope of 60° the thermal conductance for cycle 1 is presented. The Figure 6.15 shows the results for the thermal conductance (experimental thermal conductance x calculated thermal conductance) with thermal conductance uncertainty was 14% for the experimental results with the heat pipes operating at cycle 1.

The copper heat pipes obtained the highest experimental thermal conductance for the HP4 (which presented better thermal performance) and was $17.85W/^\circ C$ for the power of 100 W and $16.12W/^\circ C$ for the power of 125 W and $16.7W/^\circ C$ for the calculated thermal conductance (theoretical thermal conductance x adjustment factor). The theoretical thermal conductances presented results of approximately $16.0W/^\circ C$ for the HP4. The Table 6.9 presents results for the adjustment factor for each heat pipe. The calculated thermal conductance for each power applied and experimental error were presented by the conductances by the Eq. 4.56.

Figure 6.15 - Thermal conductance experimental x calculated for HP4, HP5 and HP6:
Cycle 1.



Source: Author.

Table 6.9 - Thermal performance for the HP4 (cycle 1) with the thermal conductance uncertainty of 14%

Power	G_E	adjustment factor	G_C	Error
25W	3.90W/°C	0.25	3.98W/°C	±1.9%
50W	10.10W/°C	0.64	10.17W/°C	±0.7%
75W	14.15W/°C	0.96	15.57W/°C	±9.1%
100W	17.85W/°C	1.15	18.81W/°C	±5.1%
125W	16.12W/°C	1.03	16.76W/°C	±3.7%

Source: Author.

6.8 Copper Heat Pipes - 90° of inclination

6.8.1 The effects of input heat

The tests performed with the heat pipes operating vertically (90 °C) presented good thermal stability during the start-up, transient and in the permanent regime and did not show tendency to drying in the evaporator in all the powers applied.

The tests performed with the heat pipes with the power step the HP4 presented the smallest temperature difference between the evaporator and the condenser for all the applied powers when compared with HP5 and HP6. The lowest temperature difference was of 6.25 °C from 75W level and the highest was of 8.15 °C from 125 W level.

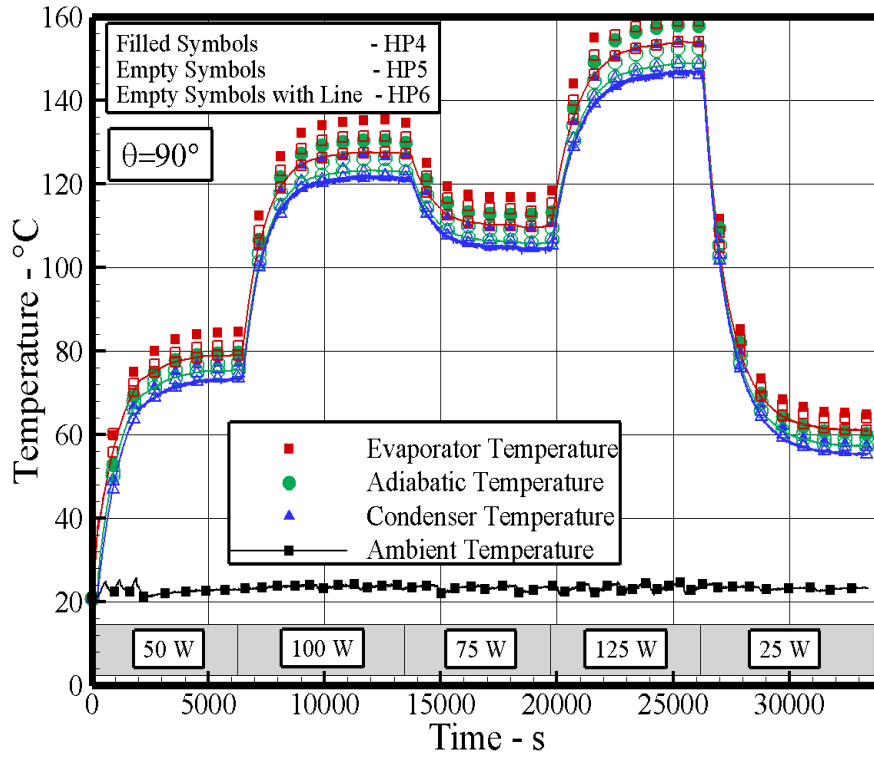
Considering the power cycles, the heat pipes showed temperature differences between the heat pipe ends below 10.0 °C for HP4, 10.5 °C for HP5 and 7.5 °C for HP6. The HP6 operating with cycle 1 obtained a temperature difference of 4.75 °C for the power of 125W, where for this slope tested the HP6 presented better return of the fluid to the evaporator, minimum losses of heat during the circulation of the working fluid and temperature differences between the evaporator and the condenser close to all applied powers.

The Figure 6.16 shows the temperature profile for the heat pipes operating with cycle 1 where it was obtained the smallest temperature difference between the ends.

For a better analysis are presented for copper heat pipes operating with cycle 1 the results between the experimental thermal conductivity x thermal conductance calculated with thermal conductance uncertainty of 18% (Fig. 6.17). The HP4 obtained experimental thermal conductance of 15.43W/°C, HP5 of 14.12W/°C and HP6 of 26.31W/°C. The theoretical thermal conductivity estimated for the HP6 was 26W/°C, value in agreement with the experimental results.

The results for the thermal performance of the heat pipes operating with cycle 1 are presented in the Table 6.10 where the adjustment facts for the experimental thermal conductance are shown for each power level applied and the calculated error.

Figure 6.16 - Temperature profiles of HP4, HP5 and HP6 for cycle 1.



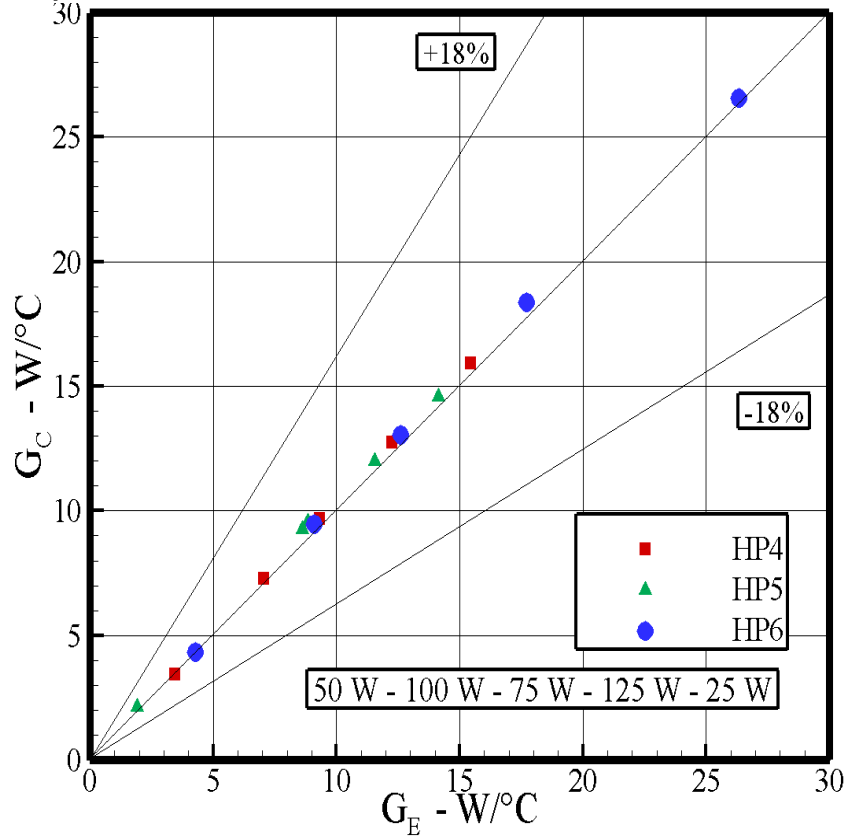
Source: Author.

Table 6.10 - Thermal performance for the HP6 (cycle 1) with the thermal conductance uncertainty of 19%

Power	G_E	adjustment factor	G_C	Error
25W	4.27W/°C	0.25	4.31W/°C	±0.8%
50W	9.10W/°C	0.64	9.45W/°C	±3.8%
75W	12.60W/°C	0.96	13.01W/°C	±3.2%
100W	17.70W/°C	1.15	18.35W/°C	±3.5%
125W	26.31W/°C	1.03	26.57W/°C	±0.9%

Source: Author.

Figure 6.17 - Thermal conductance experimental x calculated for HP4, HP5 and HP6:
Cycle 1.

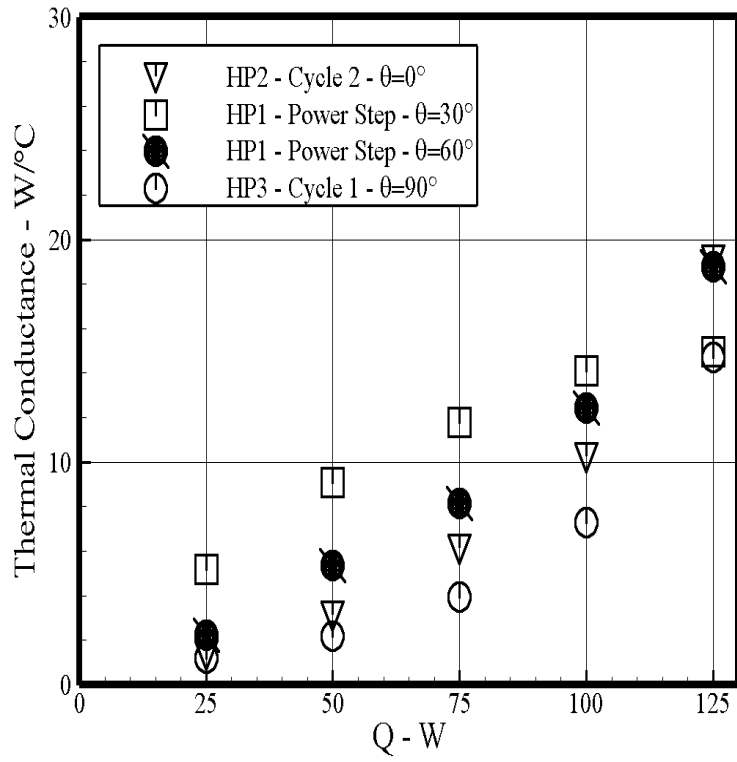


Source: Author.

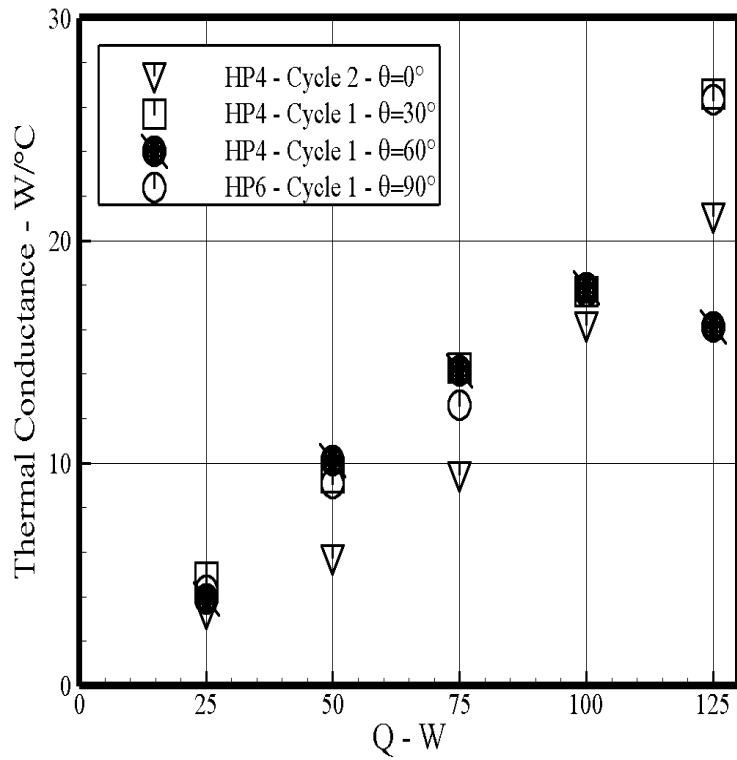
6.9 The effects of inclination angle on the heat pipe performance

The variation in the thermal conductance due to inclination slope angle for gravity-assisted orientations for five input heat levels are shown in Figure 6.18(a) for stainless steel heat pipes and Figure 6.18(b) for copper heat pipes. The results show that the heat pipe clearly performs well for all inclinations angles and that the performance qualities of the heat pipe change significantly for different gravity-assisted inclination angles due the different mesh wick numbers.

Figure 6.18 - The effects of inclination on the heat pipes performance (a) Stainless steel heat pipes and (b) Copper heat pipes.



(a)



(b)

Source: Author.

Heat pipes with the same geometry parameters, differing only on the mesh number, show higher thermal conductance when copper was used. This is compatible with a higher thermal conductivity of the material and thus resulting on higher thermal conductances for the heat pipes. For 0° , regarding the thermal conductances, the copper heat pipes demonstrated higher values when using screen mesh number 100, also influenced by the higher permeability and porosity of the wick. Stainless steel heat pipes demonstrated higher thermal conductance values by using screen mesh number 200 due to its higher capillary pumping capability. However, higher thermal conductance is obtained for the inclination angle of the 30° for HP4 (cycle 1), which is because of the role of gravity helping the liquid going back to the evaporator. While the lower thermal conductance corresponds to the inclination angle of 90° for HP3 (cycle 1), especially at lower heat input levels, which is likely the result of slightly overfilling the evaporator section. For this reason, the effect of inclination angle can't be neglected for gravity assisted operation where the condenser is located above the evaporator.

6.10 Application of screen mesh wick heat pipes operating in mid-level temperature

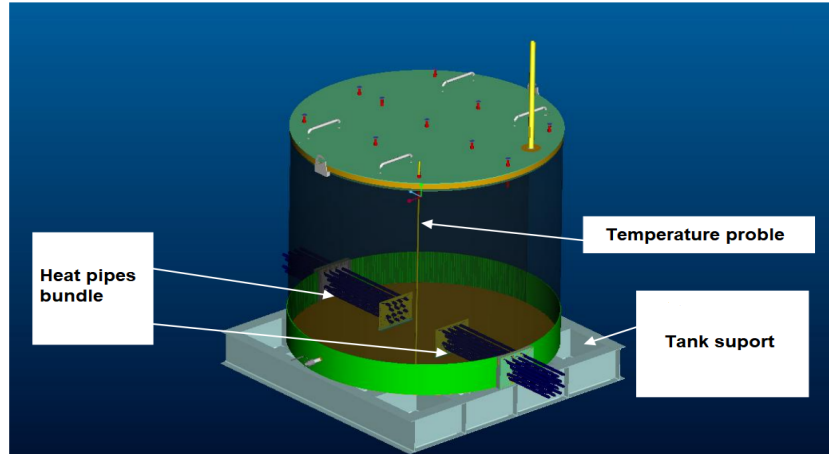
The results of this work served as a basis for the application of heat pipes in a storage tank of the Petroleum Asphalt Cement (PAC). In ambient temperature, the PAC behaves as viscoelastic fluid and in temperatures above 140°C it is presented as Newtonian fluid. The PAC on leaving the distillation tower is pumped through pipes to the storage tanks where it is kept warm. To prevent solidification of the PAC, which reduces its fluidity and prevents its handling, the tanks are heated through serpentine with saturated water vapor. The problems with this type of heating are steam leakage in the transmission line, low power of the heating serpentine of the tank, inadequate control of the average temperature of the PAC during its delivery and inadequacy of the insulators used along the vapor transmission line.

In view of the problems shown, the heat pipe presents an effective alternative for heating the PAC storage tank. The main advantage of the use of heat pipes is the homogeneous temperature in the heating surface, since the degradation of the structure and chemical decomposition of the PAC are associated with high temperatures.

As a proposal for the application of heat pipes, a project is presented for possible experimental tests. The preliminary design consists of a simulation of the heating of the PAC storage tank with a bundle of heat pipes in a set of electrical resistances by an adjustable power source. The model is simulated in a cylinder 2 m high with 2 m

in diameter with a beam with 14 heat pipes of 0.0254 m in external diameter with 2 m is in length being that 1 m in the inner part of the tank as shown in Figure 6.19.

Figure 6.19 - Heat pipes in a storage tank.



Source: Author.

Boundary conditions are shown in the table 6.11

Table 6.11 - Boundary conditions

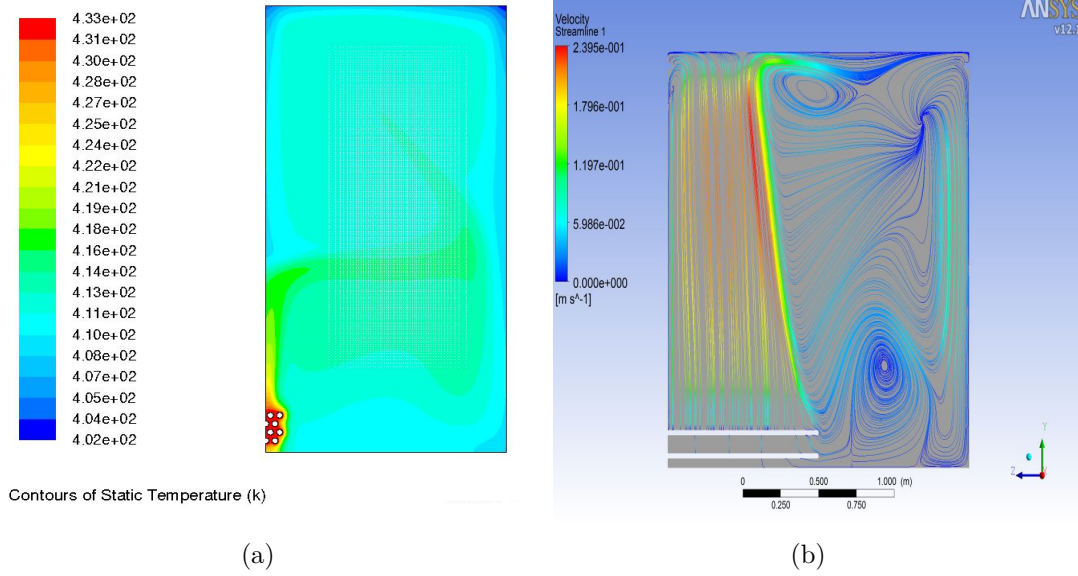
Location	Boundary Conditions
Walls of heat pipes	Temperature of HPs = $160^{\circ}C$
Bottom wall of the PAC tank	Adiabatic
Side walls of the PAC tank	Coefficient of heat transfer $4W/m^2K$, $T_{\infty} = 27^{\circ}C$
Top wall of PAC tank	Coefficient of heat transfer $11W/m^2K$, $T_{\infty} = 27^{\circ}C$

Source: Author.

The simulations were performed for a bi-dimensional and three-dimensional model using the FLUENT software taking into account the density variation of the temperature and pressure. For the two-dimensional model, a computational mesh of approximately 500 thousand quadrangular elements was used and the three-dimensional model used mesh of 5 million tetrahedral and prismatic elements. The Fig. 6.20(a) shows the temperature distribution obtained by the simulation with 30.000 iterations and the velocity field Fig. 6.20(b), both simulations shown numerically converged. Fig. 6.21(a) and Fig. 6.21(b) show, respectively, the temperature field and the velocity vectors obtained in the plane of symmetry of the computational domain in

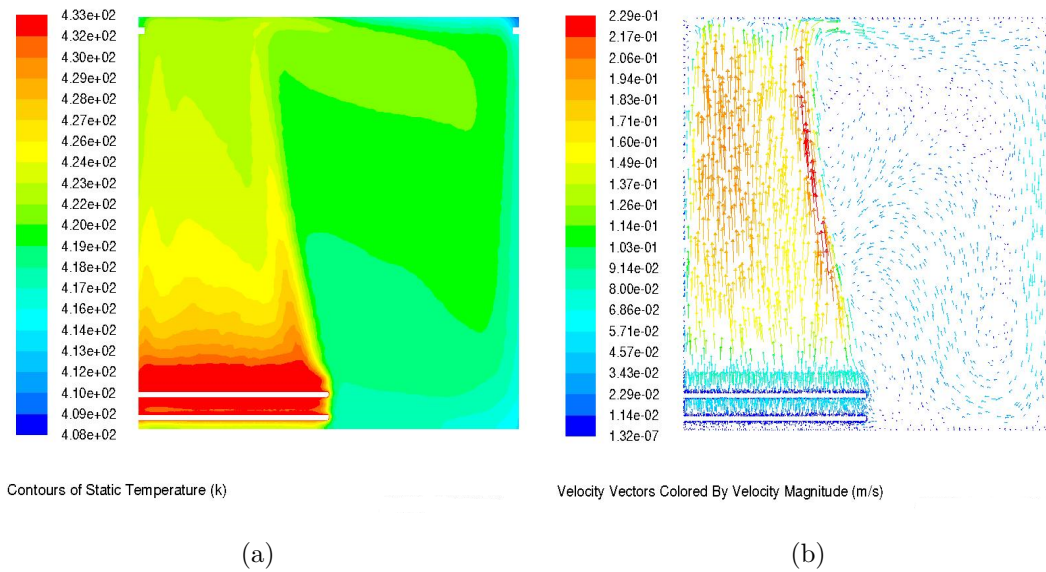
three dimensions.

Figure 6.20 - (a) Temperature distribution in the PAC tank, (b) Speed vector in the PAC tank (3D model).



Source: Author.

Figure 6.21 - (a) Temperature distribution in the PAC tank (3D model, (b) Speed vector in the PAC tank (3D model).



Source: Author.

As in the two-dimensional analysis, the solutions obtained for the equations of motion were obtained in steady state and fully converged according to the criteria adopted here. The qualitative analysis of the presented results allows to say that the calculation methodology developed is sufficiently verified and can be used in the application of heat pipes in a storage tank of petroleum asphalt cement (PAC).

6.11 Application of heat pipes for thermal control of electronic equipment in a honeycomb panel

Consider a honeycomb panel with dimensions of 1.5 m X 2.0 m and 20 mm thickness, located in the central part of a satellite that is in an equatorial orbit at 650 km altitude and 55° inclination, being it totally thermally isolated from the rest of the satellite structure, but thermally connected to a radiator.

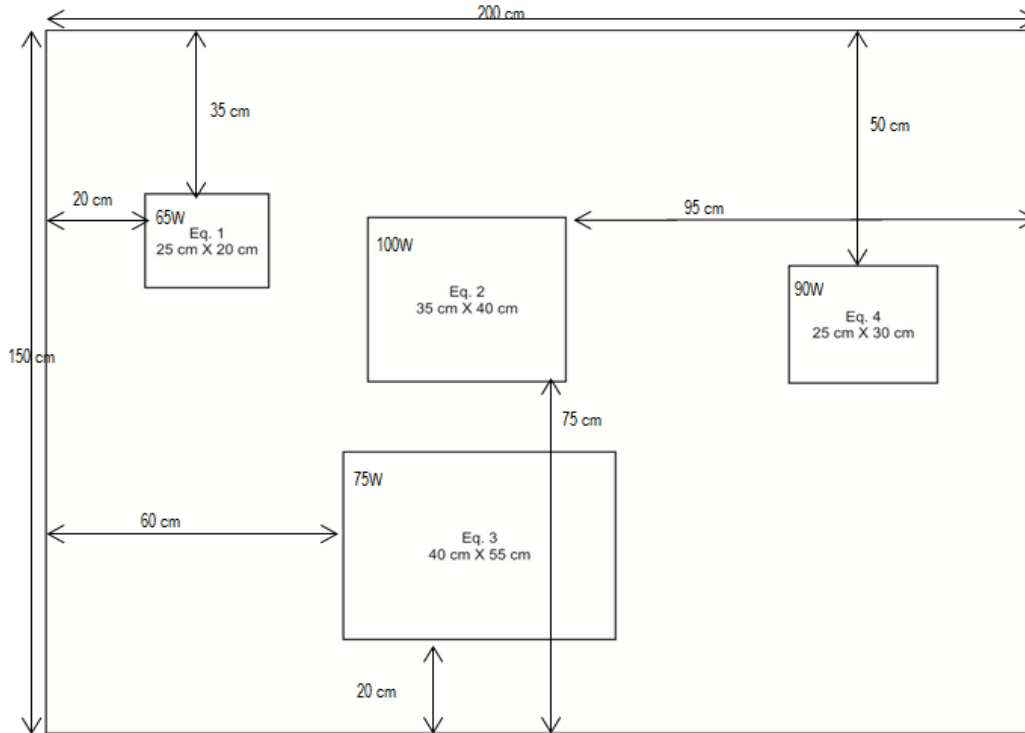
The honeycomb panel is used as the base for the assembly of electronic equipments that integrate the satellite, and 4 electronic equipments are arranged as shown in Fig. 6.22. The equipment 1 (25 cm X 20 cm) dissipates 65 W of heat to the panel by means of the mechanical contact between them; the equipment 2 (35 cm X 40 cm) dissipates 100 W, the equipment 3 (40 cm X 55 cm) dissipates 75 W and the last 90 W (25 cm X 30 cm). Due to the characteristics of the mission, the heat generated during the operation of these components must be rejected into space by means of a radiator, which, for purposes of design, only considers the case where the radiator operates in hot mode, presenting a constant temperature of 0°C , and is arranged perpendicular to the panel.

For the numerical determination of the temperature distribution, the energy balance method was used, where the finite difference equations were developed.

In the energy balance method, the finite difference equation for a nodal point is obtained by applying energy conservation in a control volume around the nodal region. Since the actual direction of thermal flow (entering or leaving the node) is often unknown, it is convenient to formulate the energy balance assuming that all thermal flows are directed into the nodal point. Such a condition is obviously impossible, but if the rate equations are represented in a manner consistent with this assumption, the correct form of the finite difference equation is obtained, for stationary regime condition with energy generation.

Once the nodal network is established and the finite difference equations appropriate for each nodal point are established, the temperature distribution can be determined.

Figure 6.22 - Position of electronic equipment on honeycomb panel.



Source: Author.

The problem is reduced to the solution of a system of linear algebraic equations. To solve the finite difference equations, the matrix inversion method was used. Here is the temperature distribution on the panel (Fig. 6.23).

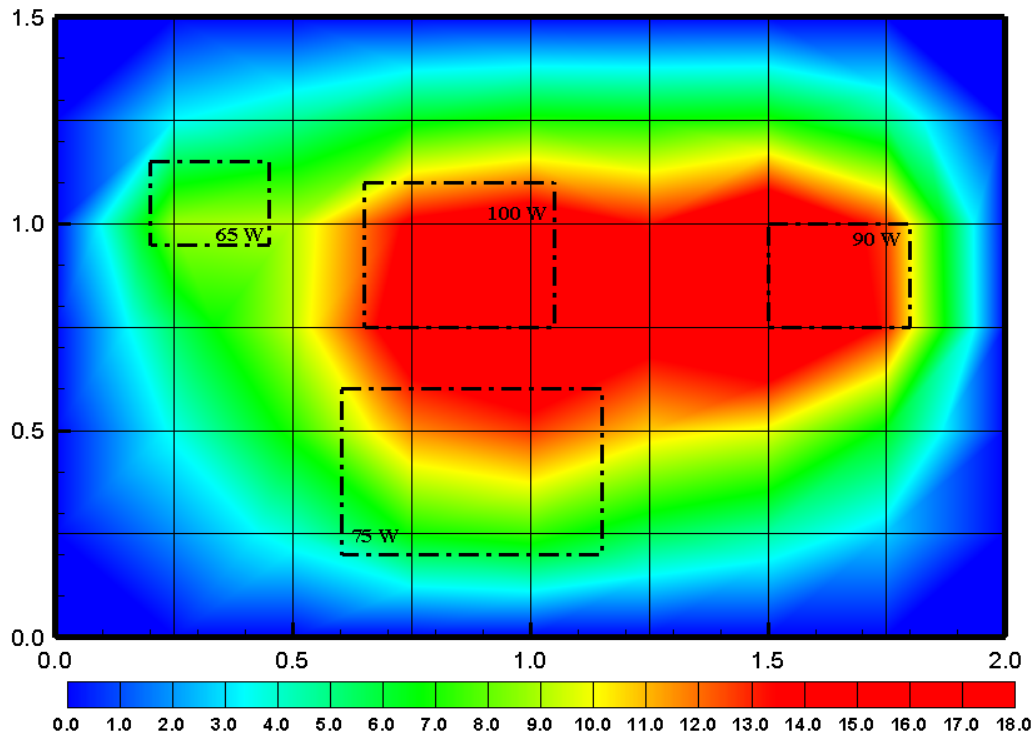
6.11.1 Heat pipe for honeycomb panel

For the design of the heat pipes to be coupled to the honeycomb panel, the following geometric characteristics were considered in the table 6.12.

Extruded aluminum tube 6061-T6 for the evaporator and condenser for the heat pipes coupled in the honeycomb panel and for the heat pipes for connection of the panel with the radiator with rectangular grooves and integrated flanges are shown in Fig. 6.24.

The heat pipes are designed to carry 165 W, and the amount of heat being dissipated by the four electronic equipment is 330 W, so it would take two heat pipes, with the geometric characteristics of Table. 6.12. However, by prevention and effect of redundancy, four heat pipes conforming to the characteristics shown in Tab. 6.12 will be inserted into the panel.

Figure 6.23 - Temperature distribution on honeycomb panel.



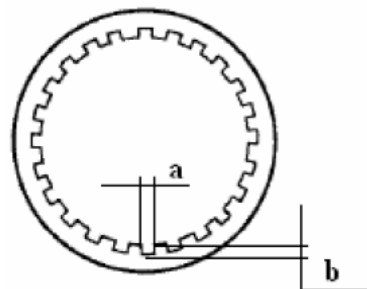
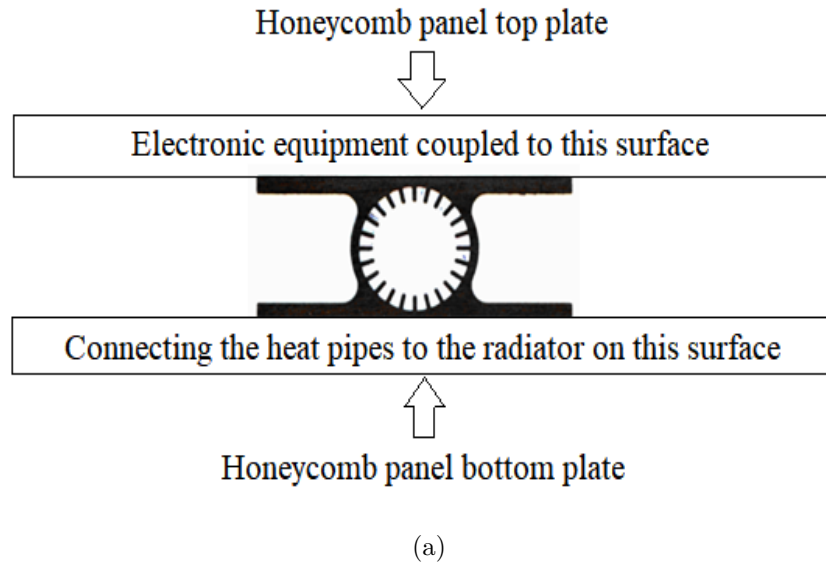
Source: Author.

Table 6.12 - Geometric characteristics of the heat pipe (panel)

Evaporator/Condenser/Total length, m	0.925/0.925/1.85
Working fluid	Ammonia
Tube material	Aluminum
Outside diameter, m	0.0127
Inside diameter, m	0.0082
Number of grooves	30
Width grooves, m	0.00035
Depth grooves, m	0.00082
Flange width, m	0.027
Flange thickness, m	0.00265
Flange height, m	0.018

Source: Author.

Figure 6.24 - (a) Aluminum extruded profile with flanges for panel heat pipes and for panel connecting pipes with radiator, (b) Aluminum extruded profile without flanges for adiabatic section of panel heat pipes with radiator.



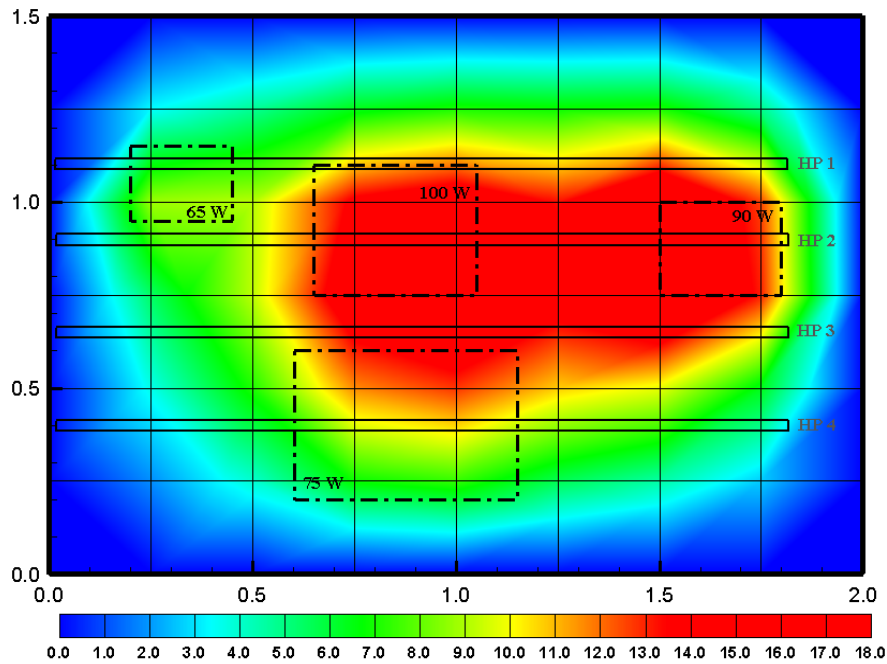
Source: Author.

The heat pipes are inserted inside the honeycomb panel where the electronic equipment dissipates a large amount of heat, so that it can efficiently reject the heat generated by these equipments and uniform the heat to a larger area, for its rejection in the space. Fig. 6.25 shows the position of the heat pipes inserted in the panel. The heat pipes occupy 92% of the total length of the panel to facilitate the absorption of heat, and also its rejection where the temperature is lower.

6.11.2 Capillary Pressure/Pressure Drops and Operating Limits

When the maximum capillary pressure is equal to or greater than the summation of these pressures drops, the capillary structure is capable of returning an adequate amount of working fluid to prevent dry out of the evaporator wicking structure.

Figure 6.25 - Position of the heat pipes in the panel.



Source: Author.

Therefore, for all temperature range the capillary pressure is higher than the pressure drops of the vapor and liquid (see Fig. 6.26), Guaranteeing the return of the working fluid to the evaporator.

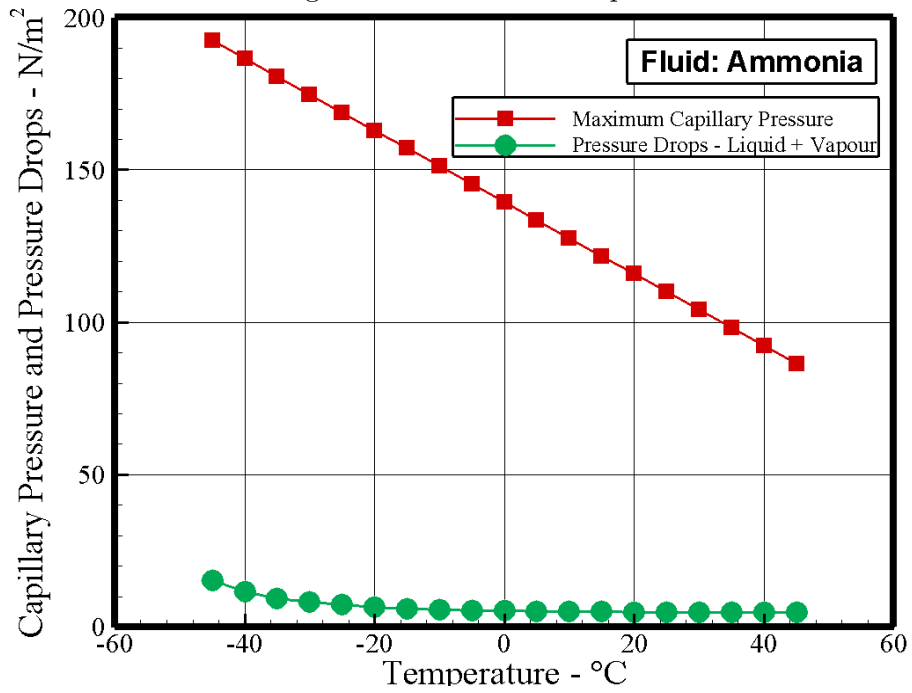
The understanding of the phenomena that occur with the phase change of the working fluid during the operation of the heat pipe is of fundamental importance for the development of the thermodynamic process and for the design of heat pipes. The maximum amount of heat that a heat pipe can carry is determined by operating limits (Fig. 6.27): capillary limit, sonic limit, entrainment limit, boiling limit and viscous limit. Each of these limitations is dependent upon the porous structure, working fluid, temperature and pipe dimensions.

As the heat load to be dissipated by the heat pipe is 165 W none of the operating limits will be reached. The main limits affecting the heat transfer capacity in the heat pipes are the entrainment limits and the boiling limit.

6.11.3 Heat pipes for connecting the honeycomb panel to the radiator

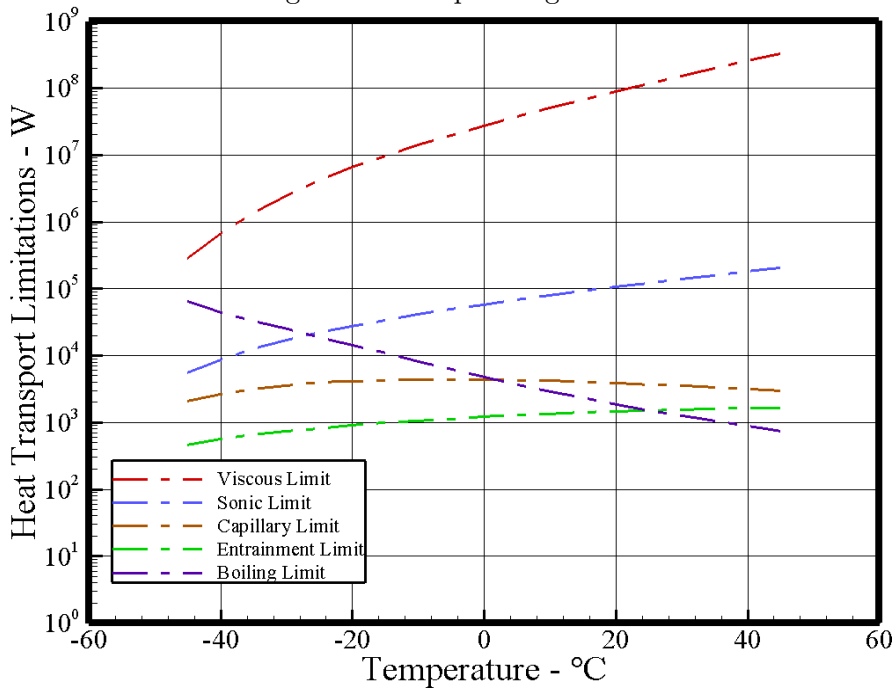
As each heat pipe was designed to carry 330 W, and the amount of heat being dissipated by the four electronic equipments is 330 W, then only one heat pipe,

Figure 6.26 - Pressure drops



Source: Author.

Figure 6.27 - Operating Limits



Source: Author.

with the geometric characteristics of Tab. 6.13 is needed. However, by prevention and redundancy effect, two heat pipes will be inserted to the panel according to the characteristics presented in Tab. 6.13.

Table 6.13 - Geometric characteristics of the heat pipe (panel/radiator)

Evaporator/adiabatic/Condenser/Total length, m	1.38/1.1/1.38/3.86
Working fluid	Ammonia
Tube material	Aluminum
Outside diameter, m	0.0127
Inside diameter, m	0.0082
Number of grooves	30
Width grooves, m	0.00035
Depth grooves, m	0.00082
Flange width, m	0.027
Flange thickness, m	0.002
Flange height, m	0.018

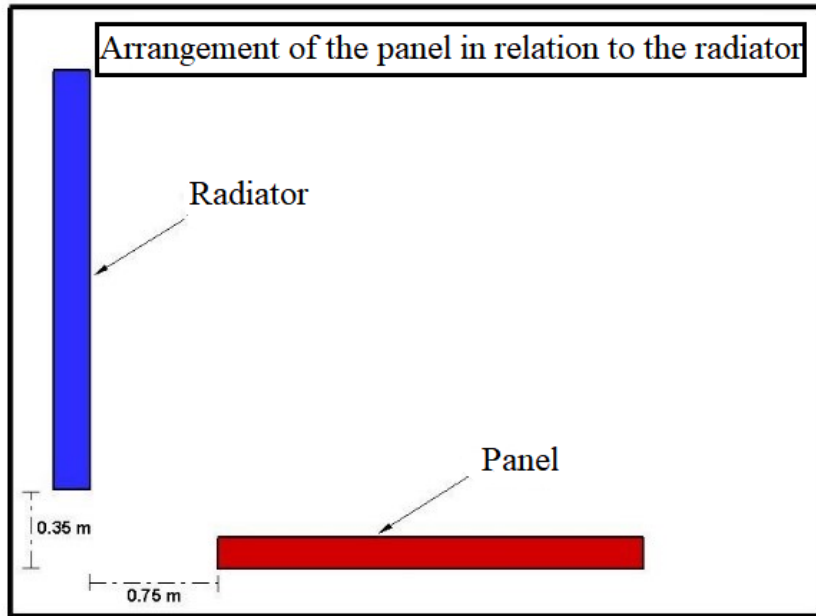
Source: Author.

Fig. 6.28 shows the positioning of the panel relative to the radiator. The arrangement of the heat pipe for connection of the panel with the radiator to dissipate the heat contained in the panel is shown by Fig. 6.29.

Just as heat pipes for the honeycomb panel, the heat pipes for connection to the radiator have not reached any operating limit and the capillary pressure is greater than the pressure drops of the liquid and the vapour. The power to be rejected to space is 330 W and the minimum area required of the radiator to dissipate the heat is $1.05 m^2$.

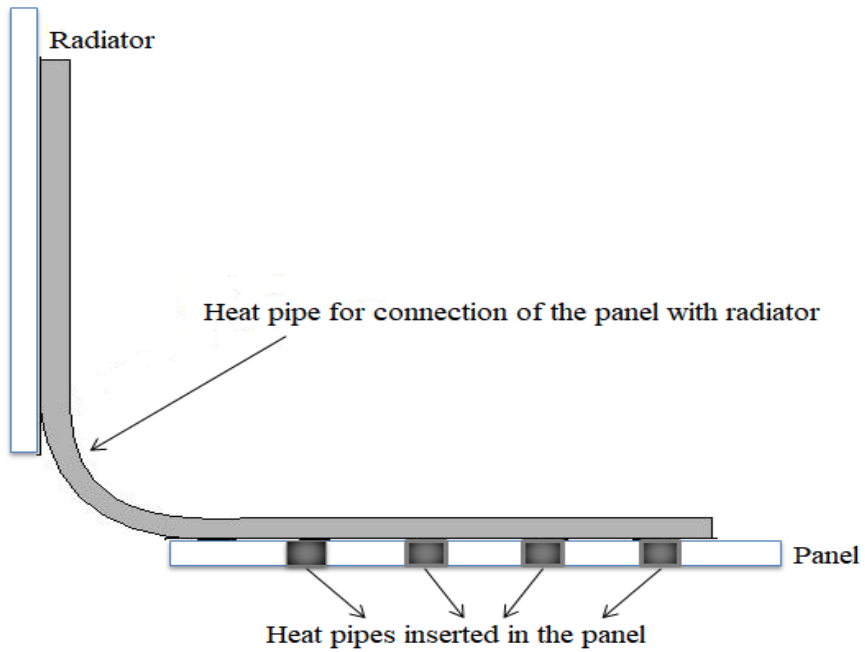
The charge of the fluid chosen for the heat pipes is for the fluid in the cold mode (the lowest temperature at which the tube can operate) because the charge is made with less fluid, ensuring that only in the grooves have liquid during the operation, not the steam channel.

Figure 6.28 - Arrangement of the panel in relation to the radiator.



Source: Author.

Figure 6.29 - Heat pipe arrangement for connecting the panel to the radiator.



Source: Author.

7 NUMERICAL MODEL

7.1 Governing Equations

The working fluid is assumed to be in liquid phase in the wick region (liquid zone) and vapour phase in the vapour region. When the evaporator is heated, the working fluid in the wick region is vaporized to the vapour space and the vapour flows to the condenser section. In the condenser section, after the vapour releases its latent heat to the environment through the outer surface of the condenser, it returns to the wick region as saturated liquid.

For the mathematical formulation of this numerical unsteady simulation work, the following assumptions were made:

- Vapour and liquid flow are unsteady, 2-D, laminar and incompressible;
- Viscous dissipation and gravity effects are negligible;
- Heat generation or dissipation due to the phase change process in the heat pipe is ignored;
- The physical properties are constant;

With the above assumptions, the resulted governing equations in cartesian coordinates were as follows:

7.1.1 Vapour Flow Region

Continuity:

$$\frac{\partial u_v}{\partial x} + \frac{\partial v_v}{\partial y} = 0 \quad (7.1)$$

Momentum in the x-direction:

$$\rho_v \left(\frac{\partial u_v}{\partial t} + u_v \frac{\partial u_v}{\partial x} + v_v \frac{\partial u_v}{\partial y} \right) = \mu_v \left(\frac{\partial^2 u_v}{\partial x^2} + \frac{\partial^2 u_v}{\partial y^2} \right) - \frac{\partial P_v}{\partial x} \quad (7.2)$$

Momentum in the y-direction:

$$\rho_v \left(\frac{\partial v_v}{\partial t} + u_v \frac{\partial v_v}{\partial x} + v_v \frac{\partial v_v}{\partial y} \right) = \mu_v \left(\frac{\partial^2 v_v}{\partial x^2} + \frac{\partial^2 v_v}{\partial y^2} \right) - \frac{\partial P_v}{\partial y} \quad (7.3)$$

Energy:

$$\rho_v C_{p,v} \left(\frac{\partial T_v}{\partial t} + u_v \frac{\partial T_v}{\partial x} + v_v \frac{\partial T_v}{\partial y} \right) = k_v \left(\frac{\partial^2 T_v}{\partial x^2} + \frac{\partial^2 T_v}{\partial y^2} \right) \quad (7.4)$$

7.1.2 Liquid Flow Region

The liquid flow in the wick is due to capillary action and is usually modeled as flow through porous medium. Liquid is considered as unsteady, incompressible flow with negligible body force.

Continuity:

$$\frac{\partial u_l}{\partial x} + \frac{\partial v_l}{\partial y} = 0 \quad (7.5)$$

The Darcy's Law is employed in the momentum equation for the porous liquid-wick region. The permeability K (Eq. 4.13) and the porosity ϵ (Eq. 4.14) of the liquid-wick region is considered to be isotropic. The resulted unsteady momentum equations are:

Momentum in the x-direction:

$$\rho_l \left(\frac{\partial u_l}{\partial t} + u_l \frac{\partial u_l}{\partial x} + v_l \frac{\partial u_l}{\partial y} \right) = \mu_l \left(\frac{\partial^2 u_l}{\partial x^2} + \frac{\partial^2 u_l}{\partial y^2} \right) - \frac{\partial P_l}{\partial x} - \frac{\mu_l u_l \epsilon}{K} \quad (7.6)$$

Momentum in the y-direction:

$$\rho_l \left(\frac{\partial v_l}{\partial t} + u_l \frac{\partial v_l}{\partial x} + v_l \frac{\partial v_l}{\partial y} \right) = \mu_l \left(\frac{\partial^2 v_l}{\partial x^2} + \frac{\partial^2 v_l}{\partial y^2} \right) - \frac{\partial P_l}{\partial y} - \frac{\mu_l v_l \epsilon}{K} \quad (7.7)$$

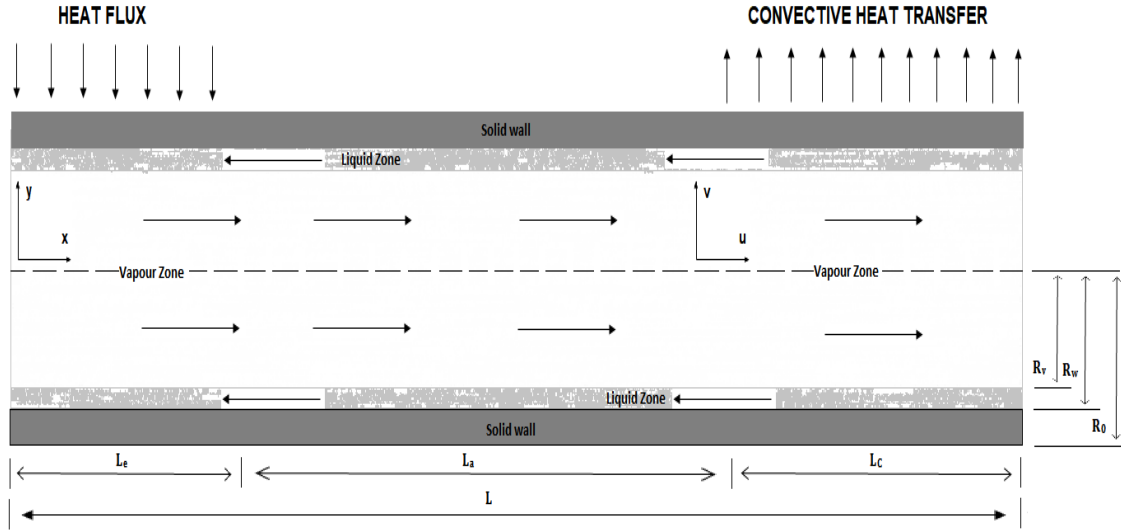
Energy:

$$\rho_l C_{p,l} \left(\frac{\partial T_l}{\partial t} + u_l \frac{\partial T_l}{\partial x} + v_l \frac{\partial T_l}{\partial y} \right) = k_{eff} \left(\frac{\partial^2 T_l}{\partial x^2} + \frac{\partial^2 T_l}{\partial y^2} \right) \quad (7.8)$$

7.2 Boundary Conditions

The imposed boundary conditions are illustrated in Figure. 7.1. The heat transfer coefficient, h can be determined using the Churchill and Chu correlation for the

Figure 7.1 - Boundary conditions of heat pipe.



Source: Author.

Nusselt number given below.

$$\overline{Nu}_d = \left\{ 0.60 + \frac{0.387 Ra_d^{1/6}}{[1 + (0.559/Pr)^{9/16}]^{8/27}} \right\}^2 \quad (7.9)$$

where the Rayleigh number

$$Ra_d = \frac{g\beta(T_p - T_\infty)d^3}{\nu\alpha} \quad (7.10)$$

where Pr is the Prandtl number, ν is the kinematic viscosity, α is thermal diffusivity and β is the volumetric thermal expansion coefficient. The detailed boundary conditions for evaporator, adiabatic and condenser region at the various radius and also at the ends of the heat pipe are given in Table 7.1 below.

Table 7.1 - Boundary Conditions

N°	Locations	Evaporator	Adiabatic	Condenser
1	Both ends of HP ($x = 0, L$)	$u = v = 0$ $\dot{m}_v = \frac{\dot{Q}}{h_{f,g}}$		$u = v = 0$
2	Centreline of HP ($y = 0$)	$v_v = 0, \frac{\partial v_v}{\partial y} = 0, \frac{\partial T_v}{\partial y} = 0$		
3	Liquid-vapour interface ($y = R_v$)	$\rho_v v_v = \rho_l v_l$		
4	Wick-wall interface ($y = R_w$)	$k_p \frac{\partial T_p}{\partial y} = k_{eff} \frac{\partial T_l}{\partial y}$, $u_l = v_l = 0, \rho_v v_v = \rho_l v_l = 0$		
5	Outer pipe wall ($y = R_0$)	$\dot{q} = k_p \frac{\partial T_p}{\partial y}$	$\frac{\partial T_p}{\partial y} = 0, \frac{\partial T_p}{\partial x} = 0$	$\frac{\partial T_p}{\partial y} = h(T_p - T_\infty)$

Source: Author.

7.3 Method of Solution

In this model, the commercial code ANSYS FLUENT 18.1 and the Volume of Fluid (VOF) method have been applied for the modelling of a heat pipe. Numerical simulations based on the finite volume method are more difficult for multiphase flows than for a single-phase flow. The reasons for this difficulty are that the interfaces between the phases are not stationary and physical properties such as density and viscosity change at interfaces between the different phases, which requires an intensive computational effort.

The VOF technique can be applied to model two immiscible fluids with a clearly defined interface between the phases, and is used for surface-tracking applied to a fixed mesh. In the VOF model, one set of Navier-Stokes equations are solved through the computational domain and used to track the motion of the different phases by defining the volume fraction of each phase.

A transient simulation with a time step of 0.0005 s is carried out to model the dynamic behaviour of the two-phase flow. A Combination of the SIMPLE algorithm for pressure-velocity coupling and a first-order upwind scheme for the determination of momentum and energy is included in the model. Geo-Reconstruct and PRESTO discretization for the volume fraction and pressure interpolation scheme, respectively, are also performed in the simulation.

The physical domain of problem was separated into 2 regions as follows.

1. vapour region;
2. liquid region and pipe wall

The numerical analysis was performed in both separated regions. The solution procedure is as follows.

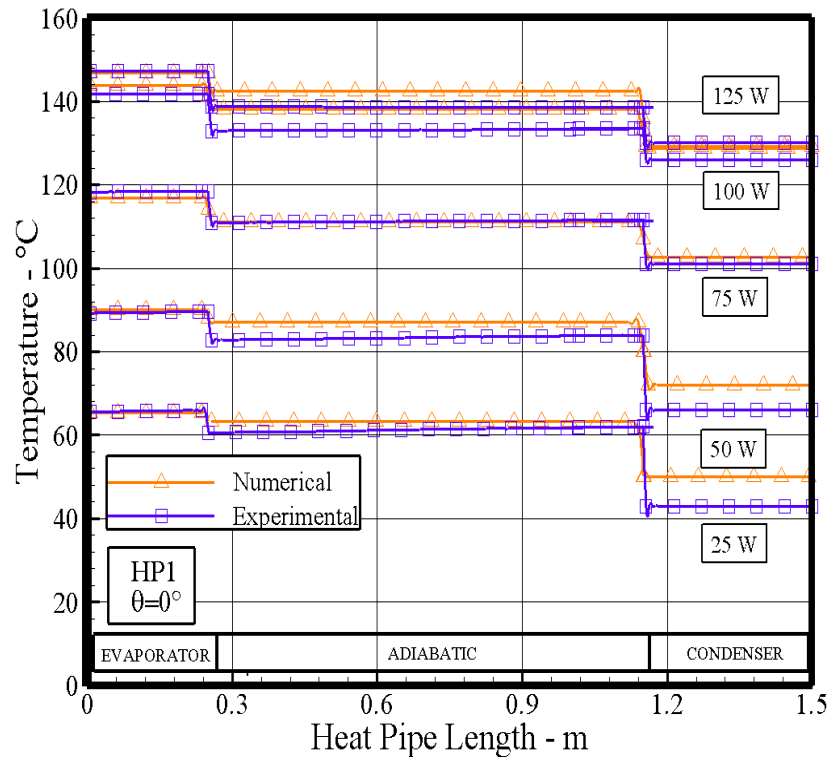
1. Continuity and momentum equation are solved in vapour region with mentioned boundary conditions to find the pressure distribution;
2. Clausius-Clapeyron equation has been used to find temperature boundary condition at the liquid-vapour interface;
3. All of the equations have been solved in vapour region;
4. The mentioned equations with related boundary condition have been solved in liquid region and pipe wall simultaneously;

It is expected to obtain a very good agreement between the numerically results and those from the experiment thus validating the numerical technique developed presented above.

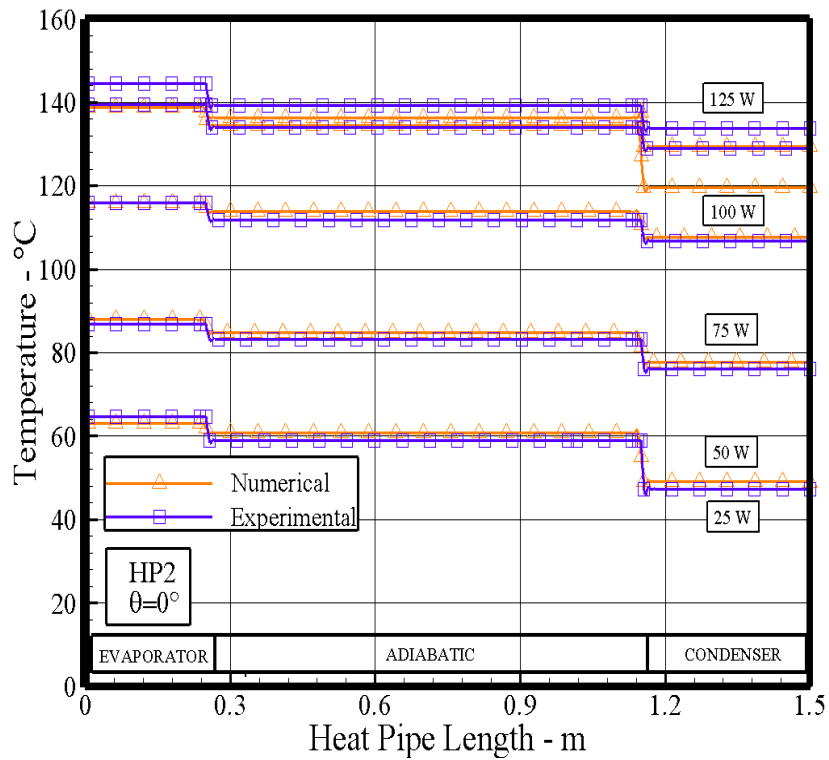
7.4 Numerical Results

In this study, the results of the simulation of the temperature in the evaporator, adiabatic and condenser walls of a screen mesh wick heat pipe were compared with that obtained from experimental results. The comparison is illustrated in Figure. 7.2. As observed in the figure that numerical models predict evaporator, adiabatic and condenser temperatures that are in good agreement with the experimental results. As a result of no heat loss in adiabatic section, the temperature is raised in the surface of this section due to the axial conduction heat transfer.

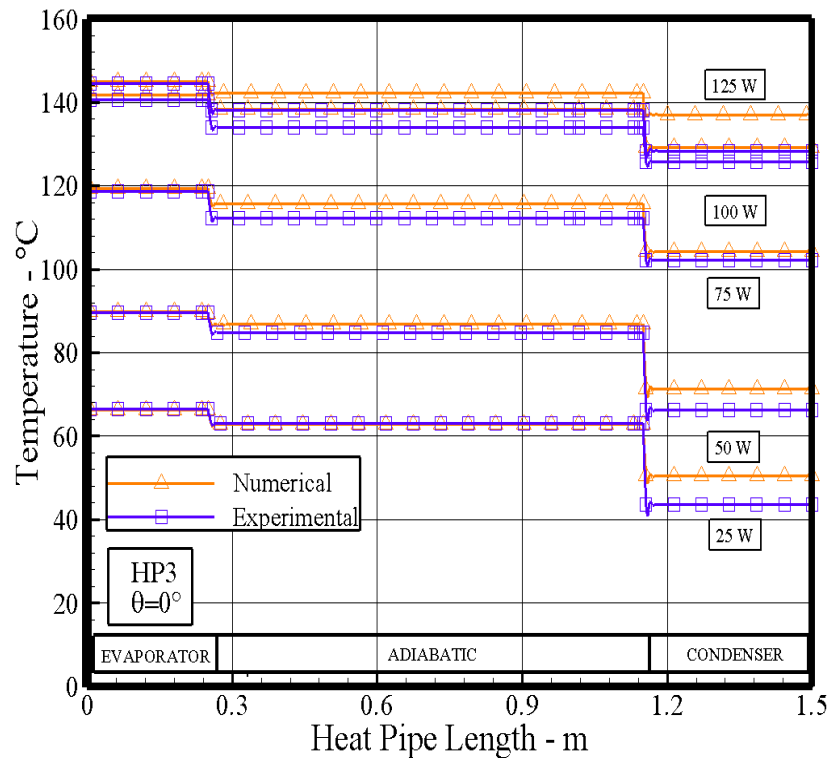
Figure 7.2 - Temperature comparison between experimental and numerical for different heat inputs.(a) HP1, (b) HP2, (c) HP3, (d) HP4 and (e) HP5.



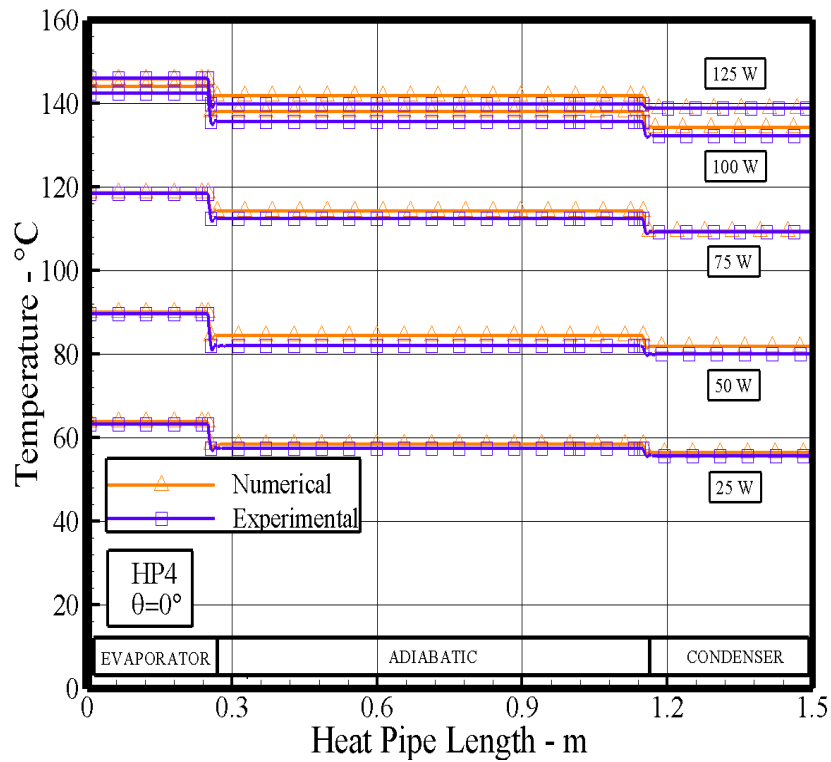
(a)



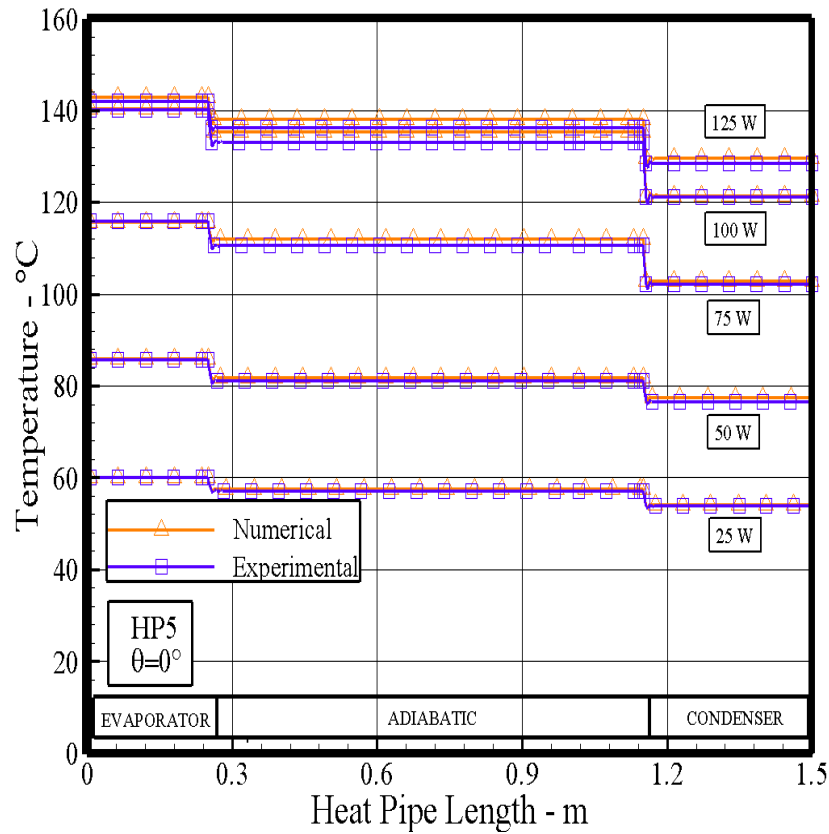
(b)



(c)



(d)



(e)

Source: Author.

One of the key assumptions in heat pipe modeling is that the evaporation and condensation occur at the interface between the wick and vapor core. This condition may not exist as the heat input increases. By increasing the heat input, the evaporation and condensation rates increase, and more liquid becomes vapour. Faster rate of evaporation and condensation may lead to the condition that entire section of the wick is not completely saturated with the working fluid and the phase change is not occurring at the wick-vapour interface. In addition, saturation condition is assumed at this interface, while at higher heat flux values, the vapour at the evaporator may be superheated.

Six different positions have been used to monitor the average temperature for the evaporator, adiabatic and condenser section. Table 7.2- 7.3 show the surface average temperatures in evaporator ($T_{e_{av}}$), adiabatic ($T_{a_{av}}$) and condenser ($T_{c_{av}}$) sections, in addition the thermal conductance of the system and the Relative Error (R_E) between numerical simulation and experimental results (EXP). The numerical results of the VOF model showed the same trend as the experimental data. The average

relative error of evaporator, adiabatic and condenser average temperatures are 1.0%, 1.87% and 1.75%, respectively for HP2 (stainless steel heat pipe) and 0.52%, 1.84% and 1.08%, respectively for HP4 (copper heat pipe).

Table 7.2 - Comparison between experimental and numerical results for different heat inputs - HP2

Power	Evaporator			Adiabatic			Condenser			G	
	T_{exp} (°C)	T_{num} (°C)	R_E (%)	T_{exp} (°C)	T_{num} (°C)	R_E (%)	T_{exp} (°C)	T_{num} (°C)	R_E (%)	G_{exp} (W/°C)	G_{num} (W/°C)
25W	64.7	62.9	±2.6	59.0	60.8	±3.1	47.4	49.2	±3.8	1.4	1.8
50W	86.9	87.8	±1.1	83.3	83.3	±0.03	76.1	77.7	±2.2	4.6	4.9
75W	115.8	115.8	±0.04	111.8	113.7	±1.7	106.7	107.5	±0.7	8.2	9.1
100	139.3	138.8	±0.3	134.0	136.3	±1.7	128.9	129.3	±0.3	9.5	10.4
125W	144.4	145.7	±0.9	139.2	143.1	±2.8	133.7	135.9	±1.6	11.7	12.7
Average Relative Error%			±1.00			±1.87			±1.75		

Source: Author.

Table 7.3 - Comparison between experimental and numerical results for different heat inputs - HP4

Power	Evaporator			Adiabatic			Condenser			G	
	T_{exp} (°C)	T_{num} (°C)	R_E (%)	T_{exp} (°C)	T_{num} (°C)	R_E (%)	T_{exp} (°C)	T_{num} (°C)	R_E (%)	G_{exp} (W/°C)	G_{num} (W/°C)
25W	63.2	63.8	±0.9	57.5	58.3	±1.4	55.7	56.5	±1.4	3.3	3.4
50W	89.6	89.9	±0.3	81.9	84.4	±3.0	79.9	81.7	±2.3	5.1	6.1
75W	118.4	118.5	±0.01	112.4	114.2	±1.6	109.1	109.2	±0.1	8.0	8.1
100	142.3	143.9	±1.2	135.6	137.9	±1.7	132.2	134.1	±1.4	9.9	10.2
125W	146.0	145.8	±0.1	139.7	141.7	±1.4	138.8	138.8	±0.03	17.36	17.85
Average Relative Error%			±0.52			±1.84			±1.08		

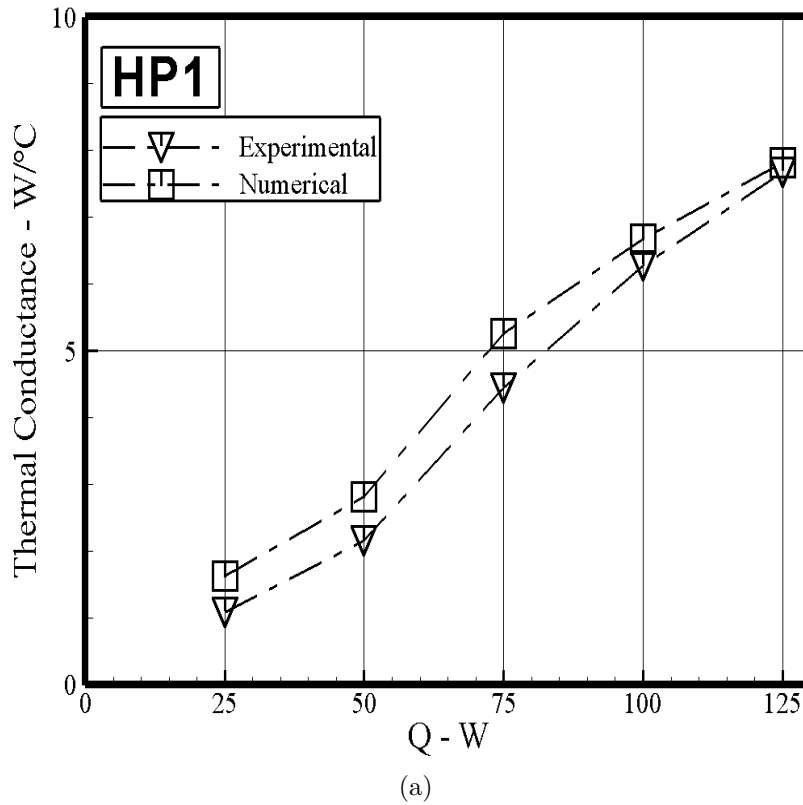
Source: Author.

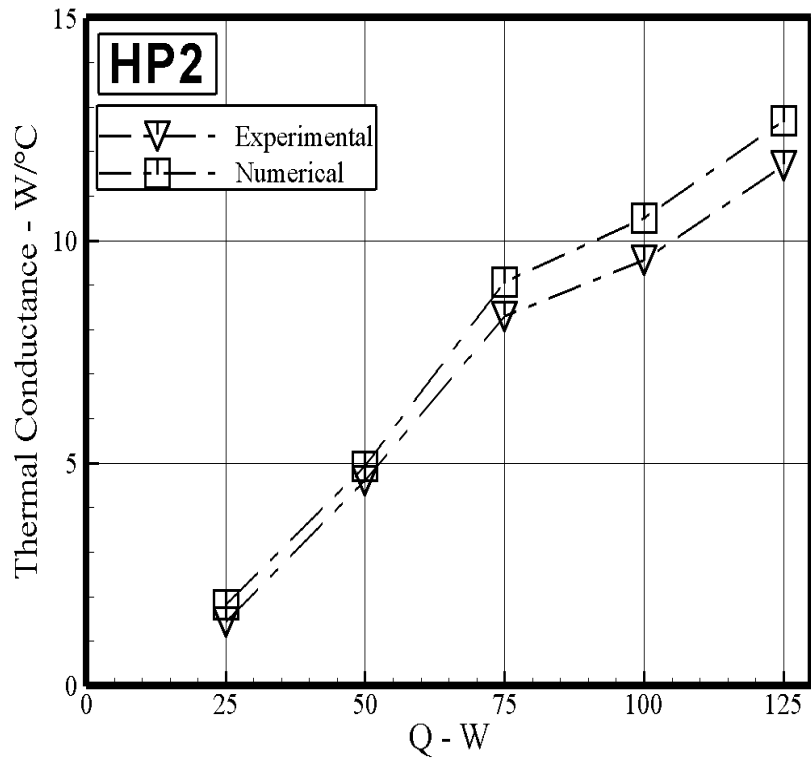
Figure 7.3 illustrates that the predicted thermal conductance is in good agreement with the experimental data as the thermal conductance of the heat pipes increases with increasing heating power load. The heat pipe has a smaller thermal conductance at lower heat inputs because more liquid resides in the evaporator section. Additionally, as the heat input increases, the operating temperature and pressure of the heat pipe increases. This indicates that the vapour temperature drop along the

length of the heat pipe is relatively small on comparison with the heat pipe's operating temperature. Furthermore, the temperature difference between the evaporator and condenser increases at a lower rate than that of the heat input.

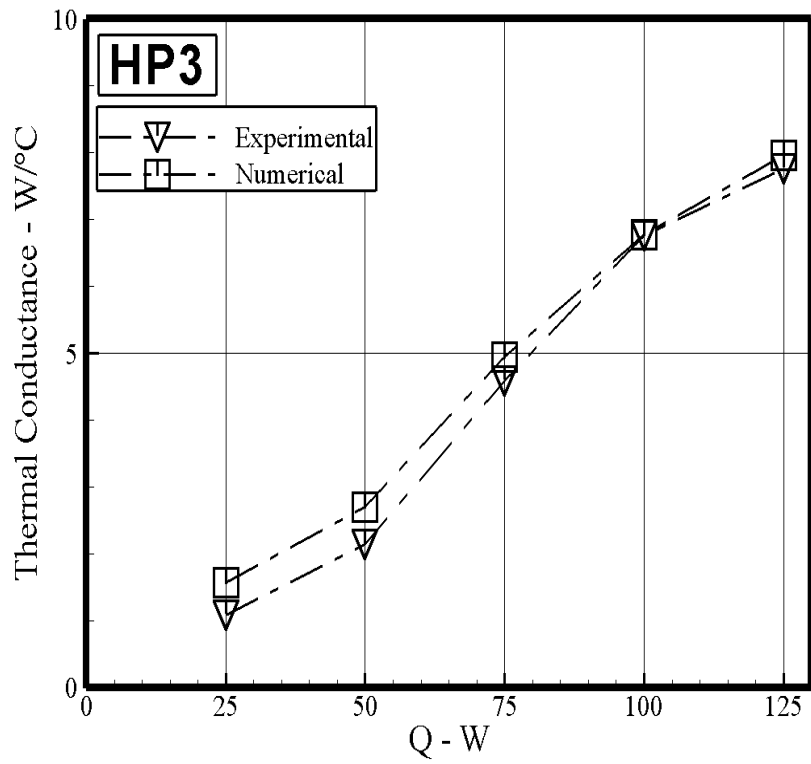
The differences between numerical and experimental results can be attributed to a non-uniformity in the wick thickness, in rolling the screen mesh wick that may have affected its porosity and, therefore, its effective thermal conductivity. The thermal conductivity of the wick directly influences the temperature distribution at the outer surface of the heat pipe and the numerical model does not consider any excess liquid, which resides in the evaporator particularly at lower heat inputs.

Figure 7.3 - Thermal conductance comparison between experimental and numerical for different heat inputs.(a) HP1, (b) HP2, (c) HP3, (d) HP4 and (e) HP5.

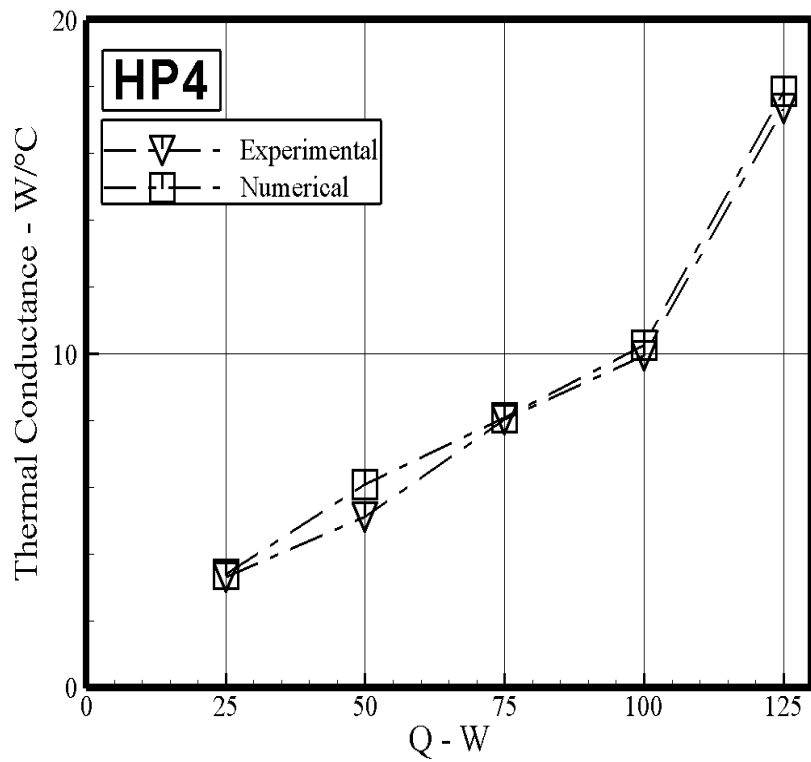




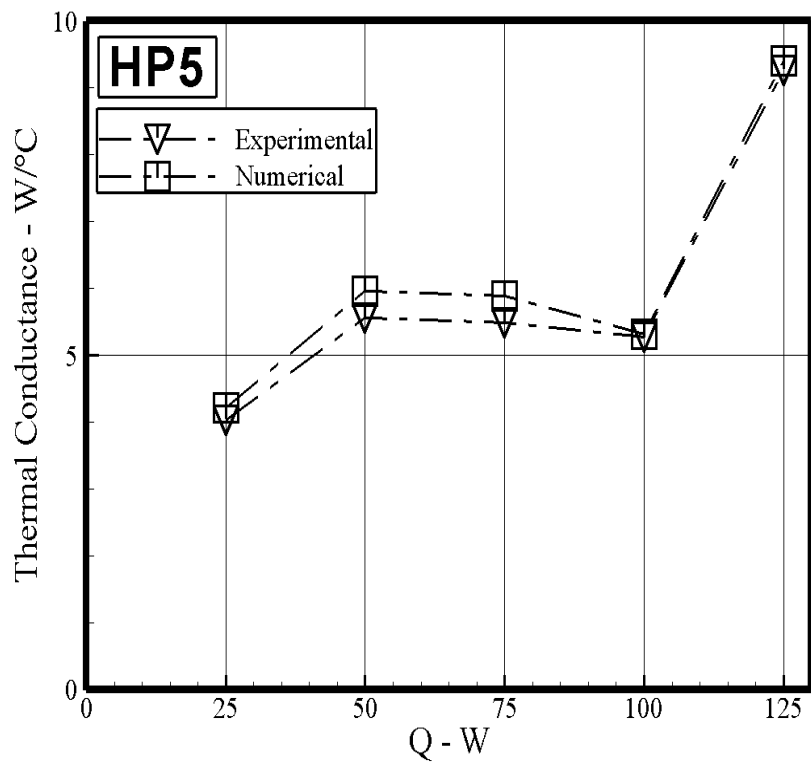
(b)



(c)



(d)



(e)

Source: Author.

8 CONCLUSIONS

The development of the heat pipe technology for industrial applications presents to be very important to improve the heat recovery systems performance, since they can greatly contribute to increase heat exchangers performances without great increase on their final costs. The continuous development of this technology for industrial and aerospace purposes is highly desirable in order to give more degrees of freedom to thermal engineers to face the increase of heat dissipation and new challenges on thermal management issues.

Stainless steel heat pipes and copper heat pipes with screen mesh wick were manufactured for the application of heat pipes technology in the industrial and aerospace sector. The results of analysis of experimental and calculated thermal conductances for heat pipes operating at mid-level temperature using water as working fluid, with mesh numbers 100, 200 and 400 were presented. With the experimental results, the thermal adjustment was calculated to obtain the thermal conductance that corresponds to each heat pipe. For better thermal performance and conditions evaluation: the thermal profiles before and after the start-up, transient behavior during the changes on applying power, thermal behavior under steady state conditions were analyzed. The following conclusions were drawn from this study.

- Referring to the design of stainless steel and copper heat pipes with metal mesh, six units of each were successfully manufactured and extensively tested, presenting reliable results considering their expected lifetime operation of 15 years. The heat pipes presented stable behavior, for both transient and steady-state conditions, when operated using the power levels of 25-125W (power step and power cycles). During the experimental tests, heat pipes did not present dry-out tendencies or superheating in the evaporator.
- With the test bench constructed the heat pipes were tested in order to obtain the temperature profiles of the stainless steel and copper heat pipes. For stainless steel heat pipes operating at 0° the HP2 presented the smallest temperature difference between the evaporator and the condenser in relation to the other two heat pipes operating with cycle 2. This difference is due to the fact that the powers were increased and decreased in each heat pipe during each test. When decreased to a lower power, a higher temperature was reached in the evaporator section due to the accumulated energy of the higher power used previously. It presented lower re-

sistance of the liquid in returning to the evaporator due the combination of important characteristics of the heat pipe: pore size, permeability and porosity. Test results showed a reliable operation during the cycles, with fast start-ups and transients, achieving experimental thermal conductance of $19.10W/^\circ C$. For copper heat pipes the HP4 showed faster start-up and without oscillations of temperatures, reaching the temperature of the evaporator, adiabatic and condenser near the isothermal condition, configuring better performance when analyzed by its thermal conductance due to the higher permeability and porosity, leading to fast fluid circulation at the start-up. Higher thermal conductance for HP4 operating with cycle 1 at 30° due to the smallest temperature difference between the evaporator and the condenser ($4.7^\circ C$). Test results showed reliable operation during the cycles, with fast start-ups and transients, achieving experimental thermal conductance of to $26.59.10W/^\circ C$.

- Referring to the thermal stability during the start-up, transient and steady-state regime, the largest temperature difference between the evaporator and the condenser occurred in the heat pipe (HP6) operating at 0° inclination, which does not occurred when operating at 90° , that was designed with stainless steel wire mesh. The results are consistent with the presence of non-condensable gases (NCG) that tend to accumulate at the condenser end of the heat pipe. At low heat flux, the non-condensable gases occupy a larger portion of the condenser due to the lower vapour pressure. As the heat flux increases, the operating (vapour) temperature of the heat pipe raising, increasing the vapour pressure which compresses the non-condensable gases thereby increasing the active region of the condenser. The results with the power cycle tests have showed no dry-out tendency in the evaporate section and little temperature difference between the evaporator section and the condenser section due to the high thermal conductivity of the copper. In order to minimize NCGs, the procedure for the manufacturing process was as follows: cleaning, passivation of stainless steel components, high vacuum ($10^{-5}mbar$) and use of deionized water with prior degassing before being inserted into the heat pipe. Then, the aging process was performed for NCGs in accelerated mode.
- An adjustment factor was considered for the calculated thermal conductance, in order to add uncontrolled variables that are inherent to the heat pipe manufacturing process, such as: porous structure thickness, correct

amount of working fluid inside the heat pipe, the mesh folding to the closing of the heat pipe, etc. The results of the thermal conductance calculated with the adjustment factor were within the experimental error for each test performed with the heat pipes.

- Applications for heat pipes operating in mid-level temperature were presented to the industrial sector in cooling in a storage tank of the petroleum asphalt cement (PAC) and in the space sector in the thermal control of electronic equipment in panel honeycomb.
- Very good agreement was obtained between the experimental results and the results obtained from the numerical model for heat inputs, thus validating the numerical methods employed.

Based on this investigation, continuity on the development of heat pipes able to operate in this temperature range must be carried on. Future development must comply with the use of alternative working fluids such as toluene, acetone and methanol, which could contribute to the application of this type of heat pipe in temperatures below freezing when necessary. Additionally, refinement in the numerical model can be done by evaluating the phase change processes in the evaporation and condensation interfaces in the heat pipes coupled with their interfacial behavior with the wick, which can highly contribute to the optimization of the heat pipe design and operation.

REFERENCES

- AKACHI, H.; POLASEK, F.; STULC, P. Pulsating heat pipes. In: INTERNATIONAL HEAT PIPE SYMPOSIUM, 5., 1996. **Proceedings...** [S.l.], 1996. p. 208–217. 16
- ANDERSON, W. G.; ELLIS, M. C.; HARTENSTINE, J. R.; PETERS, C. J.; TARAU, C.; WALKER, K. L. Variable conductance heat pipes for variable thermal links. In: INTERNATIONAL CONFERENCE ON ENVIROMENTAL SYSTEM, 42., 2012, San Diego, California. **Proceedings...** [S.l.], 2012. 11
- BEJAN, A.; KRAUS, A. D. **Heat transfer handbook**. [S.l.]: John Wiley & Sons, 2003. 23, 31, 53, 57, 58, 61, 62
- BIRUR, G.; PAUKEN, M.; NOVAK, K. Thermal control of mars rovers and landers using miniature loop heat pipes. In: INTERNATIONAL HEAT PIPE CONFERENCE, 12., 2002. **Proceedings...** [S.l.], 2002. p. 189–194. 6, 13
- BUSSE, C. Theory of the ultimate heat transfer limit of cylindrical heat pipes. **International Journal of Heat and Mass Transfer**, v. 16, n. 1, p. 169–186, 1973. 57, 60
- CAREY, V. **Liquid vapor phase change phenomena: an introduction to the thermophysics of vaporization and condensation processes in heat transfer equipment**. [S.l.]: Taylor and Francis, 1992. ISBN 9781591690351. 41, 42, 46
- CHAN, C.; SIQUEIROS, E.; LING-CHIN, J.; ROYAPOOR, M.; ROSKILLY, A. heat utilisation technologies: a critical review of heat pipes. **Renewable and Sustainable Energy Reviews**, v. 50, p. 615–627, 2015. 3, 12, 14, 17
- CHI, S. **Heat pipe theory and practice**. Washington, EUA: Hemisphere Publishing, 1976. 3, 23, 25, 31, 40, 43, 45, 46, 48, 49, 50, 51, 58, 63, 64, 65
- COTTER, T. **Theory of heat pipes**. Los Alamos, New Mexico, EUA: University of California, 1965. 7
- _____. **Heat pipe startup dynamics**. [S.l.: s.n.], 1968. 61
- _____. Principles and prospect for micro heat pipes. In: INTERNATIONAL HEAT TRANSFER CONFERENCE, 5., 1984, Tusbuba, Japan. **Proceeding...** [S.l.], 1984. p. 328–335. 8

FAGHRI, A. **Heat pipe science and technology**. Washington, EUA: Taylor and Francis, 1995. 1, 3, 4, 6, 8, 23, 24, 25, 28, 29, 33, 35, 37, 38, 41, 43, 44, 46, 47, 49, 53, 57, 69, 70

_____. Heat pipes: review, opportunities and challenges. **Frontiers in Heat Pipes (FHP)**, v. 5, n. 1, 2014. 9, 33, 57

GERASIMOV, Y. F.; KISEEV, V.; MAIDANIK, Y. F. et al. Heat pipe. **USSR Inventors Certificate**, v. 449213, 1974. 13

GERASIMOV, Y. F.; MAIDANIK, Y. F.; SHCHEGOLEV, G.; FILIPPOV, G.; STARIKOV, L.; KISEEV, V.; DOLGIREV, Y. E. Low-temperature heat pipes with separate channels for vapor and liquid. **Journal of Engineering Physics and Thermophysics**, Springer, v. 28, n. 6, p. 683–685, 1975. 13

GERNER, F.; LONGTIN, J.; HENDERSON, H.; HSIEH, W.; RAMDAS, P.; CHANG, W. Flow limitations in micro heat pipes. In: ASME NATIONAL HEAT TRANSFER CONFERENCE, 28., 1992, San Diego, California. **Proceeding...** [S.l.], 1992. p. 99–104. 9

GONCHAROV, K. Development and application of space radiators with loop heat pipes. In: MINSK INTERNATIONAL SEMINAR HEAT PIPES, HEAT PUMPS, REFRIGERATORS, POWER SOURCES, 8., 2011. **Proceedings...** Belarus, 2011. 13

GROVER, G.; COTTER, T.; ERIKSON, G. Structures of very high thermal conductivity. **Journal of Applied Physics**, v. 35, n. 6, p. 1190–1191, 1964. 1

IVANOVSKII, M.; SOROKIN, V.; YAGODKIN, I. **The Physical Properties of Heat Pipes**. [S.l.]: Clarendon Press, 1982. (Oxford studies in physics). 31

KEMME, J. E. Ultimate heat pipe performance. **IEEE Transactions on Electron Devices**, v. 16, n. 8, p. 717–723, 1969. 58

KEW, P. A.; REAY, D. A. **Heat pipes: theory, design and applications**. 5.ed. ed. Oxford, UK: Elsevier's, 2006. 1, 2, 4, 5, 6, 11, 15, 16, 17, 26, 27, 28, 29, 32, 33, 34, 35, 36, 37, 38, 39, 40, 43, 44, 53, 62, 69, 70

KIRKPATRICK, J.; MARCUS, B. A variable conductance heat pipe experiment. **AIAA Paper**, n. 71-411, 1971. 5

KRAUS, A. D.; BAR-COHEN, A. **Thermal analysis and control of electronic equipment**. Washington, DC: Hemisphere, 1983. 633 p., 1983. 51

LERICHE, M.; HARMAND, S.; LIPPERT, M.; DESMET, B. An experimental and analytical study of a variable conductance heat pipe: Application to vehicle thermal management. **Applied Thermal Engineering**, v. 38, p. 48–57, 2012. 11, 12

LEVY, E. Theoretical investigation of heat pipes operating at low vapor pressures. **Journal of Engineering for Industry**, v. 90, n. 4, p. 547–552, 1968. 59

LI, H.; LIU, Z.; CHEN, B.; LIU, W.; LI, C.; YANG, J. Development of biporous wicks for flat-plate loop heat pipe. **Experimental Thermal and Fluid Science**, v. 37, p. 91–97, 2012. 37

LIU, D.; TANG, G.; ZHAO, F.; WANG, H. Modeling and experimental investigation of looped separate heat pipe as waste heat recovery facility. **Applied Thermal Engineering**, v. 26, n. 17, p. 2433–2441, 2006. 6

MARCUS, B. D. **Theory and design of variable conductance heat pipes**. Washington DC, EUA: NASA, 1972. 47, 48, 62

MAYDANIK, Y.; FERSHTATER, Y.; PASTUKHOV, V.; GONCHAROV, K.; ZAGAR, O.; GOLOVANOV, Y. Thermoregulation of loops with capillary pumping for space use. In: . [S.l.]: INTERNATIONAL CONFERENCE ON ENVIRONMENTAL SYSTEMS, 1992. 13

MAYDANIK, Y. F. Loop heat pipes. **Applied Thermal Engineering**, v. 25, n. 5, p. 635–657, 2005. 13, 14, 16

MOFFAT, R. J. Describing the uncertainties in experimental results. **Experimental Thermal and Fluid Science**, v. 1, n. 1, p. 3–17, 1988. 67

MUENZEL, W. Compatibility tests of various heat pipe working fluids and structural materials at different temperatures. In: INTERNATIONAL HEAT PIPE CONFERENCE, 3., 1978. **Proceedings...** [S.l.], 1978. p. 398. 84

PETERSON, G. An overview of micro heat pipe research and development. **Journal Applied Mechanics Review**, v. 45, n. 5, p. 175–189, 1992. 8, 10

_____. **An introduction to heat pipe modeling, testing and applications**. New York, EUA: John Wiley and Sons, 1994. 1, 8, 10, 25, 26, 27, 28, 30, 31, 32, 39, 40, 41, 47, 48, 49, 50, 51, 52, 55, 57, 58, 59, 60, 61, 62, 63, 64, 65, 70

REYES, A.; BROWN, J.; CHANG, W.; PONNAPPAN, R. Gas generation test data and life tests of low temperature heat pipes. In: JOINT THERMOPHYSICS

AND HEAT TRANSFER CONFERENCE, 5., 1990. **Proceedings...** [S.l.], 1990. 84, 85

RIEHL, R.; SIQUEIRA, T. C. Heat transport capability and compensation chamber influence in loop heat pipes performance. **Applied Thermal Engineering**, v. 26, n. 11, p. 1158–1168, 2006. 13

RIEHL, R. R. Extensive development of the loop heat pipe technology. In: **INTERNATIONAL CONFERENCE ON ENVIRONMENTAL SYSTEMS, 2006**. [S.l.: s.n.]. 13

_____. Heat pipes and loop heat pipes acceptance tests for satellites applications. In: **American Institute of Physics Conference Series**. [S.l.: s.n.]. v. 1103, p. 82–90, 2009. 6, 13

_____. **Passive Two-Thermal Control - Terrestrial and Space Applications, 2018**. [S.l.]: in preparation. 84

_____. design and operation of capillary driven two-phase loops as cpl/lhp. **São Paulo, Brazil: National Institute for Intellectual Property, 2002. Software Register**, v. 3003, 2002. 80

_____. Thermal performance and development of a dual evaporator loop heat pipe. **Heat Pipe Science and Technology, an International Journal**, v. 4, n. 1-2, 2013. 14, 15

_____. Passive thermal management of surveillance systems using pulsating heat pipes. In: **INTERNATIONAL SEMINAR SEMINAR HEAT PIPES, HEAT PUMPS, REFRIGERATORS, HEAT SOURCES, 9.**, 2015. **Proceedings...** [S.l.], 2015. 6

_____. Copper-methanol heat pipes development for electronics cooling of surveillance equipment. In: **INTERNATIONAL ENERGY CONVERSION ENGINEERING CONFERENCE, 14.**, 2016. **Proceedings...** [S.l.], 2016. p. 4796. 9

_____. Utilization of passive thermal control technologies in cooling electronics: A brief review. **Heat Pipe Science and Technology: an International Journal**, v. 7, n. 3-4, p. 161–183, 2016. 6, 7, 9, 13, 14, 17, 18, 19

RIEHL, R. R.; CACHUTÉ, L. O. Pulsating heat pipes used for thermal control of electronics on surveillance systems. In: **43RD INTERNATIONAL CONFERENCE**

ON ENVIRONMENTAL SYSTEMS, 43., 2013, Colorado, United States.

Proceedings... [S.l.], 2013. 6, 7, 18

RIEHL, R. R.; SANTOS, N. Loop heat pipe development overview. In: **AIP Conference Proceedings**. [S.l.: s.n.]. v. 969, n. 1, p. 29–36, 2008. 6, 13

_____. Loop heat pipes and heat pipes technologies development and qualification for space applications. In: INTERNATIONAL SEMINAR SEMINAR HEAT PIPES, HEAT PUMPS, REFRIGERATORS, HEAT SOURCES, 7., 2008.

Proceedings... [S.l.], 2008. p. 8–11. 6, 13, 15

SANTOS, N. **Desenvolvimento de tubo de calor circuitado (Loop Heat Pipe-LHP) para aplicações Espaciais**. 188 p. Thesis (Doctor in Engineering and Space Technology - Space Mechanics and Control) — National Institute for Space Research, São José dos Campos- SP, Brazil, 2009. Disponível em: <<http://mtc-m16c.sid.inpe.br/col/sid.inpe.br/mtc-m18@80/2009/04.07.18.33/doc/publicacao.pdf>>. 7

SARNO, C. Application of phase change systems in avionics. In: INTERNATIONAL HEAT PIPE CONFERENCE, 16., 2012, Lyon, France.

Proceedings... [S.l.], 2012. 82

SHI, C.; WANG, Y.; LIAO, Q.; YANG, Y. Analysis and application of variable conductance heat pipe air preheater. **Journal of Thermal Science**, v. 20, n. 3, p. 248–253, 2011. 12

SHUKLA, K. Heat transfer limitation of a micro heat pipe. **Journal of Electronic Packaging**, v. 131, n. 2, p. 024502, 2009. 9

_____. Heat pipe for aerospace applications - an overview. **Journal of Electronics Cooling and Thermal Control**, v. 5, n. 1-14, p. 1313–1319, 2015. 5, 9, 12

SILVA, D. O.; MARCELINO, E.; RIEHL, R. R. Thermal performance comparison between water-copper and water-stainless steel heat pipes. In: INTERNATIONAL ENERGY CONVERSION ENGINEERING CONFERENCE, 13., 2015.

Proceedings... [S.l.], 2015. p. 3981. 4, 92

SILVA, D. O.; RIEHL, R. R. Development of heat pipes operating at mid-level temperature range applied for industry, defense and aerospace. In: **AIAA PROPULSION AND ENERGY FORUM**. [S.l.: s.n.], 2014. 6, 7

- _____. Experimental investigation of water-stainless steel heat pipes operating in power cycles. In: **HEAT POWERED CYCLES CONFERENCE, Nottingham, UK.** [S.l.: s.n.], 2016. 104
- SINGH, R.; AKBARZADEH, A.; MOCHIZUKI, M. Operational characteristics of a miniature loop heat pipe with flat evaporator. **International Journal of Thermal Sciences**, v. 47, n. 11, p. 1504–1515, 2008. 14
- TORRES, A.; MISHKINIS, D.; KULAKOV, A.; ROMERA, F.; GREGORI, C.; KAYA, T. Thermal control of loop heat pipe with pressure regulating valve. **Heat Pipe Science and Technology, An International Journal**, v. 1, n. 4, 2010. 15
- TULIN, D.; TULIN, I.; SEROV, G.; SHABARCHIN, A. In-flight experience of heat pipe based thermal control system for geostationary orbiting service module. In: INTERNATIONAL SEMINAR HEAT PIPES, HEAT PUMPS, REFRIGERATORS, POWER SOURCES, 8., 2011. **Proceedings...** [S.l.], 2011. v. 15. 13
- VASILIEV, L. L. Heat pipes in modern heat exchangers. **Applied Thermal Engineering**, v. 25, n. 1, p. 1–19, 2005. 6
- VLASSOV, V. V.; RIEHL, R. R.; SOUZA, F. L. **CBERS3 STM heat pipes set acceptance test data report.** [S.l.: s.n.], 2007. 68 p. 6
- WALLIN, P. heat pipe, selection of working fluid. **Lund, Sweden, 2012. (Project Report, MVK160)**, 2012. 72
- WAYNER, P. Long range intermolecular forces in change-of-phase heat transfer(1998 donald q. kern award review). In: NATIONAL HEAT TRANSFER CONFERENCE, 33., 1999. **Proceedings...** Albuquerque, 1999. 45
- YANG, H.; KHANDEKAR, S.; GROLL, M. Operational limit of closed loop pulsating heat pipes. **Applied Thermal Engineering**, v. 28, n. 1, p. 49–59, 2008. 18
- YANG, X.; YAN, Y.; MULLEN, D. Recent developments of lightweight, high performance heat pipes. **Applied Thermal Engineering**, v. 33, p. 1–14, 2012. 3
- YOSHIHARA, J.; CAMPBELL, C. T. Methanol synthesis and reverse water gas shift kinetics over cu (110) model catalysts: structural sensitivity. **Journal of Catalysis**, v. 161, n. 2, p. 776–782, 1996. 85

ZHANG, C.; CHEN, Y.; SHI, M.; PETERSON, G. Optimization of heat pipe with axial shaped micro grooves based on a niched pareto genetic algorithm npga. **Applied Thermal Engineering**, v. 29, n. 16, p. 3340–3345, 2009. 38

PUBLICAÇÕES TÉCNICO-CIENTÍFICAS EDITADAS PELO INPE

Teses e Dissertações (TDI)

Teses e Dissertações apresentadas nos Cursos de Pós-Graduação do INPE.

Manuais Técnicos (MAN)

São publicações de caráter técnico que incluem normas, procedimentos, instruções e orientações.

Notas Técnico-Científicas (NTC)

Incluem resultados preliminares de pesquisa, descrição de equipamentos, descrição e ou documentação de programas de computador, descrição de sistemas e experimentos, apresentação de testes, dados, atlas, e documentação de projetos de engenharia.

Relatórios de Pesquisa (RPQ)

Reportam resultados ou progressos de pesquisas tanto de natureza técnica quanto científica, cujo nível seja compatível com o de uma publicação em periódico nacional ou internacional.

Propostas e Relatórios de Projetos (PRP)

São propostas de projetos técnico-científicos e relatórios de acompanhamento de projetos, atividades e convênios.

Publicações Didáticas (PUD)

Incluem apostilas, notas de aula e manuais didáticos.

Publicações Seriadas

São os seriados técnico-científicos: boletins, periódicos, anuários e anais de eventos (simpósios e congressos). Constam destas publicações o Internacional Standard Serial Number (ISSN), que é um código único e definitivo para identificação de títulos de seriados.

Programas de Computador (PDC)

São a seqüência de instruções ou códigos, expressos em uma linguagem de programação compilada ou interpretada, a ser executada por um computador para alcançar um determinado objetivo. Aceitam-se tanto programas fonte quanto os executáveis.

Pré-publicações (PRE)

Todos os artigos publicados em periódicos, anais e como capítulos de livros.